National Library of Canada
Acquisitions and Bibliographic Services Branch
395 Wellington Street
Ottawa, Ontario
K1A 0N4

Bibliothèque nationale du Canada
Direction des acquisitions et des services bibliographiques
395, rue Wellington
Ottawa (Ontario)
K1A 0N4

Your file Votre référence

Our file Notre référence

NOTICE

The quality of this microform is heavily dependent upon the quality of the original thesis submitted for microfilming. Every effort has been made to ensure the highest quality of reproduction possible.

If pages are missing, contact the university which granted the degree.

Some pages may have indistinct print especially if the original pages were typed with a poor typewriter ribbon or if the university sent us an inferior photocopy.

AVIS

La qualité de cette microforme dépend grandement de la qualité de la thèse soumise au microfilmage. Nous avons tout fait pour assurer une qualité supérieure de reproduction.

S'il manque des pages, veuillez communiquer avec l'université qui a conféré le grade.

La qualité d'impression de certaines pages peut laisser à désirer, surtout si les pages originales ont été dactylographiées à l'aide d'un ruban usé ou si l'université nous a fait parvenir une photocopie de qualité inférieure.

Canada

TECTONIC FRAMEWORK AND RELATIVE AGES OF STRUCTURES WITHIN THE OTTAWA-BONNECHÈRE GRABEN

by

Rolly E. Rimando

A thesis submitted to the School of Graduate Studies and Research in partial fulfillment of the requirements for the degree of M.Sc. in Geology

UNIVERSITY OF OTTAWA

OTTAWA, CANADA

1994

ISBN 0-612-00494-5

UNIVERSITÉ D'OTTAWA
UNIVERSITY OF OTTAWA

ABSTRACT

The Ottawa-Bonnechère graben forms a 55 km wide topographic low extending from near Montreal through Ottawa. It is part of the St. Lawrence rift system, which also includes the Saguenay graben in Québec. Cambrian to Ordovician carbonate and fine clastic sedimentary rocks of the St. Lawrence Platform overlie Grenvillian basement rocks and, in the Ottawa-Hull area, are cut by several generations of brittle faulting. Relative ages of faults and associated structures are determined or inferred from field studies of key outcrops. Three periods of faulting are defined, and the orientations of the paleostress fields associated with each period are modelled using fault and fault surface lineations orientation data. The oldest generation of fault structures, referred to as D_1, formed in response to a stress field in which the greatest principal horizontal stress was oriented northwest. The second and third periods of faulting (D_2,D_3) occurred when the greatest principal horizontal stress was oriented west-northwest and southwest, respectively. Both D_2 and D_3 involved the reactivation of the existing faults and the development of new faults. D_1 structures are kinematically congruent with the compressional direction associated with the closing of the proto-Atlantic ocean during the Paleozoic, though absolute ages of these structures are not yet determined. Emplacement of Cretaceous carbonatite

dykes coincided with D_2, which therefore occurred during the Mesozoic when the stress regime was associated with the opening of the Atlantic ocean. D_3 structures are consistent with the post-Cretaceous stress field in eastern North America. Periods of Phanerozoic faulting in the Ottawa-Bonnechère graben record a counterclockwise rotation of the regional stress field by about 90° since Paleozoic time. The occurrence of strong historical earthquakes and present-day microseismic events within the Ottawa-Bonnechère graben suggests that faulting continues under the current stress field, perhaps involving the reactivation of families of faults identified in this paper. Analysis of epicentral distribution using a Geographic Information System indicate spatial association between seismicity and geophysical lineaments that are similar in orientation to some D_1 to D_3 faults. Gravity and magnetic anomalies are only weakly associated with seismicity. Though the spatial associations are not strong, the data suggest a departure from spatial independence. A predictive map showing elevated potential for earthquake occurrence indicate high posterior probabilities for areas with high magnetic and gravity anomalies and within 7 km from northeast-trending gravity lineaments.

TABLE OF CONTENTS

LIST OF FIGURES

LIST OF TABLES

ACKNOWLEDGEMENTS

The Canadian International Development Agency (CIDA) granted a scholarship to the author under the long-term component of the Canada-ASEAN Regional Training Program and through the Philippine Institute of Volcanology and Seismology (Department of Science and Technology). Sincere thanks are due to Dr. Keith Benn for his supervision and contribution to the author's education; to Dr. Joseph Wallach for introduction to this study's problem, for providing field trips, data, photos and useful discussions on many aspects of the study; to Dr. Graeme Bonham-Carter for his contribution to my learning of GIS, and; to Mark Mihalasky, Kevin Telmer, Danny Wright and Quiming Cheng, teaching assistants, for helping the author untangle the intricacies of the GIS hardware and software. Thanks is also extended to Mario Funai and Lynn Bourdeau of Francon-Lafarge Inc. for providing access to the Francon and Permanent quarries; to the Ottawa-Carleton Transit Commission for providing access to the transitway; to Janet Drysdale of the Geological Survey of Canada for sharing earthquake data; to Dr. O. Laborde for providing the fault kinematics program, and; to Edward Hearn for assistance in preparing the photographs.

My deepest thanks to Marilou and Jeremy for their love and support.

1. INTRODUCTION

1.1 Introduction

Although the existence of the Ottawa-Bonnechère graben has been recognized for some time (Kay 1942; Wilson 1946; Hewitt 1964; Norris 1967; Williams and Rae 1983; Williams and Telford 1986, 1987; Williams *et al.* 1992), very little is known about its structural geology. This is because most previous studies have focused mainly on stratigraphy. Important evidence, based on surface structural geology, regarding the history of graben development, the kinematics of movement on faults, and the evolution of the regional stress field orientations has remained undocumented.

The reactivation of faults within the graben has become a generally accepted notion (Kay 1942; Wilson 1946; Kumarapeli and Saull 1966; Kumarapeli 1976, 1978; Williams and Telford 1986), and the occurrence of historical earthquakes and numerous microseismic events in the Ottawa-Bonnechère graben and adjoining areas (Smith 1962, 1966; Basham *et al.* 1979; Adams and Basham 1989) demonstrates that some faults are currently active. Examples of significant historical earthquakes from within the Ottawa-Bonnechère graben are listed in Table 1. A major earthquake (1988; mN6.5) also occurred within the Saguenay graben near Chicoutimi (Du Berger *et al.* 1991). This historical and recent seismic activity

TABLE 1. Some significant historical earthquakes. (After Adams and Basham 1989 and references therein)

Latitude (deg.)	Longitude (deg.)	Location	Magnitude (mN)	Date
45.50N	73.60W	Montreal	5.8	Sept.16,1732
45.40N	75.40W	Ottawa	- *	July 12,1861
46.78N	79.06W	Timiskaming	6.2	Nov.1,1935
44.98N	74.90W	Cornwall-Massena	5.6	Sept.5,1944
46.66N	78.61W	Timiskaming	4.3	Aug.13,1982
45.20N	75.75W	North Gower (near Ottawa)	4.1	Oct.11,1983
45.11N	74.61W	Cornwall	3.3	July 1981

* intensity VII on the Modified Mercalli Intensity scale.

within the St. Lawrence rift system, and in particular in the Ottawa-Bonnechère graben, underscores the necessity of undertaking structural and tectonic studies in the region. Spatial analysis of earthquake distribution to identify correlations between recent seismicity, structural geology and geophysical anomalies is complementary to our knowledge of recent fault activation acquired from analysis of field data. Any correlation established between seismicity and geophysical anomalies, geology and other geoscientific parameters would provide additional constraints for future assesment of earthquake source zones, hazards and risks.

1.2 Location of Study Area

The Ottawa-Bonnechère graben forms a 55 km wide topographic low (the Ottawa River valley) which extends from near Montreal through Ottawa, then branches northwestward (Fig. 1). It is linked to the St. Lawrence rift system, which also includes the Saguenay graben in Québec (Kumarapeli and Saull 1966). In the Ottawa-Hull area, several generations of brittle faulting cut Cambrian to Ordovician carbonate and fine clastic sedimentary rocks of the St. Lawrence Platform (Fig. 2).

Field work was carried out at three (3) localities (Fig. 3), along the Ottawa-Carleton Transit Commission transitway

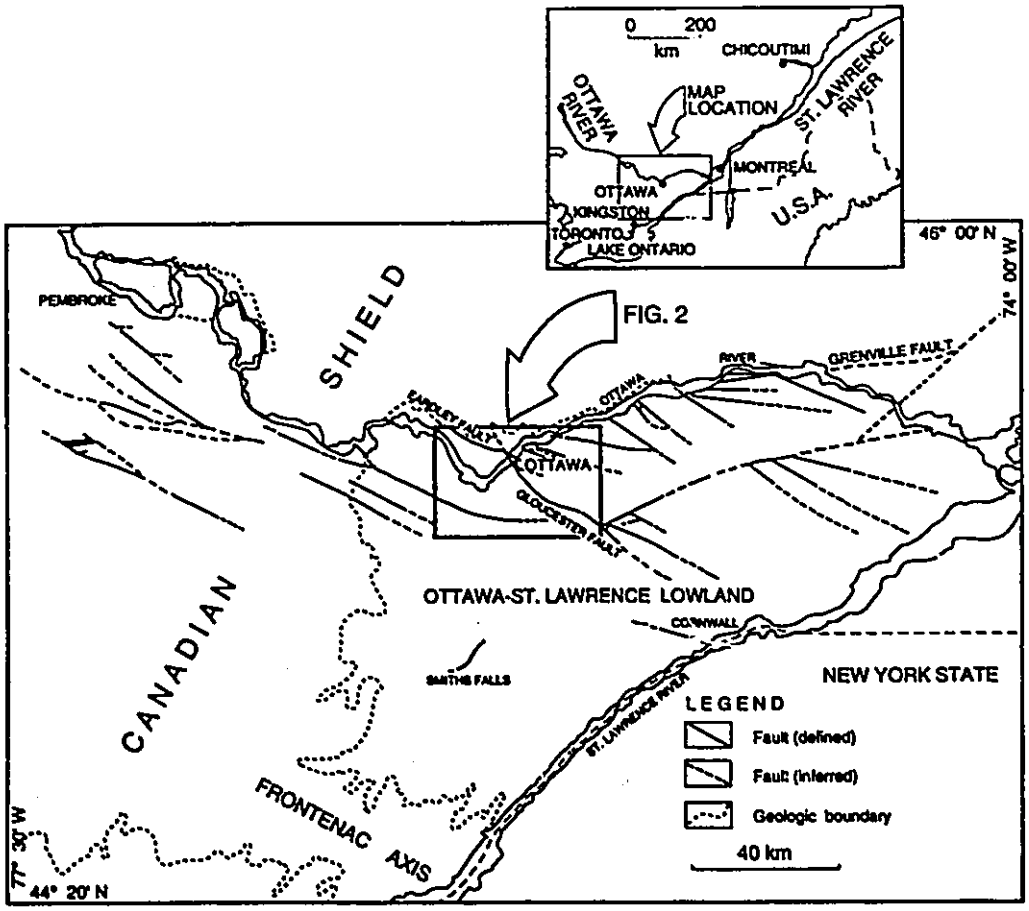

FIG. 1. Regional structures of the Ottawa-Bonnechère graben in the Ottawa-St. Lawrence Lowland and adjoining Canadian Shield. After Wilson (1946).

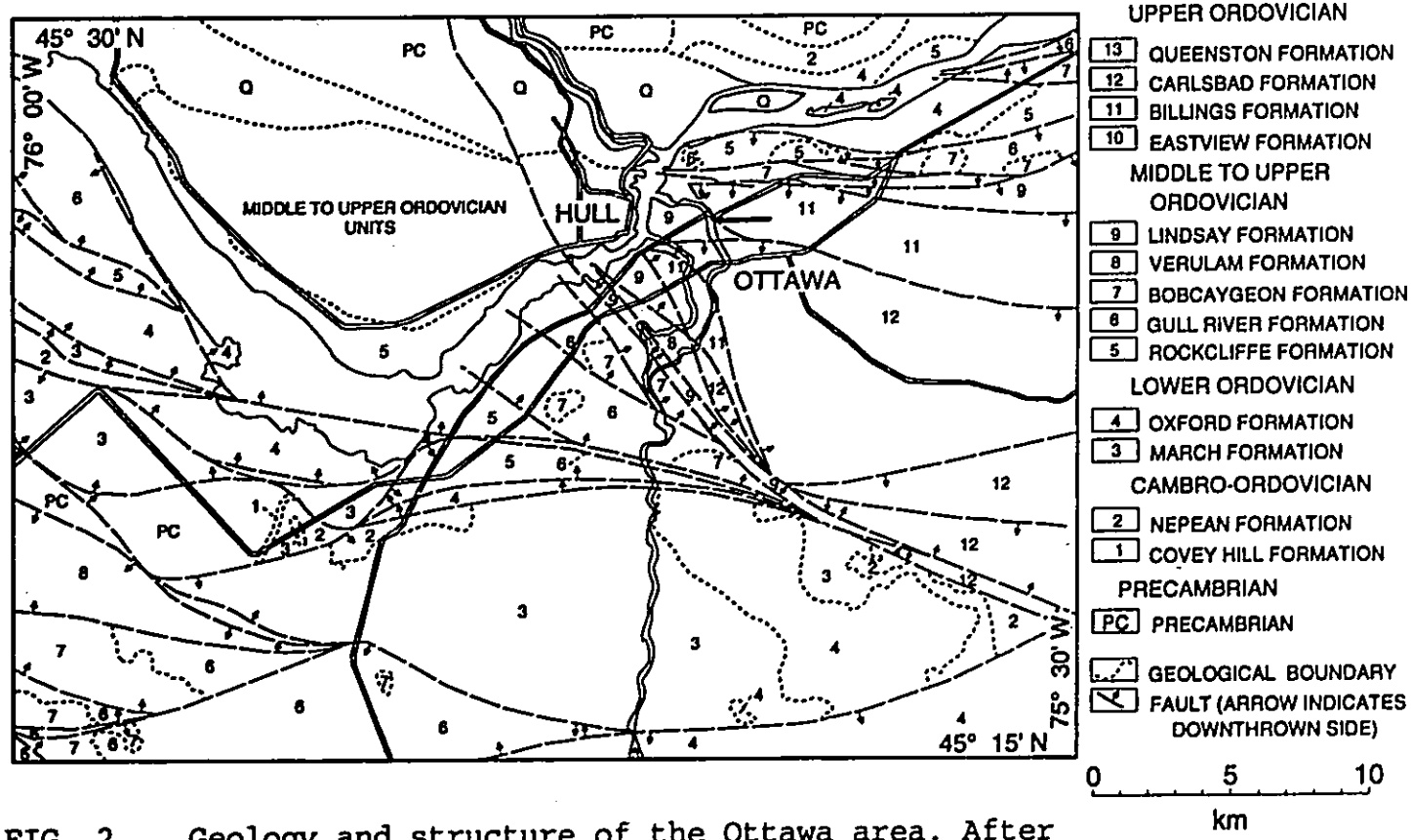

FIG. 2. Geology and structure of the Ottawa area. After Williams, D. A., Rae, A. M., and Wolf, R. R. (1984) and Wilson (1946).

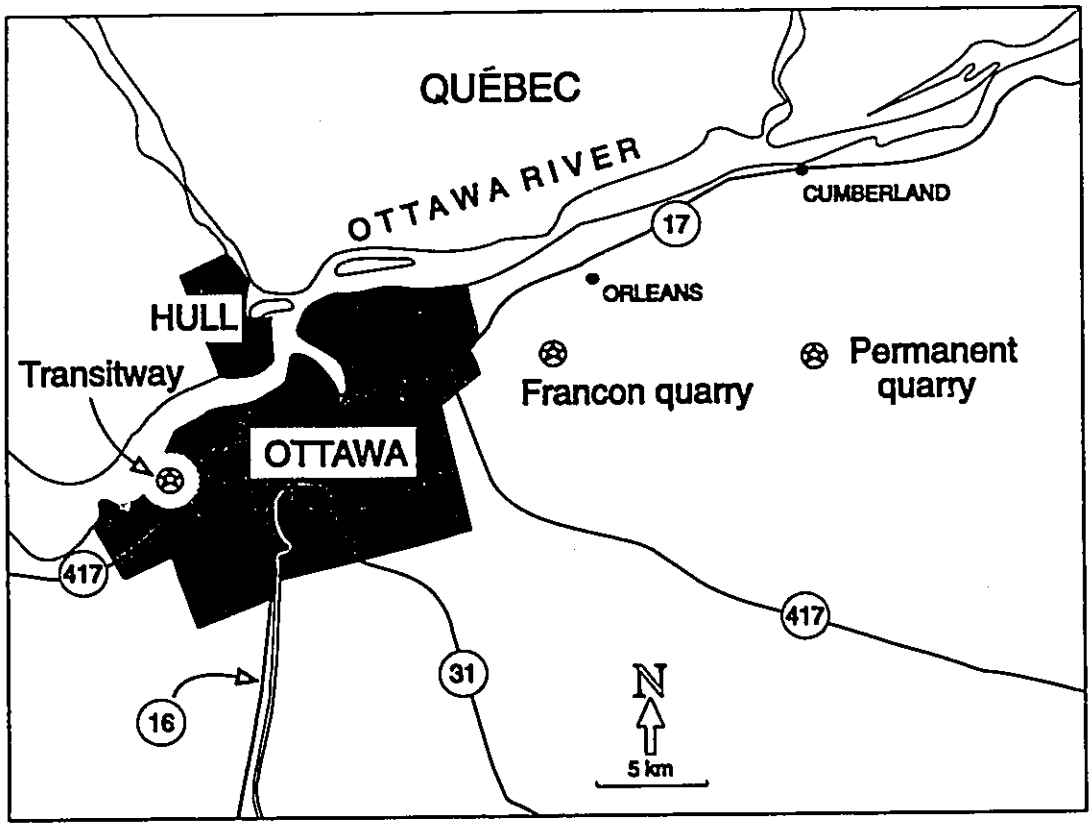

FIG. 3. Location of sites studied in more detail, namely: Ottawa-Carleton Transit Commission transitway (between Holland Avenue and Bayview Road); Francon Quarry (municipality of Gloucester), and; Permanent quarry (municipality of Navan).

(between Holland Avenue and Bayview Road in Ottawa), at the Francon quarry (municipality of Gloucester), and at the Permanent quarry (municipality of Navan). These three localities were chosen because of the presence of excellent, continuous outcrop which allows very detailed study and the collection of accurate orientation data. Geoscientific data used for spatial correlation with seismicity covers portions of the Ottawa-Bonnechère graben and the Grenville Province within 75°-77° West longitude and 45°-46° North latitude.

1.3 Previous Work

References to structural geology of the Ottawa Valley in existing literature are vague on the subject of the regional structural evolution. No defintive account on this point has been made partly because previous studies (Kay 1942; Wilson 1946; Hewitt 1964; Norris 1967; Lumbers 1976; Williams and Rae 1983; Williams and Telford 1987, 1986; Williams *et al.* 1992) do not specifically tackle the subject. Not much field data has been available to make determination of the relative ages of structures of the Ottawa-Bonnechère graben possible. Crucial evidence regarding stress orientations, based on surface geology, has been largely ignored for several decades. Kay (1942) documented some macrofaults and compiled joint trends within what he termed the Ottawa-Bonnechère graben. Using orientation data for both faults and joints to establish

the genetic relationship of these structures, he surmised that the "Early Tertiary" faults could be reactivated pre-Paleozoic joints rather than reactivated pre-Paleozoic faults. This interpretation was largely based on the similarity of the trends. Wilson (1946) described some major and lesser faults in the Ottawa-St. Lawrence Lowland but expressed uncertainty on the number and ages of faulting periods. The presence of different generations of structures and their possible reactivation has been discussed by later authors. Lumbers (1976) suggested intermittent reactivation of faults in the Ottawa-Bonnechère graben since its formation in late-Precambrian time. It has also been suggested that although many of the prominent features of the St. Lawrence rift system, that includes the Ottawa-Bonnechère graben, resulted largely from mid-Mesozoic reactivation of earlier tensional structures (Kumarapeli and Saull 1966; Kumarapeli 1976, 1978) resulting from tensional stresses related to the opening of the Atlantic Ocean, much of the fracture system was formed in the late Pre-cambrian (Philpotts 1978). Williams and Telford (1986) believed that the faults post-dating the Cambrian-Ordovician sedimentary sequence resulted from reactivation of pre-existing faults during the Mesozoic, but added that an earlier age is possible. Adams and Basham (1989) maintained that no significant reactivation occured during the Mesozoic and that the last significant extensional movement occurred during the Paleozoic.

Descriptions of structures, in particular, the relative displacement of beds along faults, from several outcrops in the Ottawa-Hull area were documented by Williams and Telford (1986, 1987). Norris (1967) related bedding- and fault-plane lineations measured from outcrops of the Queensway at Parkdale Avenue to folding and movement along the adjacent Gloucester fault (Fig. 2). Generalized descriptions of structures in quarries based mainly on the works of Williams and Telford (1986) were prepared by Derry *et al.* (1989) for the Ontario Ministry of Natural Resources. Maps depicting large-scale structures include the 1:63 360 scale Ottawa Sheet (Maps 414A and 413A) of the Department of Mines and Resources (1938) based on Wilson (1938a, 1938b); 1:50 000 scale Paleozoic geology of the Ottawa area of the Ontario Geological Survey (1984) based on Williams *et al.* (1984); 1: 125 000 scale Ottawa-Hull Sheet (Map 1508A) of the Geological Survey of Canada (1979) based on compilations by MacDonald (1967) and Harrison (1976); 1:253 440 scale Ottawa-Cornwall Sheet (Map 852A) of the Department of Mines and Resources (1946) based on Wilson (1929, 1935 to 1940); 1:1 340 833 scale Structural Map of the Ottawa-St. Lawrence Lowland of the Geological Survey of Canada (1976) based on Wilson (1946), and; 1: 1 000 000 scale Southern Ontario Sheet 30S (Map 1335A) of the Geological Survey of Canada based on the compilations by Sanford and Baer (1971).

Known ages of carbonatite dykes exposed in the study area are used to bracket the absolute ages of associated faulting and paleostress orientations. Carbonatite dykes are exposed at both the Francon and the Permanent quarries. Those at the Francon quarry were the subject of study by Hogarth *et al.* (1988), who obtained ages of about 115.2 ± 7.2 Ma. and 103.1 ± 7.0 based on fission-track dating. These ages are much younger than those obtained by Shafiqullah (1971) based on K-Ar dating of possibly contaminated samples. The ages obtained by Hogarth *et al.* (1988) are supported by similarity in composition of the dykes at Francon quarry (Hon 1970; Bolton and Liberty 1972; Hogarth *et al.* 1988) with those of the Monteregian Hills in Québec, and by paleomagnetic study of the carbonatite dykes indicating a pole coincident with that of the Oka carbonatite complex of the Monteregian Hills (Bolton and Liberty 1972). Samples from the Monteregian Hills have ages of about 118 Ma (Rb-Sr and fission-track dating, Eby 1984). The emplacement of these alkaline rocks at the eastward extension of the Ottawa-Ottawa-Bonnechère graben are also believed to be graben-controlled, and believed to represent a reactivation of the older late-Precambrian rift (Sykes 1978).

Very few studies dealing with the analysis of distribution of epicentres in the study area have been done previously. The spatial association between earthquake epicentres and geological, drainage lineament and magnetic

anomaly maps were investigated by Goodacre *et al.* 1993 using a statistical method implemented on a PC-based Geographic Information System called SPANS (Spatial Analysis Systems) for an area in west Québec that overlaps the eastern half of this work's study area. The method (weights of evidence method) used in this study is also discussed in their paper. Examples of applications, including the analysis of seismic epicentre distribution and assessment of gold potential in eastern Nova Scotia and northeastern New Brunswick, were also described by Bonham-Carter (1991). The principles of this approach and more detailed discussions of applications are also found in the works of Bonham-Carter (In Press) and in recent works relating to the prediction of mineral occurrence (Agterberg *et al.* 1990; Bonham-Carter and Agterberg 1990; Bonham-Carter *et al.* 1990; Bonham-Carter *et al.* 1988; Wright 1988; Watson *et al.* 1989; Watson and Rencz 1989). Through visual inspection, Forsyth (1981) suggested possible correlation between seismicity and drainage lineaments, geology, magnetic and gravity anomaly in and near the western Québec seismic zone (43° to 48° North and 72° to 80° West). Forsyth (1981) proposed a correlation between seismicity and the eastern shear zone boundary of the Central Metasedimentary Belt, and the belt itself.

1.4 Objectives

This work is composed of two main parts. The first part represents the first detailed study of the structural geology in the Ottawa-Hull area. The principal goals are to document families of Phanerozoic faults and their relative ages and movement histories, to demonstrate the evolution in the orientation of the paleostress field in the study area based on the kinematic analysis of faults and fault surface features, and to bracket the absolute ages of faulting and of paleostress orientations by known ages of associated or cross-cutting magmatic rocks, thereby establishing the relationships between periods of faulting and periods in the tectonic evolution of eastern North America. Knowledge of the history of faulting and of the evolution of the paleostress orientations should aid in the rigorous assessment of seismic hazard in this earthquake-source and earthquake-prone region. A better knowledge of the structural geology in the area should also lead to more accurate stratigraphic correlations, and therefore to a clearer understanding of the local geological history.

The second part of the study aims to determine spatial association between seismicity and larger-scale structures, that either belong to the families of faults identified from key outcrops in the Ottawa-Hull area or are older but similar in orientation to the Phanerozoic faults. This was accomplished using SPANS (Spatial Analysis Systems), a PC-

based Geographic Information System. Although earthquakes in eastern North America are relatively infrequent, seismic risk and hazard may be great because of the large affected areas and high population density (Slemmons and dePolo 1986). Delineation of possible earthquake generators and determination of structures, among lineaments delineated from gravity and magnetic maps, geological maps, LANDSAT and Radar imageries and topographic maps, which are most spatially associated with seismicity is thus warranted. To provide additional constraints in future assessment of earthquake source zones, hazard and risk within the study area, the possible correlation of seismicity with gravity anomalies, magnetic anomalies and other geological features will also be tested. This study also aims to generate a predictive map showing areas with elevated probabilities of earthquake occurrence per unit area over a given period by combining several maps using the overlay function of SPANS and the weights of evidence model.

2. GEOLOGY AND TECTONIC SETTING

The Ottawa-Bonnechère graben is bounded by nearly vertical faults trending along an east-west to west-northwest direction (Fig. 1). The graben has long been recognized as a rift valley system based on geomorphological, topographical, and structural evidence (Kumarapeli and Saull 1966; Kumarapeli 1978, 1985), and on the association of intrusive rocks of alkaline affinity (Philpotts 1978). The association of major faults bounding and within the graben, along with the presence of alkaline igneous rocks, is typical of well-documented continental rift zones such as the Rhine graben and the East African rift system (Kumarapeli 1978; Illies 1981).

The geology of the Ottawa Valley consists of Paleozoic sedimentary rocks of the Ottawa-St. Lawrence Lowland, and inliers and uplifted blocks of Precambrian (Grenvillian) basement consisting of highly deformed metasedimentary and metavolcanic rocks intruded by felsic to mafic plutons (Hewitt 1964; Williams *et al.* 1992). A major unconformity separates the Precambrian basement and the overlying Paleozoic sedimentary package (Williams *et al.* 1992). The present stratigraphic nomenclature for the Ottawa region evolved through adaptation and modification (Williams and Rae 1983; Williams and Telford 1986; Williams *et al.* 1992) of Wilson's (1946) and Liberty's (1964; 1967) nomenclature. Stratigraphy

is presented in Table 2. Formations are composed of coarse to fine clastics and pure and impure carbonates that are commonly interbedded with fine clastics. Environments of deposition consist of both terrestrial and shallow marine with the coarse clastics representing alluvial fan-braided fluvial (Wolf and Dalrymple 1984) and coastal dune facies, and the carbonates and fine clastics representing intertidal to subtidal, and supratidal to subtidal intracontinental shelf environments (Wilson 1946; Williams and Telford 1986; Williams *et al.* 1992; Steele-Petrovich 1986).

In the Ottawa-Hull area, the Paleozoic rocks consist mainly of a sequence of Middle to Upper Ordovician limestones with interbeds of dolostone, shale, and quartz sandstone belonging to formations of the Ottawa Group (Uyeno 1974). These formations include the Shadow Lake, Gull River, Bobcaygeon, Verulam and Lindsay (Williams and Rae, 1983; Table 2; Fig. 2). In many cases, lithologic boundaries correspond to mapped faults.

Rocks that underlie the Ottawa-St. Lawrence Lowland and exposed within the area included in the analysis of epicentre distribution, belong to the Central Metasedimentary Belt (CMB) Subprovince of the Grenville Province. It was accreted adjacent to neighbouring terranes during the Grenville and possibly earlier orogenies (Cullota *et al.* 1990). The

TABLE 2. Stratigraphy and lithological composition of formations in the Ottawa region. (From Williams and Telford 1986, Williams et al. 1992 and references therein)

PERIOD	STRATIGRAPHY			LITHOLOGY
	GROUP	FORMATION	MEMBER	
ORDOVICIAN		QUEENSTON		Interbedded siltstone and shale.
		CARLSBAD		Interbedded shale, calcareous siltstone, and silty limestone.
		BILLINGS		Shale with laminae of finely crystalline dark grey limestone in the lower part and calcareous siltstone interbeds up to 2 cm thick in the upper part.
	OTTAWA	LINDSAY	UPPER	Limestone with shale interbeds; shale interbeds greater than 5 cm restricted to the upper member.
			LOWER	
		VERULAM		Limestone with shale interbeds.
		BOBCAYGEON	UPPER	Limestone with planar to undulating shaly partings; subdivision into lower, middle, and upper members based on higher shale content of middle member.
			MIDDLE	
			LOWER	
		GULL RIVER	UPPER	Upper member consists of limestone with shaly partings; lower member composed of interbedded limestone, silty dolostone, quartz sandstone, and shale.
			LOWER	
		SHADOW LAKE		Silty to sandy dolostone , with shaly partings and thin interbeds of quartz sandstone.
		ROCKCLIFFE	UPPER	Quartz sandstone , shale and limestone and silty dolostone interbeds; lower member consists of interbedded quartz sandstone and shale only.
			LOWER	
	BEEKMANTOWN	OXFORD		Dolostcne with subordinate shaly and sandy interbeds.
		MARCH		Quartz sandstone, dolomitic quartz sandstone, sandy dolostone, and dolostone.
	POTSDAM	NEPEAN		Interbedded quartz sandstone and conglomerate.
CAMBRIAN		COVEY HILL		Interbedded, non-calcareous, feldspathic conglomerate and sandstone.

supracrustal rocks and plutonic suites comprising the CMB were deposited and emplaced during the Grenvillian orogenic cycle (ca. 1.3 to 1.0 Ga, Moore and Thompson 1980). Following previous subdivision of the belt into smaller units (Brock and Moore 1983; Moore 1982; Wynne-Edwards 1972) the belt was divided from west to east into the Bancroft, Elzevier and Frontenac terranes (Davidson 1986; Corriveau 1990) based on lithological, structural and metamorphic grade differences. Flanking the CMB to the northwest and to the east are the Ontario Gneiss Belt and Central Granulite terrane, respectively (Fig. 4). The CMB is transected mainly by northeast- and east-trending to northeast-trending ductile and brittle faults displaying dip variation across the study, and reflecting terrane transitions from west to east. From the west, shallow-dipping layering and west-vergent thrust sheets become steeply-dipping to vertical until steep northwest-dips are attained further to the east (Beardsley and Cable 1983; Davidson 1986; Hanmer 1988; Wiener *et al.* 1984). Within the Frontenac terrane, steep, southeast dips in the northwest become vertical along the St. Lawrence river and give way to gentler but northwest-dipping structures in New York State (Davidson 1986).

The oldest structures that cut the basement rocks of the Grenville Province were the result of accretion of terranes during the Grenvillian orogeny (ca. 1.3-1.0 Ga; van Breemen

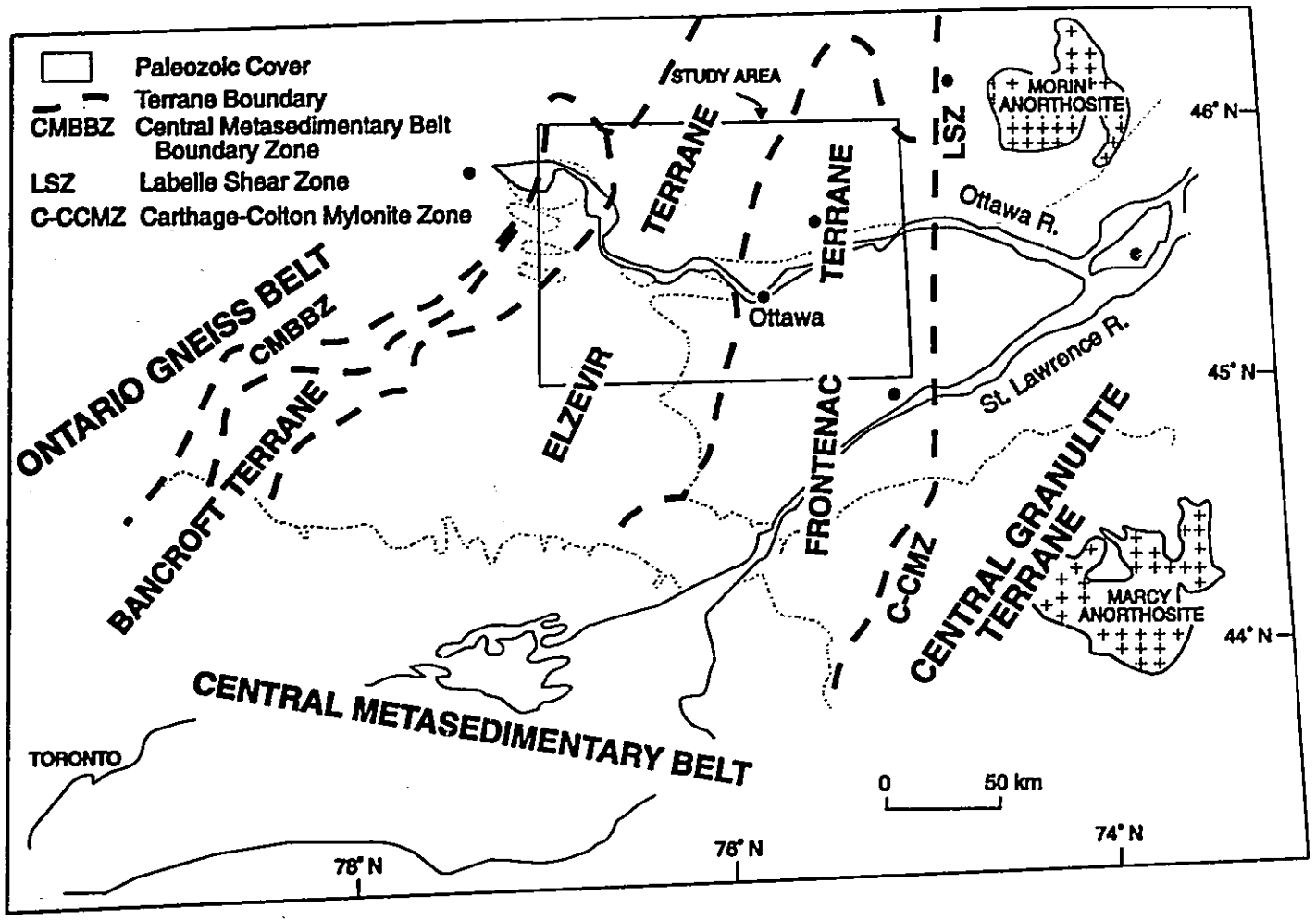

FIG. 4. Major lithotectonic units of the Central Metasedimentary Belt and adjoining areas. After Corriveau (1990). Eastern Canadian Telemetered Network (ECTN) stations (•) within and near the study area are also shown.

and Davidson 1988). This is illustrated by one tectonic evolution model (Fig. 5; Cullota *et al.* 1990) suggesting a series of collisions between terranes. The Grenville Front Tectonic Zone (GFTZ) marks the site of collision along an east-dipping subduction zone between the Ontario Gneiss BElt and the North American Craton. Collision between the Central Granulite Terrane (CGT) and the CMB is marked by the west-dipping Coshocton Zone and Carthage-Colton Mylonite Zone (or Labelle shear Zone for the north). The Central Metasedimentary Belt Boundary Zone is believed to mark the site along which the CMB has been thrust onto the west around 1060 Ma (syntectonic pegmatites, van Breemen and Hanmer 1986)

The Ottawa-Bonnechère graben has been interpreted as a failed arm of a triple junction (Burke and Dewey 1973; Kumarapeli 1976, 1978, 1985; Rankin 1976) along the St. Lawrence rift system, formed during the Hadrynian (late Precambrian) to early Paleozoic event that led to the formation of the Iapetus (Kumarapeli 1978, 1985). Hadrynian to Cambrian age arenites (Hofmann 1972) filling early graben structures in the Montreal area and further to the east (Kumarapeli 1976; 1985) provide geological evidence of a rifting episode dating back to late Precambrian to early Paleozoic time. Magmatic activity associated with this period of extensional tectonics is represented by diabase dykes dated at approximately 700 million years (paleomagnetic pole

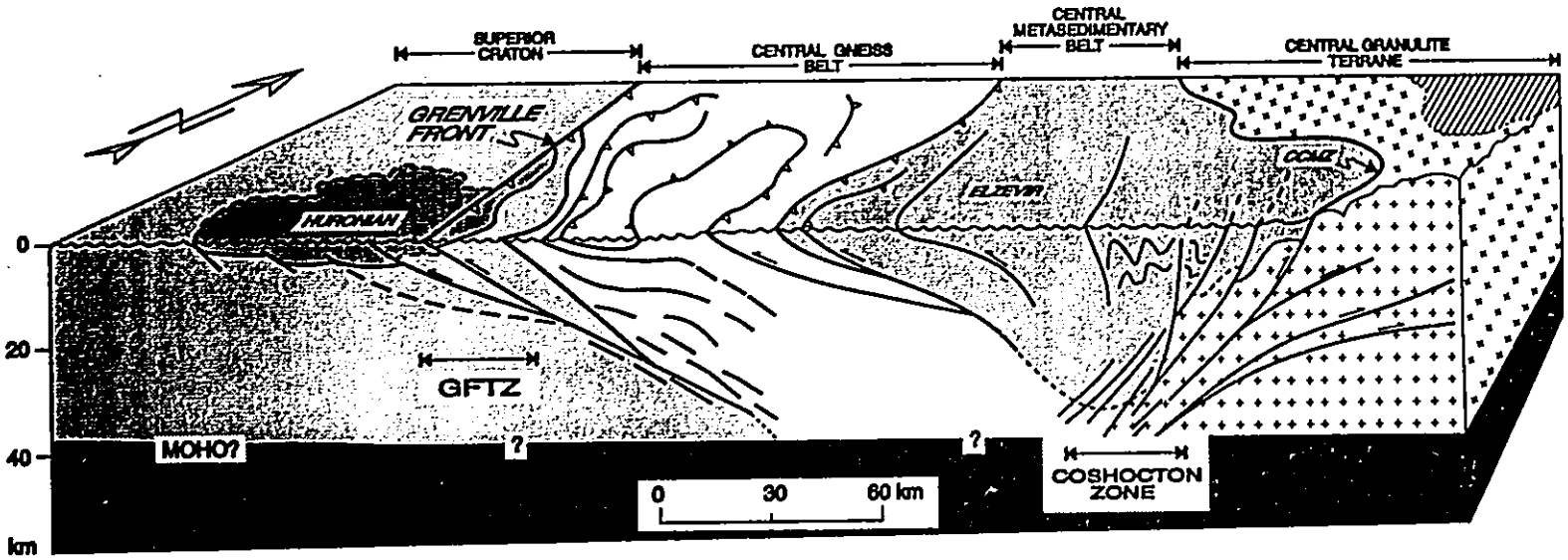

FIG. 5. Generalized diagram of the structural framework across the Grenville province illustrating the transition from southeast-dipping structures, near the western boundary of the Central Metasedimentary Belt, through near vertical and northwest-dipping structures towards the eastern boundary of the belt. After Cullota *et al.* (1990) and references therein.

determination; Murthy 1971), which intruded Grenvillian basement rocks along the north side of the Ottawa-Bonnechère graben, and by alkalic and carbonatite complexes which intruded the graben floor at Lake Nipissing (Doig 1970; Kumarapeli 1985) about 565 Ma ago (K-Ar dating by Gittins *et al* 1967). The bimodal character of alkalic or transitional Tibbit Hill volcanic rocks in southern Québec may represent late Hadrynian to early Cambrian volcanism (based on stratigraphic relations; Pintson *et al*. 1985) associated with this period of extensional tectonics (Rankin 1976; Kumarapeli 1985; Pintson *et al*. 1985).

Closure of the Iapetus ocean during the Ordovician resulted in the Taconian orogeny, and collision of Atlantic Canada with northwestern Africa in the Early Devonian gave rise to the Acadian orogeny which is obviously the main diastrophic event with which final closure of the Iapetus Ocean is related (Dewey 1969; Schenck 1971; McKerrow and Cocks 1977; Keppie 1977a, 1977b). Compression during this ocean-closing episode most likely generated structures, in the Paleozoic cover, some of which are probably early graben structures that underwent reactivation and propagation into the overlying sediments.

The Atlantic Ocean opened along a line close to the position of the Iapetus (Miyashiro *et al*. 1982). The Central

Atlantic opened in the early Jurassic (Miyashiro *et al.* 1982) or in late Triassic time, concurrent with the break-up of North America and Africa (Dewey and Bird 1984). Opening of the north Atlantic in the early Cretaceous or early Jurassic (US Geodynamics Committee 1989) followed. An episode of Mesozoic crustal extension in the Ottawa-Hull area is supported by the presence of carbonatite dykes (Hon 1970; Bolton and Liberty 1972; Hogarth *et al.* 1988) with ages of about 115.2 ± 7.2 Ma. and 103.1 ± 7.0 (fission-track dating by Hogarth *et al.* 1988), and by the alkaline Monteregian intrusions that were emplaced at about 118 Ma (Rb-Sr and fission-track dating of apatite and sphene; Eby 1984) along a west to west-northwest lineament at the eastward extension of the Ottawa-Bonnechère graben. The emplacement of these alkaline rocks was graben-controlled, and represents a reactivation of the older late-Precambrian rift (Sykes 1978).

Following Mesozoic extension, another episode of compression began and is still operative at the present time. Inferences made on the orientation of the current stress field in eastern North America indicate an east-northeast to northeast direction of the greatest horizontal principal stress (Sbar and Sykes 1973, 1977; Yang and Aggarwal 1981; Hasegawa *et al.* 1985; McKay 1986; Adams and Basham 1989; Zoback 1992).

3. METHODOLOGY

3.1 Field Method

Field-based structural analysis consisted largely of documenting outcrop-scale faults and their associated mesoscale structures. All observed faults are essentially brittle, and the kinematics of faulting and of bedding-plane slip can be determined using structural criteria which are documented in the literature. Displacement trajectories were determined from orientations of friction-related slickenlines (Fleuty 1975) and of fibrous calcite growths (Durney and Ramsay 1973; Means 1987; Twiss 1992) on fault surfaces and on bedding planes. Where possible, offset of marker beds, dykes or earlier fractures was used to determine sense of displacement. In other cases, the sense of displacement was determined using steps on fault surfaces (e.g. congruous accretion steps, Petit 1987 and Norris and Barron 1969; PT type of Petit [1987] or congruous synthetic fracture steps of Norris and Barron [1969]; congruous pluck fracture steps of Norris and Barron [1969]) which are often filled with fibrous calcite, or using fault-associated features such as en-echelon gashes (Twiss 1992; Groshong 1988), riedel shears (Groshong 1988; Hancock 1985) and drag folding.

Several families of faults were recognized based on

similarity of fault-plane orientations and kinematics, and where possible, relative ages of the different families were established by cross-cutting and offset relationships. Since the relative ages of families of faults could not always be clearly established by field observations, faults were inferred to have the same relative age as other faults and structures with which their orientations and kinematics are congruent (Fig. 6). Absolute ages of families were bracketed using published ages for associated or cross-cutting igneous dykes. In this way, families of faults were assigned to three sets representing three distinct periods of faulting, referred to herein as D_1, D_2, and D_3. This is depicted in Table 3, where the criteria used to determine the kinematics and age relationships for each family of faults are also summarized. Some faults can be part of two or three periods of movement as indicated by the presence of different sets of lineations recognized on the same fault surface. Lineations preserved on wall rock (slickenlines; Fleuty 1975) were interpreted as recording earlier movements than lineations defined by fibrous calcite coating the fault surface. The results of the detailed field study will be presented and illustrated by line drawings and photographs of key structural features.

There are many methods for determining paleostress orientations based on fault-slip data. The method of Etchecopar *et al.* (1981) is applicable to polyphase data and

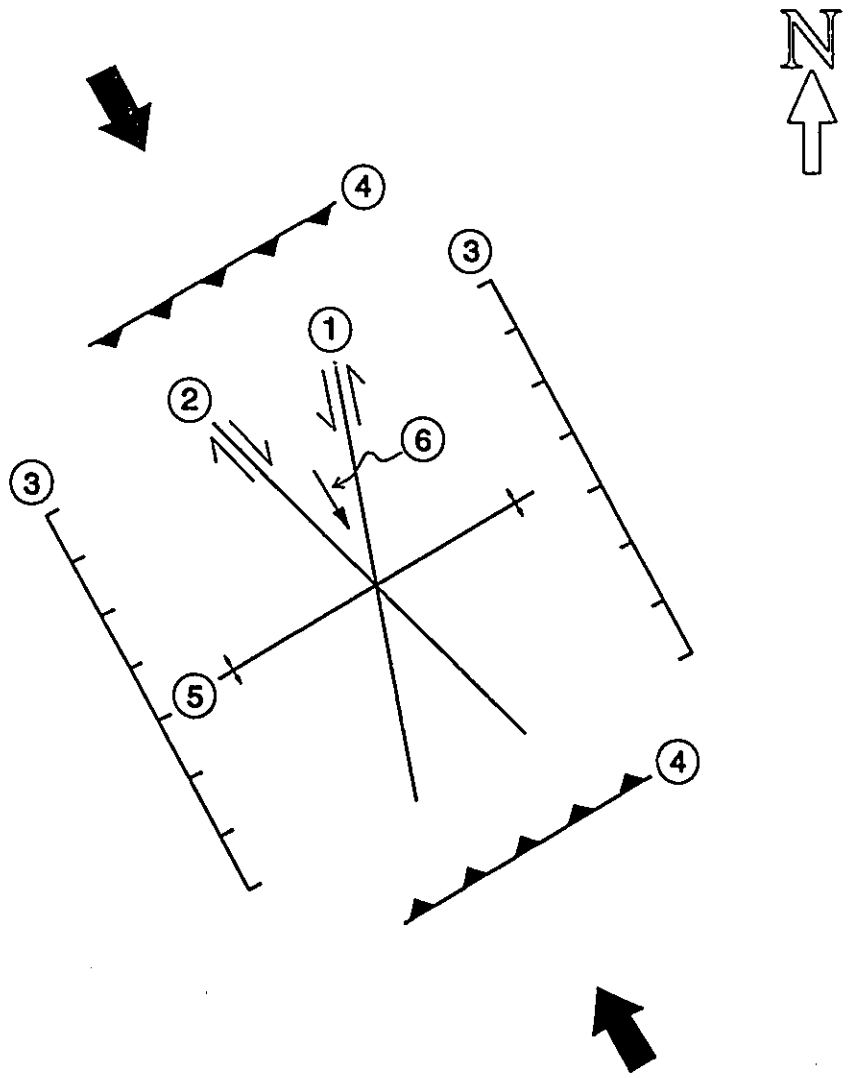

FIG. 6. Diagram of kinematically congruent families of structures that include north-northwest-trending sinistral strike-slip fault (1), northwest-trending dextral strike-slip fault (2), northwest-trending normal faults (3), northeast-trending thrust faults (4) and folds (5), and northwest-trending bedding plane lineations (6), for a region undergoing compression along the northwest-southeast direction.

TABLE 3. Criteria for classifying faults and fault movements within the Ottawa-Hull area into families and determining their kinematics.

Period of faulting	Families of faults	Criteria
D_1	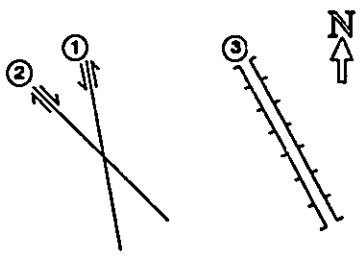	1 North-northwest-trending dextral strike-slip faults; lineations and steps; orientation and kinematics consistent with northwest-trending bedding plane lineations. 2 Northwest-trending dextral strike-slip faults; lineations and steps; orientation and kinematics consistent with orientation of northwest-trending bedding plane lineations. 3 Northwest-trending normal faults; lineations and steps; drag; displacement of beds; offset by slip along bedding plane with northeast- trending lineations; rotated by northwest folds.
D_2	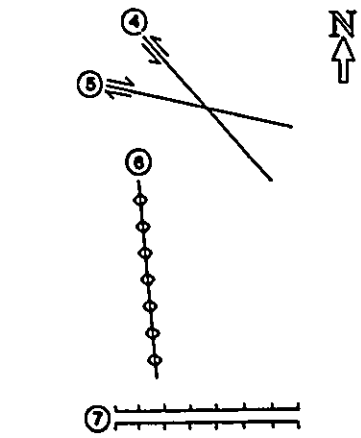	4 Northwest-trending sinistral strike-slip faults; lineations and steps; orientation and kinematics consistent with east-west- to west-northwest-trending bedding plane lineation. 5 East-west- to west-northwest-trending dextral strike-slip faults; lineations and steps; displacement of beds; orientation and kinematics consistent with east-west- to west-northwest-trending bedding plane lineations. 6 South-southeast– to south-trending thrust faults; lineations and steps; displacement of beds; orientation and kinematics consistent with east-west to west-northwest-trending bedding plane lineations. 7 West-northwest- to west-southwest-trending normal faults; lineations and steps; drag; displacement of beds; offsets beds with northwest lineations; offset by D_3 thrust fault.
D_3	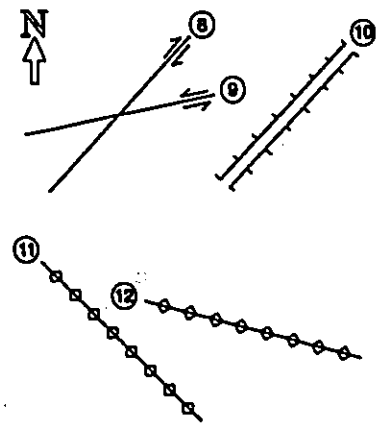	8 Northeast-trending dextral strike-slip faults; lineations and steps; orientation and kinematics consistent with D_3 northeast-trending bedding plane lineations. 9 East-southeast- to northeast-trending sinistral strike-slip faults; lineations and steps; orientation and kinematics consistent with D_3 northeast-trending bedding-plane lineations. 10 Northeast-trending normal faults; lineations and steps; displacement of beds. 11 North- to north-northwest-trending thrust faults; lineations and steps. 12 East-west- to northwest-trending thrust faults; lineations and steps; offsets D_2 east-west-trending normal faults and D_1 northwest-trending normal faults.

is based on the minimization of the angular deviation between observed and computed lineations. This is an iterative method that segregates the data into subsets and enables these to be assigned to distinct stress orientations associated with corresponding tectonic phases. A computer program based on this approach, written by Laborde *et al.* (no date) and kindly provided by them, was used to compute the characteristics of the paleostress tensor associated with the periods of faulting established using the above criteria.

3.2 Measuring Spatial Association and the Weights of Evidence Method

Spatial association among seismicity, lineaments and other geoscientific data was carried out using a PC-based Geographic Information System and the weights of evidence model. The weights of evidence method employs conditional probabilities and Bayes' Rule to determine spatial correlation between map patterns and epicenters. Weights are assigned to indicator maps in order to generate maps that predict seismicity. The principles of this method were discussed by Bonham-Carter (In Press) and in recent works relating to the prediction of mineral occurrence in Nova Scotia (Agterberg *et al.* 1990; Bonham-Carter and Agterberg 1990; Bonham-Carter *et al.* 1990; Bonham-Carter *et al.* 1988; Wright 1988) and New Brunswick (Watson *et al.* 1989; Watson and Rencz 1989) and of

earthquake occurrence in western Québec (Goodacre *et al.* 1993). The following discussion on the principles of the model used for this study and the steps involved in calculating weights of evidence and related statistical parameters (see Appendix A) are based mainly on these works.

Given two (2) overlapping binary patterns, B and D (Fig. 7), the idea of probabilities and odds could be applied to ascertain spatial relationship between them. The area proportions for each of the four (4) overlap conditions are treated as estimates of probabilities. Thus the probability of B and D ($P\{B \cap D\}$), B and not D ($P\{B \cap \bar{D}\}$), not B and D ($P\{\bar{B} \cap D\}$), and not B and not D ($P\{\bar{B} \cap \bar{D}\}$) occurring together are estimated as II/(I+II+III+IV), I/(I+II+III+IV), III/(I+II+III+IV) and IV/(I+II+III+IV), respectively. For pattern B, the unconditional probability of occurrence in the study region is expressed as $P\{B\} = (I+II)/(I+II+III+IV)$ and that for pattern D, as $P\{D\} = (II+III)/(I+II+III+IV)$.

Probability of occurrence might also be expressed in terms of conditional probability. For example, the conditional probability of pattern B occurring given the presence of D is expressed as $P\{B|D\}$ and is defined as $P\{B \cap D\}/P\{D\}$. In terms of area proportions, this expression may be written as $[II/(I+II+III+IV)]/[(II+III)/(I+II+III+IV)]$ or directly in terms of areas as $II/(II+III)$. Since probability is related to

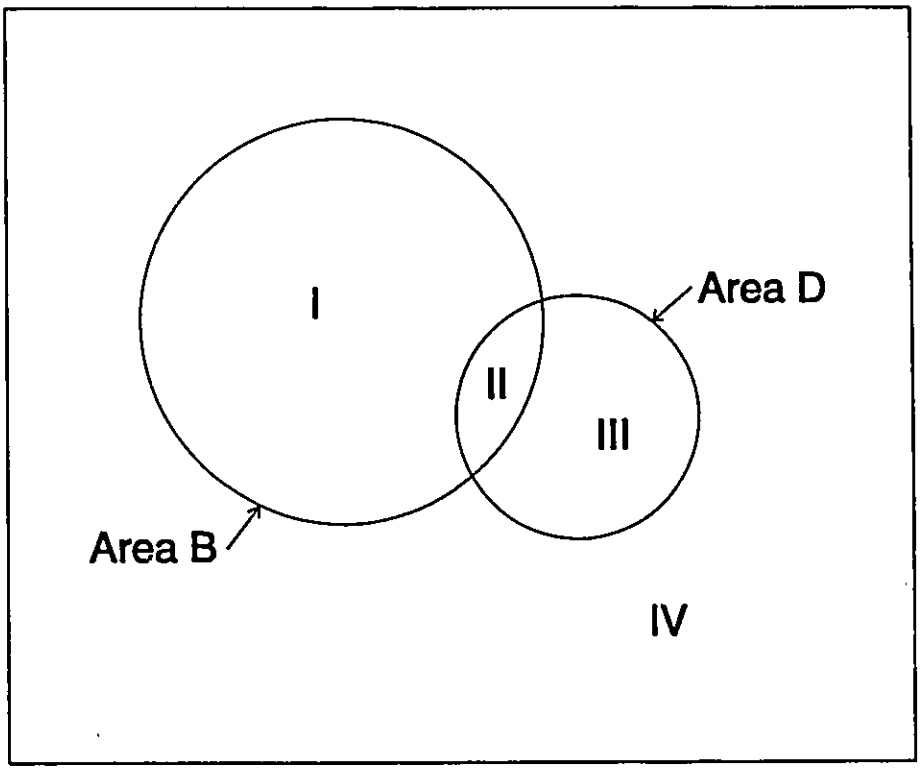

B = Presence of Pattern B
$\bar{B}$ = Absence of Pattern B
D = Presence of Pattern D
$\bar{D}$ = Absence of Pattern D

I = Area ($B \cap \bar{D}$)
II = Area ($B \cap D$)
III = Area ($\bar{B} \cap D$)
IV = Area ($\bar{B} \cap \bar{D}$)

FIG. 7. Venn diagram to illustrate the spatial overlap relationships between two binary map patterns, B and D.

odds according to the expression $O = P/(1-P)$, conditional probability may also be written as conditional odds. Thus, the conditional odds of B occurring given that D also occurs, $O(B|D)$, is written as:

$$O(B|D) = [P(B|D)]/[1-P(B|D)]$$

Since $1-P\{B|D\} = P\{\bar{B}|D\}$, it follows that

$$O(B|D) = [P(B|D)]/[P(\bar{B}|D)],$$

In terms of area proportions, O(B|D) is equal to:

$$\frac{\{[II/(I+II+III+IV)]/[(II+III)/(I+II+III+IV)]\}}{\{[III/(I+II+III+IV)]/[(II+III)/(I+II+III+IV)]\}}$$

which simplifies to the ratio of areas:

$$O(B|D) = II/III$$

A similar expression may be written for the conditional odds of B given the absence of D, using the same reasoning. Thus $O(B|\bar{D})$ is written as:

$$O(B|\bar{D}) = [P(B|\bar{D})]/[P(\bar{B}|\bar{D})],$$

which can be determined from the ratio of areas I/IV.

The same principles of determining probabilities and odds

could be applied given a binary map pattern and a set of points (e.g. epicentres) by assuming that each point occupies a small unit of area. Overlap conditions for a binary map pattern and a set of points are shown in Fig. 8. Once a unit of area is assigned for each point, computation of probabilities and odds in terms of area proportions and areas may be done as if we are dealing with two (2) binary map patterns.

The two conditional odds [$O(B|D)$ and $O(B|\tilde{D})$] expressions may be combined in various ways to provide a symmetrical measure of association between two binary map patterns. The simplest measure is the **odds ratio** O_R, defined as

$O_R = O(B|D)/O(B|\tilde{D})$ which in terms of area computation equals **(II.IV)/(I.III)**

The numerator is a measure of agreement between the patterns, and the denominator is a measure of disagreement. The odds ratio always takes a positive value. As illustrated in Fig. 8, odds ratio values greater than 1 indicate patterns that are positively associated, those with values equal to 1 indicate two patterns that are independent and patterns with values less than 1 are negatively associated. The natural logarithm of the odds ratio provides another useful and closely-related index of association called the **contrast**, C_W. The contrast is

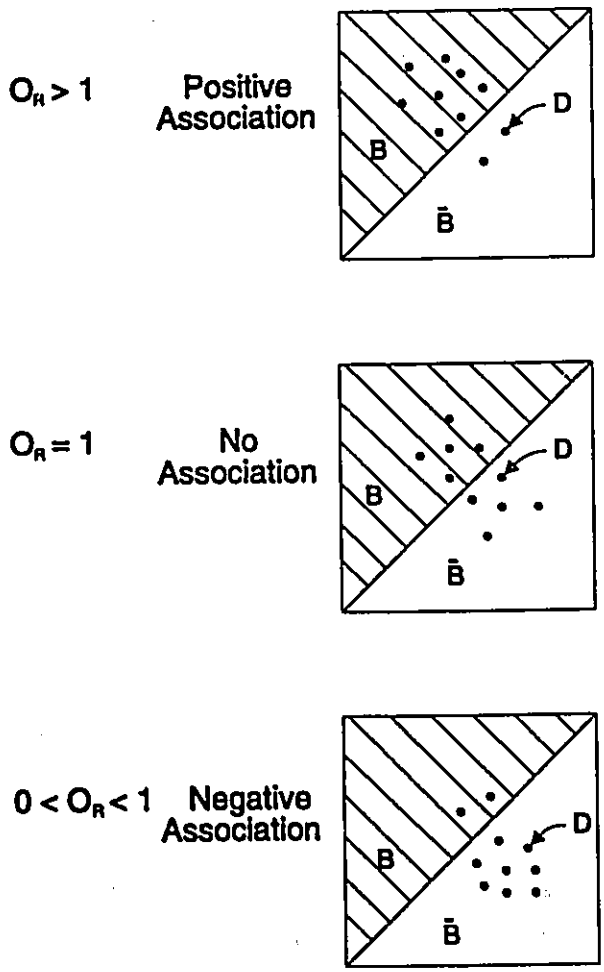

FIG. 8. Diagram to illustrate overlap relationship between a binary map pattern and a set of points. Calculation of odds ratio and contrast, C, is also shown.

0 when the patterns overlap only by the expected amount due to chance, is positive for positive associations and negative for negative associations (Fig. 8).

Another measure of association is designated by α and is equivalent to the difference of the square roots of the conditional odds, divided by their sum. It was originally proposed by Yule, as quoted by Fleiss (1981), and can be expressed by

$$\alpha = \{[O(B|D)]^{1/2}-[O(B|\bar{D})]^{1/2}\}/\{[O(B|D)]^{1/2}+[O(B|\bar{D})]^{1/2}\}$$
$$= \{[(II/III)]^{1/2}-[(I/IV)]^{1/2}\}/\{[(II/III)]^{1/2}+[(I/IV)]^{1/2}\}$$

α ranges in value between -1 and +1 like a correlation coefficient, with -1 signifying perfect negative correlation, +1 indicating perfect positive correlation and 0 implying independence of the two patterns.

Any of these measures of association between binary patterns can be applied, although Yule's α is probably the easiest to explain, because its range is like a correlation coefficient. However, the advantage of using the contrast is that it is easily linked to the weights (W^+, W^-), discussed in Appendix A, for combining binary maps.

The principles and methods of measuring spatial

association between binary patterns (or between points and a binary map pattern) can also be applied when dealing with points and multi-class maps such as geological maps and contour maps (map of continuous variable) such as geophysical maps. The determination of spatial association between a set of points and geological maps is carried out by treating one (1) or more units as one (1) class of a binary map while the remaining units are lumped together to form the second class. One (1) class of a geophysical map is likewise isolated and the remaining classes are lumped to form two (2) classes of a binary map. One alternative is to group successive classes such that spatial association is determined between cumulative areas and points. Contrast at successive cumulative intervals may then be compared. Binary predictor maps of point occurrences may be combined to produce a composite map showing probabilities of occurrence. To generate the best binary predictor of point occurrences, a contour map is reclassified into a binary map using a cut-off class that maximizes the spatial association (between the resulting binary map pattern and the point pattern).

When superimposing map layers to produce a composite predictive map, the calculation of final probabilities involves the determination of the contribution of each map unit in altering initial probability or prior probability. It is an expression of the proportion of the area occupied by

epicentres representing the point area to the total area of the study area. Its value is estimated using the following equation:

$$P(D) = D/T$$

where **D = number of unit cells containing an epicentre, equal to the number of epicentres if unit cell area (u) is small enough**

T = total number of unit cells in the study area

The prior probability of epicentre occurrence is modified using the weights of evidence method, to produce a posterior probability that depends on the presence or absence of indicator patterns. The weights of evidence method takes into account the influence of each map layer (indicator pattern) used as evidence and allows the calculation of final probabilities (or posterior probabilities) as a map. This method is presented in Appendix A.

Data used include the following: 1) seismological data (epicentre, depth and magnitude) for the study area (75° to 77° West and 45° to 46° North) recorded from 1983 to 1993 in table format); 2) total magnetic field data for the area bounded by 75° to 77° West and 45° to 46° North in raster format and pixel resolution of 200 x 200 m; 3) Bouger anomaly gravity data in raster image format, covering the same region and with

the same pixel resolution, and; 4) 1:1 000 000 geological map of southern Ontario. A PC-based Geographic Information System, Intera-Tydac's SPANS (Spatial Analysis System), was the main software used to analyze data and carry out the modelling methods used. Appendix B describes this program and the Fortran Programs used outside SPANS. Appendix C summarizes the hardware used to run these programs.

Earthquake data included in the analysis represent only an eleven-year period of record, and earthquakes occurring prior to 1983 and recorded without the benefit of an improved seismic network were excluded. This is to ensure optimum reliabilty of correlation. A total of 62 events were used for the analysis (Table 4). Appendix D shows the frequency distribution of earthquake magnitude. Magnitudes cluster around the 1.5 mN-2.0 mN range. A total of 39 epicentres representing 63 % of total number of events have magnitudes greater than 2.0. Although seismic events 1.0 mN and events related to road and other construction activities, have been screened out by seismologists at the Geological Survey of Canada, the smaller number of earthquakes with magnitudes lower than 2.0 mN could reflect lower sensitivity of the seismograph network to weaker events. Error locations are also generally associated with weaker earthquakes. A subset of 39 epicentres comprising those with magnitude 2.0 or greater was thus analyzed separately for spatial association to determine

TABLE 4. Earthquake data for the period 1983-1993. Events with magnitude <2.0 mN are written in bold italics.

Date	Time	Latitude (Degrees)	Longitude (Degrees)	Depth (km)	Magnitude (mN)
1983-03-10	06:15:42.5	45.693	-76.094	25.4	2.0
1983-10-11	04:10:55.0	45.200	-75.750	14.0	4.1
1983-10-11	***04:19:30.0***	***45.200***	***-75.750***	***14.0***	***1.7***
1983-10-13	***08:57:00.3***	***45.202***	***-75.746***	***13.7***	***1.2***
1983-10-16	03:00:47.1	45.618	-75.054	12.6	3.1
1983-10-16	03:04:38.5	45.596	-75.052	18.3	2.0
1984-01-17	19:04:46.3	45.561	-75.124	20.3	3.1
1984-05-09	***03:21:17.5***	***45.752***	***-75.023***	***18.0***	***1.7***
1984-10-11	***23:27:32.1***	***45.793***	***-75.226***	***08.7***	***1.6***
1984-10-26	02:13:22.2	45.832	-76.434	18.0	2.3
1984-10-31	***20:27:32.0***	***45.883***	***-75.646***	***07.8***	***1.0***
1984-11-26	09:03:48.1	45.166	-75.071	10.0	3.2
1984-11-26	09:03:49.0	45.220	-75.030	05.0	2.7
1984-12-08	***03:23:05.1***	***45.880***	***-75.595***	***18.0***	***1.9***
1985-01-30	09:46:13.1	45.748	-75.153	16.2	2.6
1985-08-20	15:05:46.9	45.883	-76.420	18.0	2.9
1985-08-24	06:04:02.0	45.680	-76.654	18.0	3.1
1986-05-07	17:29:57.0	45.870	-75.390	22.0	2.5
1986-05-07	***19:59:14.0***	***45.460***	***-75.400***	***01.0***	***1.7***
1986-06-04	***15:48:27.0***	***45.450***	***-75.520***	***01.0***	***1.7***
1986-06-14	16:43:13.0	45.730	-75.610	18.0	2.7
1986-07-22	22:41:31.9	45.589	-76.611	18.0	2.4
1986-07-24	***05:43:45.0***	***45.750***	***-76.550***	***18.0***	***1.6***
1986-07-24	***05:56:43.0***	***45.760***	***-76.540***	***18.0***	***1.8***
1986-08-17	21:48:03.0	45.760	-76.500	18.0	2.2
1986-12-09	13:02:33.0	45.340	-76.210	18.0	2.2
1987-05-14	11:38:57.2	45.749	-75.220	18.1	2.2
1987-06-19	***19:40:55.3***	***45.562***	***-75.597***	***01.0***	***1.8***
1987-09-30	13:55:19.4	45.663	-75.802	27.0	2.7
1987-11-11	07:58:33.1	45.769	-75.336	17.1	3.5
1987-11-11	08:00:27.4	45.776	-75.336	21.1	3.2
1987-11-16	20:25:44.0	45.804	-75.778	00.0	2.6
1988-03-31	09:28:38.4	45.893	-75.137	18.0	2.6
1988-05-15	06:10-05.4	45.156	-75.607	08.5	3.3
1988-07-16	17:35:28.1	45.269	-76.139	14.2	2.1
1988-08-14	19:48:53.9	45.822	-76.722	18.0	2.0
1988-08-14	***19:48:53.9***	***45.554***	***-75.089***	***13.7***	***1.8***
1988-12-29	***05:24:54.7***	***45.374***	***-75.452***	***18.0***	***1.2***
1989-01-29	***03:07:23.3***	***45.749***	***-76.941***	***18.0***	***1.5***
1989-02-01	18:01:13.5	45.244	-75.227	13.5	2.5
1989-07-16	***12:23:08.5***	***45.445***	***-75.971***	***20.3***	***1.8***
1990-03-03	01:12:35.4	45.224	-75.284	08.7	2.9
1990-05-13	***18:28:02.5***	***45.645***	***-75.034***	***18.0***	***1.5***

TABLE 4 (Cont'd)

1990-05-20	12:20:15.1	45.604	-75.160	18.0	2.3
1990-10-08	14:34:40.2	45.637	-75.021	01.0	2.0
1990-11-18	01:45:27.1	45.746	-75.179	09.6	2.4
1991-03-20	*21:12:29.1*	*45.264*	*-75.697*	*18.0*	*1.7*
1991-07-08	10:08:13.1	45.537	-76.723	18.0	3.1
1991-08-14	07:26:42.2	45.639	-76.273	18.0	2.0
1991-08-22	08:22:55.4	45.871	-75.110	10.6	3.1
1991-08-25	19:46:45.8	45.717	-76.219	18.0	2.3
1991-11-29	*05:23:23.5*	*45.568*	*-75.141*	*18.0*	*1.8*
1992-03-31	10:45:19.8	45.083	-75.621	18.0	2.8
1992-04-27	02:06:33.3	45.689	-75.125	18.0	2.2
1992-06-14	23:57:36.8	45.752	-76.625	18.0	2.0
1992-08-13	03:13:07.1	45.264	-75.135	18.0	2.0
1992-09-17	*04:30:57.9*	*45.834*	*-75.130*	*18.0*	*1.5*
1992-10-15	*23:34:19.0*	*45.238*	*-75.190*	*18.0*	*1.3*
1992-11-13	*02:17:44.1*	*45.822*	*-75.608*	*18.0*	*1.9*
1993-02-21	*14:56:56.6*	*45.868*	*-75.066*	*18.0*	*1.6*
1993-04-01	00:25:03.3	45.595	-75.107	03.8	2.5
1993-08-29	*10:53:18.8*	*45.316*	*-75.584*	*20.7*	*1.5*

whether non-detection of or location errors for weaker events has any effect on the results for the main set.

The correlation of seismicity with positive aeromagnetic anomalies in nearby areas (Forsyth 1981; Goodacre *et al.* 1993) had been established. To test whether this also holds true for the study area and earthquake data used, the magnetic anomaly map, originally in raster format with 255 classes, was reclassified into nine (9) classes. Spatial association between positive aeromagnetic anomalies and epicentres was measured, using the method described above. Possible correlation between seismicity and magnetic anomaly in the study area stems from the fact that magnetic anomalies are often associated with underlying lithologic units and structures. In sediment-covered areas, the high magnetic susceptibility igneous and metamorphic basement rocks are the predominant factors controlling the pattern of the anomaly field due to the inherently weaker magnetic susceptibility of sedimentary rocks (Roche and and Wohlenberg 1970). Conversely, deep sedimentary basins are likely to show low values of the anomaly and gentle field gradients. Where the basement rocks are brought nearer to the surface in structural highs the magnetic anomalies are large and characterized by strong relief (Roche and Wohlenberg 1970). Shear zones that are mineralized, especially the ferruginous patches, may be responsible for some of the linear high magnetic anomalies

(Teskey 1989; Forsyth 1981). The magnetic map is also very useful in confirming the presence of dykes (Halls 1978; Roche and Wohlenberg 1970) and the zones of weakness along which these rocks are intruded.

The gravity anomaly map, also originally in raster format with 255 classes, was likewise reclassified into thirteen (13) classes, in order to estimate the spatial association between seismicity and gravity. Gravity anomaly maps may reveal various lithologies that respond differently to applied stresses, and structures. Linear belts of steep gravity gradients may be produced by steep contacts between rocks of different density across fault planes (Dobrin and Savit 1988). Gravity highs are oftentimes associated with uplift along structures that bring older denser rocks nearer the surface, and gravity lows are associated with downfaulting of denser rock units (Kumarapeli 1978). Gravity highs may be due to the presence of dense basic intrusions while sedimentary basins and relatively less dense acid intrusions usually produce gravity lows (Mueller 1970).

Since geophysical anomalies that reflect geological structure may be associated with seismicity, a spatial relationship of epicentres with geology is also suggested (Forsyth 1981; Goodacre *et al.* 1993). The possible spatial association between seismicity and lithology was thus tested

in the study area. However, most of the earthquakes are deep-seated that correlation of earthquakes with smaller, superficial units and structures is probably not realistic. Results of the analysis show no convincing results for geological units. The correlation between seismicity and broader lithotectonic units with characteristic lithologies, metamorphic grades and structural grains within the study area was also determined but no significant association was obtained.

To prepare for correlation between epicentres and lineaments, faults and dykes from the 1:1 000 000 geological map (Appendix E) were digitized and exported into SPANS. Another lineament map was generated from the interpretation of LANDSAT imagery (Appendix F). The lineaments from both sets were combined and classified into ten (10) classes with 18° interval. Class 1 includes lineaments with orientation between 81° and 99° azimuth and higher classes are taken anticlockwise. An eleventh class was added to accommodate curved lineaments. Fifteen (15) buffer zones with 1 km interval were drawn around lineaments belonging to each orientation class. The sixteenth class was assigned to areas beyond 15 km from lineaments.

Spatial association between seismicity and lineaments, that include dykes, faults with surface manifestations and basement faults derived from magnetic and gravity anomaly maps

were also determined. Lineaments were delineated from geophysical data through visual inspection of magnetic and gravity contours displayed in SPANS to identify regions of steep, linear horizontal gradients that are often diagnostic of faulting (Dobrin and Savit 1988). As with the lineaments delineated from the geological map and through interpretation of LANDSAT imagery, magnetic and gravity lineaments were classified according to orientations. The same scheme was used in the classification; that is, ten (10) classes with each class having an 18° interval and lineaments oriented between 81° and 99° azimuth assigned to class 1. Magnetic gradients are correlated with seismicity because different structural blocks that these gradients delineate respond differently to the ambient stress field (Forsyth 1981; Mareschal and Zhu Pei-Ding 1989). The association of earthquakes epicentres with gravity gradients and structural zones have been mentioned quite often (McGinnis and Ervin 1974; McKeown 1975; Long 1976; Forsyth 1977; Campbell 1978) and have been explained in terms of yielding of these relatively weak boundaries to stresses, due to the anomalous mass, that are otherwise too weak to directly cause rock failure (Forsyth 1981). Yang and Aggarwal (1981) also noted the association of majority of epicentres with steep gravity gradients that possibly mark the location of buried faults. Similar association among seismicity, gravity anomalies, structure and lithology were mentioned in relation to studies in regions such as the Rhine graben (Mueller 1970).

4. EVOLUTION OF PHANEROZOIC FAULTING AND THE REGIONAL STRESS FIELD

4.1 Periods of Faulting

4.1.1 D_1

The earliest period of faulting (D_1) is represented by three families of faults including northwest-trending normal faults, and sinistral and dextral strike-slip faults with north-northwest and northwest orientations, respectively (Fig. 9). Northwest-trending lineations on bedding planes (Fig. 10), defined by both slickenlines (grooves, striations) observed on the limestone bedding surface (Fig. 11a) and by fibrous calcite coating (Fig. 11b), are kinematically congruent with the three families of faults and are therefore interpreted as D_1 structural elements. The orientations and kinematics of the three families of faults, and the orientation of the bedding-plane lineations, are all consistent with a northwest-southeast-oriented maximum horizontal principal compressive stress. Field observations which establish the relative age of D_1 structures include offset of bedding which bears northwest-trending lineations by later faults (Fig. 11b), the preservation of northwest-trending slickenlines on bedding surfaces where later calcite-fibre lineations are present (Fig. 11a) and offset of D_1 normal faults by bedding plane

FIG. 9. Lower hemisphere Schmidt projection of D_1 sinistral (i) and dextral (ii) strike-slip and normal (iii) faults; D_2 sinistral (i) and dextral (ii) strike-slip faults, normal faults (iii) and thrust faults (iv) , and; D_3 sinistral (i) and dextral (ii) strike-slip faults, normal (iii) and thrust (iv and v) faults.

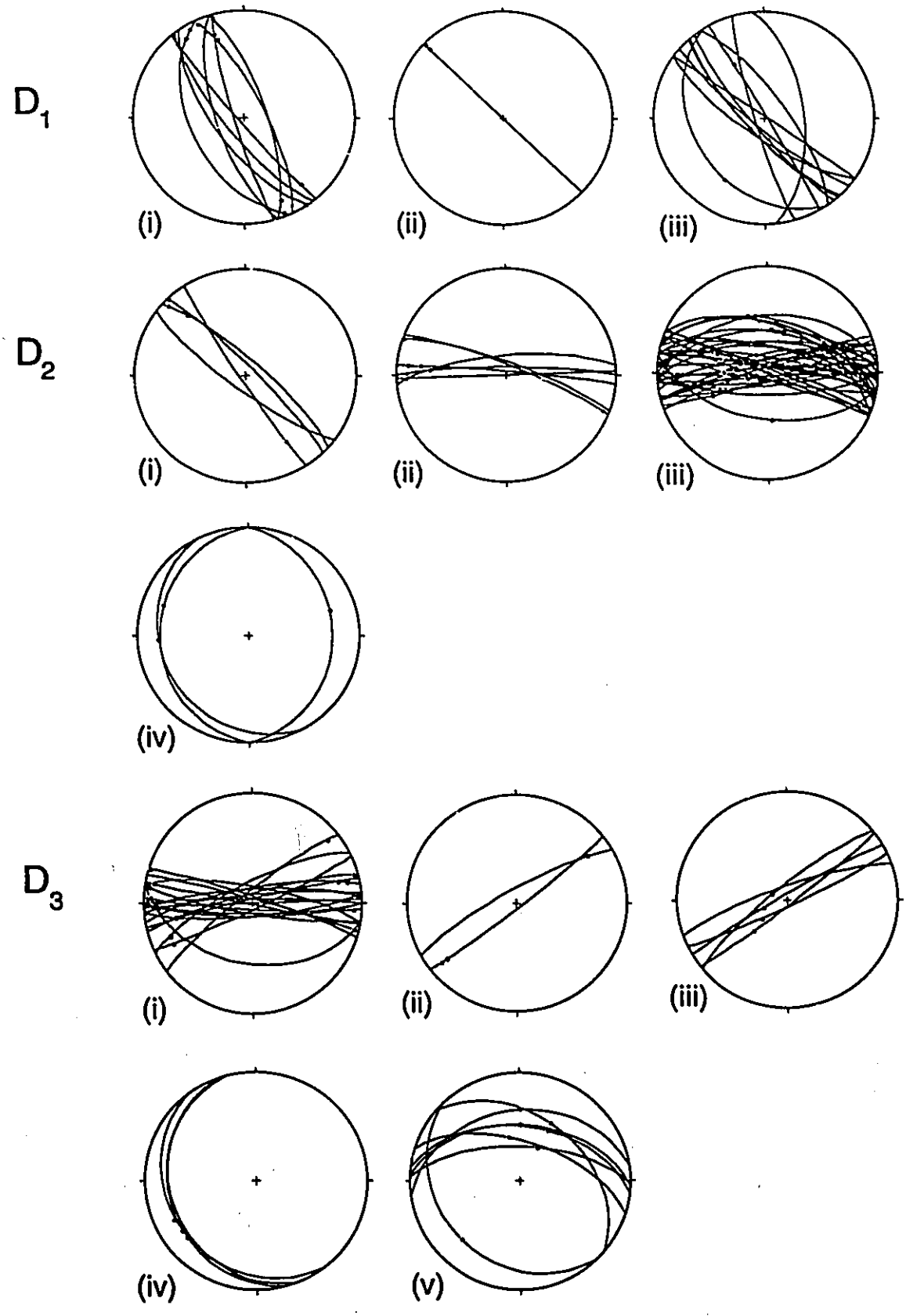
D1
(i)
(ii)
(iii)
D2
(i)
(ii)
(iii)
(iv)
D3
(i)
(ii)
(iii)
(iv)
(v)

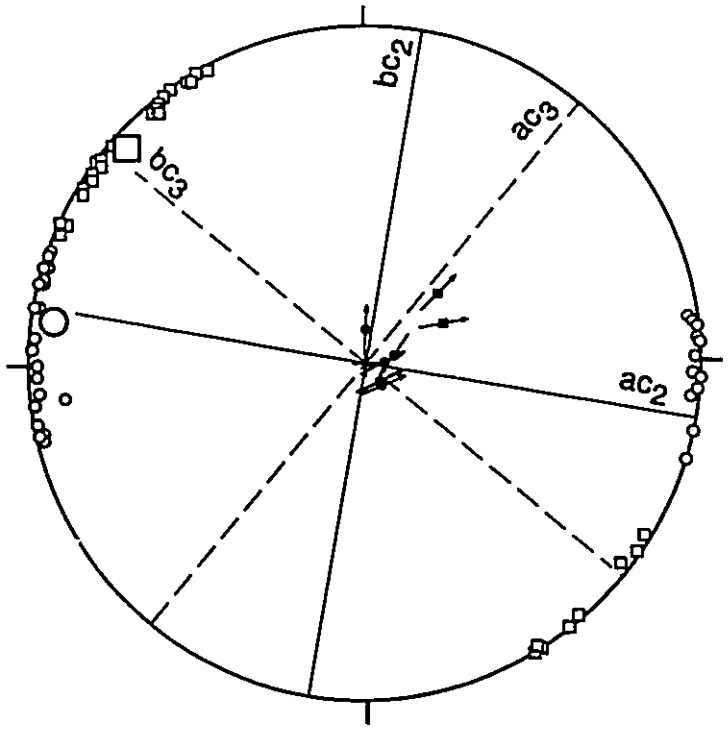

L_1 Mean Vector □
Trend and Plunge 312.3° 3.3°
L_2 Mean Vector ○
Trend and Plunge 278.5° 5.9°

FIG. 10. Lower hemisphere Schmidt projection for D_1 (□) and D_2 (○) bedding plane lineations. Data for D_1 and D_2 bedding plane lineations were gathered from the northern quarry of Francon quarry. Also shown are D_3 slip linears (→), centered on poles to bedding (●) and fault planes (■), and associated with the northwest-trending fold in the transitway (Fig. 14). The associated fold axes for D_2 (bc_2) and D_3 (bc_3) along with the deformation axes for D_2 (ac_2) and D_3 (ac_3) are also shown.

FIG. 11. (a) D_1 northwest striations along limestone bedding surface and later (D_2) east-west-oriented, fibrous calcite coating. Upper pen is 14 cm long and oriented along strike of northwest-trending striation (332°) while lower pen, parallel to east-west-trending fibrous calcite coating, is oriented 272°. (b) Bedding plane and northwest-trending, fibrous calcite coating on the same bedding plane are offset by D_2 normal faults. Photos taken at Francon quarry.

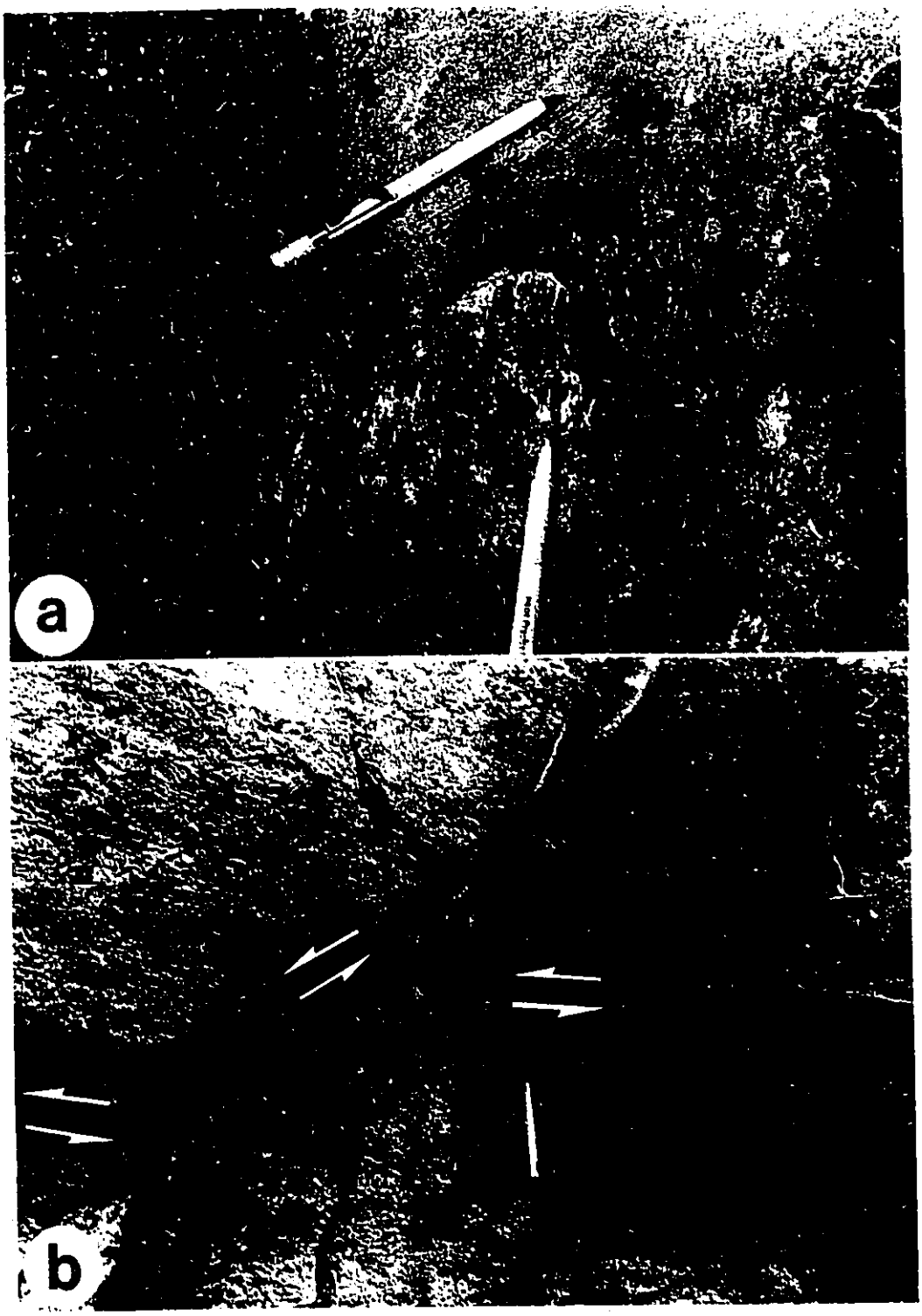
a
b

faults with northeast-trending lineations, and from which minor D_3 thrusts sometimes project (Fig. 12). A minimum age of D_1 bedding-plane lineations can be established where they are cross-cut by a carbonatite dyke of Cretaceous age (Hogarth *et al.* 1988) in the Francon quarry (Fig. 13). D_1 faults are concentrated in outcrops along the Ottawa-Carleton Transit Commission transitway and at the Permanent quarry.

4.1.2 D_2

The second period of faulting involved movement on abundant west-northwest- to west-southwest-trending normal faults, and a subordinate number of sinistral and dextral strike-slip faults oriented northwest and west-northwest, respectively, and a few thrust faults (Fig. 9). D_2 bedding-plane lineations (striations, grooves and fibrous calcite lineations; Fig. 14) are oriented east-west to west-northwest (Fig. 10) and are due to flexural-slip along bedding planes during the formation of very open north- to north-northeast-trending folds with at least 450 m of wavelength (measured based on mapped positions of synclinal and anticlinal axes), observed in the north quarry of the Francon quarry. These structures are all consistent with an east-west to west-northwest-east-southeast maximum horizontal principal stress. Within the Permanent quarry (Fig. 3), a highly sheared, west-

FIG. 12. (a), (b) Northwest-trending D_1 normal faults displaced by bedding-parallel slip during D_3. A minor, gently-dipping thrust fault plane projects from the slipped bedding plane at (b). The normal fault opened up leaving a hollow (indicated by arrow) as propagation of slip along bedding plane at right of the normal fault stepped down to a lower level on the left. Pole graduation is 0.5 m. (c) East-west- to west-northwest-trending fractures with calcite infilling, at right of fault at (b), displaced by bedding-plane slip during D_3. Pole length is 2 m. Photos taken at the Ottawa-Carleton Transit Commission transitway east of Holland Avenue.

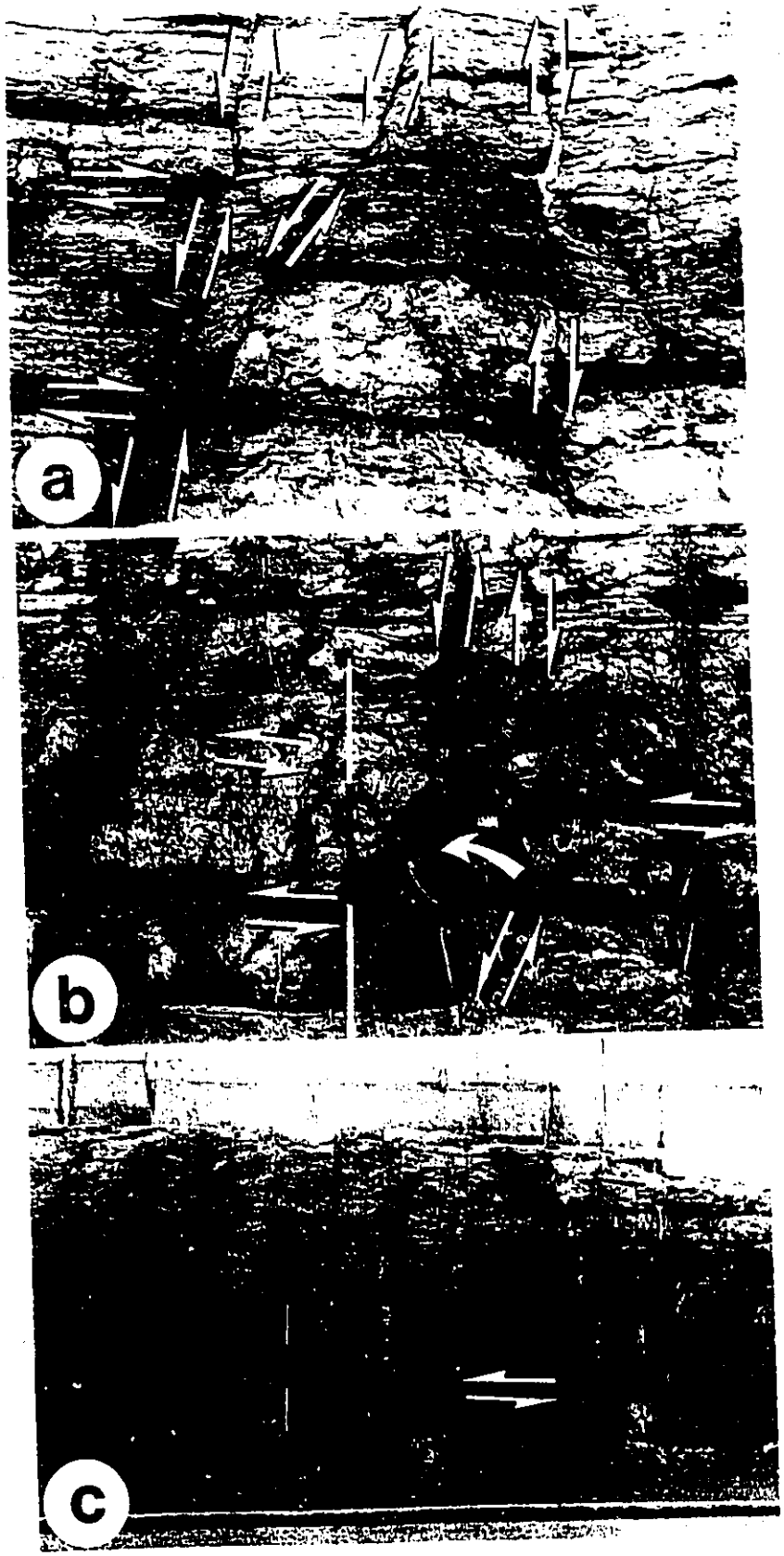
a
b
c

FIG. 13. East-west-oriented Cretaceous carbonatite dyke cross-cutting northwest-oriented D_1 bedding-plane grooves and striations on fibrous calcite coating. Pen is 14 cm long and is oriented along strike of D_1 lineation (152°). Photo taken at Francon quarry.

FIG. 14. D_2 slickenlines (striations and grooves) and steps on fibrous calcite coating of bedding plane. Pen is 14 cm long and points toward direction of slip (85°). Photo was taken at northern quarry of Francon quarry.

northwest-trending (292°) carbonatite dyke has been observed; the asymmetry of steps on the wall rock indicate a dextral strike-slip movement during shearing of the dyke. Dextral shearing of the carbonatite dyke is consistent with the compressional direction associated with D_2 dextral strike-slip faults, and it is likely that emplacement of the dyke was pre- to syn- D_2. Assuming that carbonatite dykes in the Permanent quarry belong to the same suite as those dated by Hogarth *et al.* (1988) in the Francon quarry, this would indicate that D_2 occurred during or prior to the Cretaceous.

D_1 normal faults may be shown to have been reactivated during this phase of deformation (D_2) based on drag and kinematics apparent from fault plane features. For instance, adjacent, conjugate D_1 north-northwest and northwest faults (Fig. 15), both bounded by drag indicating the original normal sense of movement, display fault lineations and steps indicating sinistral sense of movement, most likely during D_2 when the orientation of the maximum principal horizontal stress was more westerly than the northwest D_1 normal fault. Later folding during D_3 has rotated the beds and faults along a northwest axis. No evidence from northwest or west-northwest dextral-strike-slip faults (D_1) was found to show reactivation during D_2 with left-lateral sense of movement. Some west-northwest faults displaying two episodes of dextral strike-slip movement may have originated as D_1 dextral strike-

FIG. 15. Conjugate northwest-oriented D_1 normal faults on left and right were first reactivated into sinistral (strike-slip) faults during D_2. The fault on right was further reactivated as thrust fault during D_2. Both faults were subjected to rotation concurrent with folding during D_3. Photo taken at Ottawa-Carleton Transit Commission transitway east of Carruthers Avenue.

slip faults and reactivated during D_2.

4.1.3 D_3

The third period of faulting produced thrust faults oriented east-west to north-northwest, normal faults oriented northeast, and dextral and sinistral strike-slip faults trending northeast and west-northwest to northeast, respectively (Fig. 9). D_3 bedding-parallel slip, recorded by northeast-southwest-trending bedding-plane lineations, has displaced older generations of structures (Fig. 13a,b,c). D_3 bedding plane lineations are associated with northwest-trending open folds. Norris (1967) established the genetic relationship to flexural slip of some D_3 bedding plane lineations associated with the northwest-trending Queensway folds near Parkdale Avenue in Ottawa. In the transitway, a northwest-trending fold (Fig. 15), genetically related to D_3 northeast-trending bedding-plane lineations (Fig. 10), has rotated D_1 northwest-oriented, conjugate normal faults. The orientation of D_3 bedding plane lineations are consistent with the compressional direction associated with dextral and sinistral strike-slip faults trending northeast and west-northwest to northeast, respectively. Sinistral sense of movement shown by carrot-shaped grooves and steps on wall-rock of an east-west-trending, Cretaceous carbonatite dyke within the Francon quarry is also consistent with this compressional

direction. If the carbonatite dykes within the Francon and Permanent quarries were indeed emplaced during the same period, occurrence of D_3 during or after the Cretaceous is indicated.

Where structures representing all three generations of faulting are exposed, it can be demonstrated, based on offsetting relationship of these structures, that D_3 faulting followed movement along D_2 and D_1 structures. This is illustrated by an exposure at Francon quarry (Fig. 15) where D_2 east-west normal faults, vertically displacing bedding planes with D_1 northwest lineations, are in turn displaced by a D_3 thrust fault. Fault-propagation folds associated with the thrust fault are bounded by more minor reverse faults (Fig. 16). The west-northwest orientation of the fault-propagation folds and the observed D_3 bedding plane grooves trending north-northeast (12°) just above the folds suggest a north-northeast directed compression that caused thrusting. Similar flat-ramp sections, displacing D_1 and D_2 normal faults observed at Francon quarry and the transitway, with notably gentler ramp slopes display less-developed fault-propagation folds or none at all (Fig. 13b).

The relative ages of D_2 and D_3 fault surface features and reactivation during D_3 of D_2 normal (Fig. 17a, b) and dextral strike-slip faults (Fig. 18) as sinistral strike-slip faults

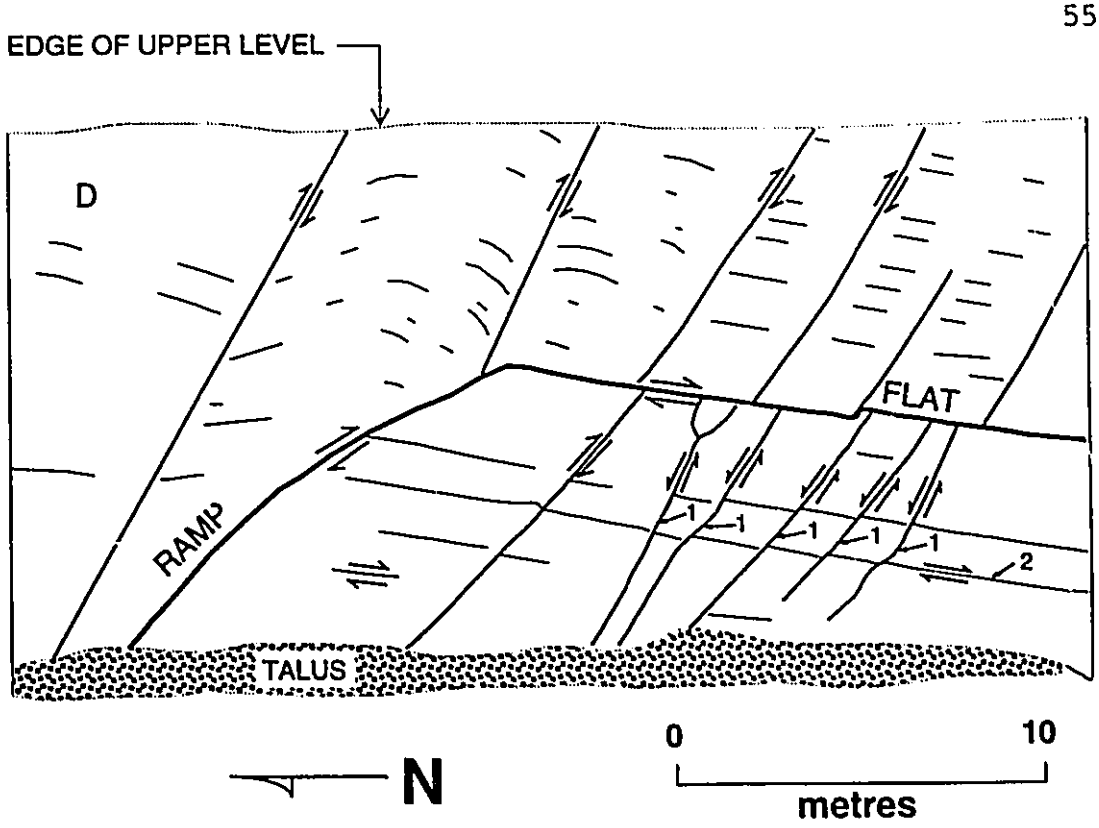

FIG. 16. Ramp-flat section on eastern wall of southern quarry of Francon quarry. Above the ramp are fault propagation folds oriented essentially east-west suggesting reverse faulting along ramp-flat thrust plane indicated by solid bold outline. Thrusting cut a series of east-west D_2 normal faults (1) that in turn vertically displaced bedding planes (2) along which northwest or southeast slip during D_1 occurred.

FIG. 17. (a) D_2 normal faults in an east-west-oriented zone. Drag pattern suggests normal faulting with dextral strike-slip component. Photo was provided by J. Wallach. (b) Lineations with more gentle plunge (indicated by white underline) on northernmost fault plane suggest reactivation with sinistral strike-slip movement during D_3 which might have slightly modified original normal faulting drag. Photo taken at southern quarry of Francon quarry.

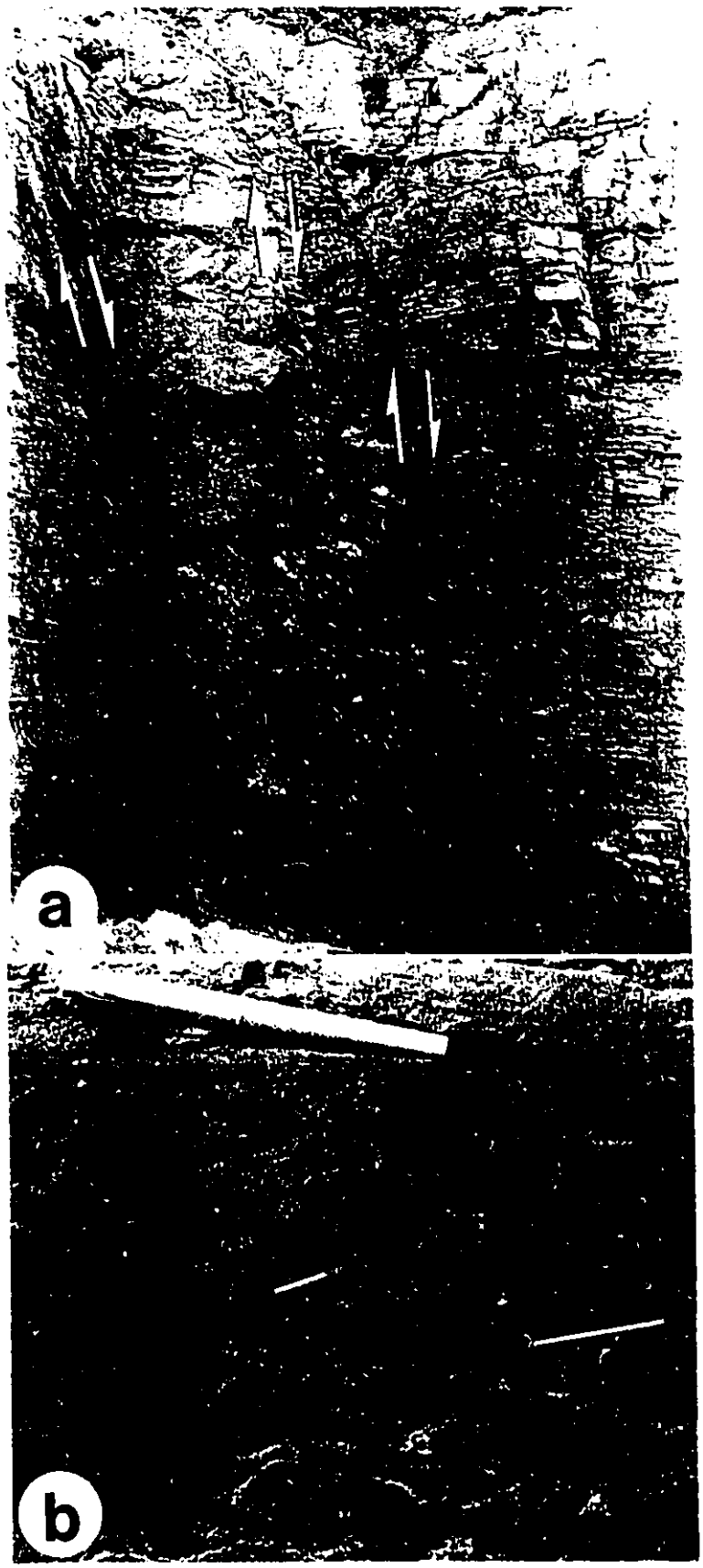
a
b

FIG. 18. An east-west-oriented D_2 fault showing evidence on wall-rock (a) of original dextral strike-slip movement. Lineations on fibrous calcite vein filling (b) came later as a result of sinistral strike-slip movement during D_3. Pen is 14 cm long. Photo taken at Ottawa-Carleton Transit Commission transitway east of Holland Avenue.

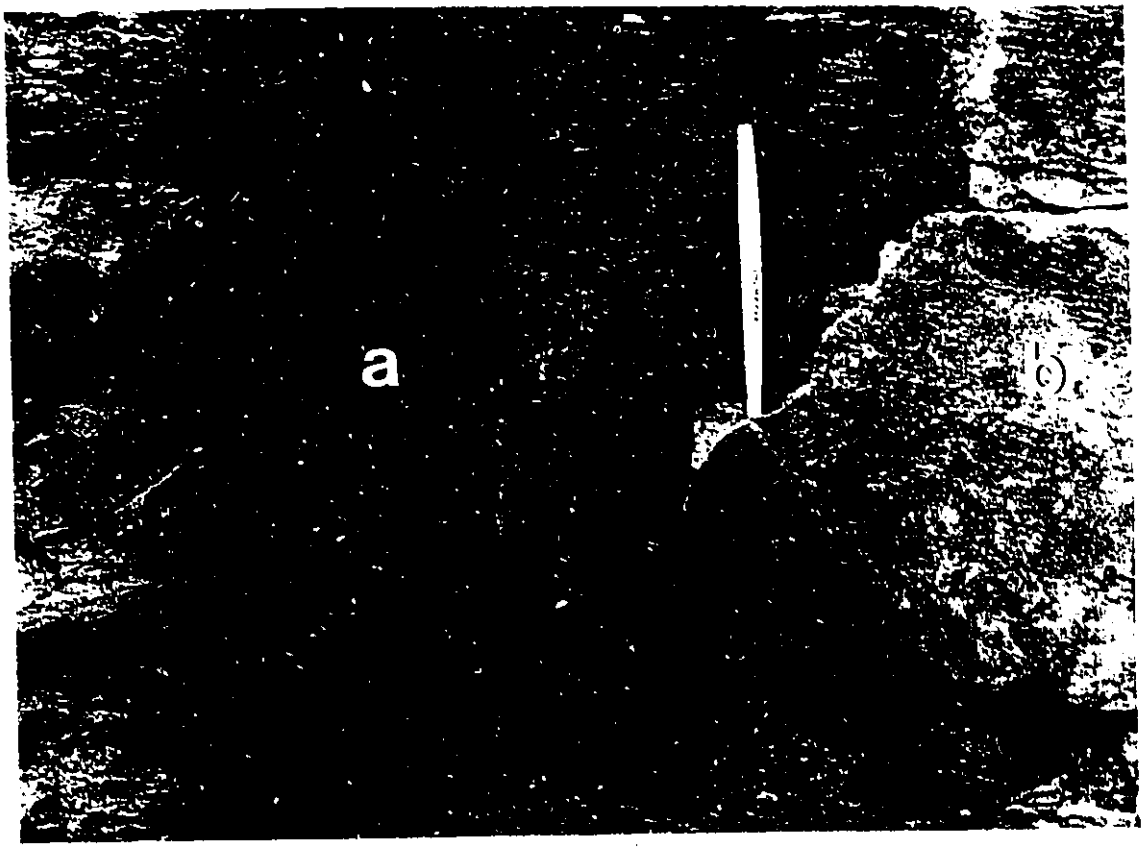
a
b

are established from outcrops in the Francon quarry and transitway. The younger age of D_3 lineations is based on cross-cutting relationship with D_2 lineations (Fig. 17b) or occurrence as fibrous calcite veins filling fracture walls with D_2 steps (Fig. 18). The D_2 steps indicate dextral sense of movement. The sinistral sense of movement displayed by the D_3 grooves (Fig. 17b) and fibrous calcite (Fig. 18) is consistent with northeast-southwest compression.

Some D_1 normal faults had also been reactivated into thrust faults during D_3 (Fig. 15) as shown by lineations and steps, associated with thrusting, on fault planes bounded by drag indicating an original normal sense of movement. Table 5 lists faults with more than one set of lineations. Fault plane lineation data demonstrate mainly reactivation of D_2 strike-slip, reverse and normal faults during D_3 involving either strike-slip or reverse faulting.

4.2 Paleostress Orientations Based On Lineation Data

Fault-plane and fault plane lineation measurements, and stress tensor solutions are presented in Fig. 19. Fault planes and lineations were rotated back to original positions where folding occurring after faulting has tilted beds. The D_1 sinistral and dextral strike-slip faults imply that the greatest principal horizontal stress (σ_1) was oriented

TABLE 5. Fault planes with more than one set of lineations belonging to any of the three periods of faulting.

Strike	Dip	Pitch of Slicken-lines	Sense of Displ.	Faulting Period
088	90 -	09 W	D	D_2
	-	10 W	S	D_3
083	75 W	87 W	N	D_2
		04 E	S	D_3
090	84 W	10 W	D	D_2
		10 W	S	D_3
070	85 W	85 W	N	D_2
		04 W	S	D_3
085	84 W	14 W	S	D_3
		01 W	S	D_3
095	87 E	23 W	D	D_2
		11 W	D	D_2
053	86 E	56 W	N	D_3
		19 W	D	D_3
		13 W	D	D_3
155	50 W	15 W	S	D_1
		22 W	S	D_1
		05 W	S	D_1
142	76 W	11 W	S	D_2
		45 W	R	D_3
132	78 E	07 W	S	D_2
		26 W	S	D_2
065	85 E	67 W	N	D_3
		20 W	S	D_3
118	08 E	18 W	R	D_3
		56 E	R	D_3
090	57 E	87 E	N	D_2
		35 E	N	D_2
100	78 E	58 E	N	D_2
		72 W	N	D_2
087	66 W	65 E	N	D_2
		85 E	N	D_2
107	51 E	85 W	N	D_2
		59 E	N	D_2
093	84 E	85 W	N	D_2
		53 W	N	D_3
		21 W	S	D_3
085	80 E	30 W	N	D_2
		53 W	N	D_2
077	83 E	60 W	N	D_2
		10 W	S	D_3
153	22 W	25 W	R	D_2
		66 W	R	D_2
		54 E	R	D_3

NOTE: Sense of displacement is designated by N (normal), S (sinistral), D (dextral), and R (reverse).

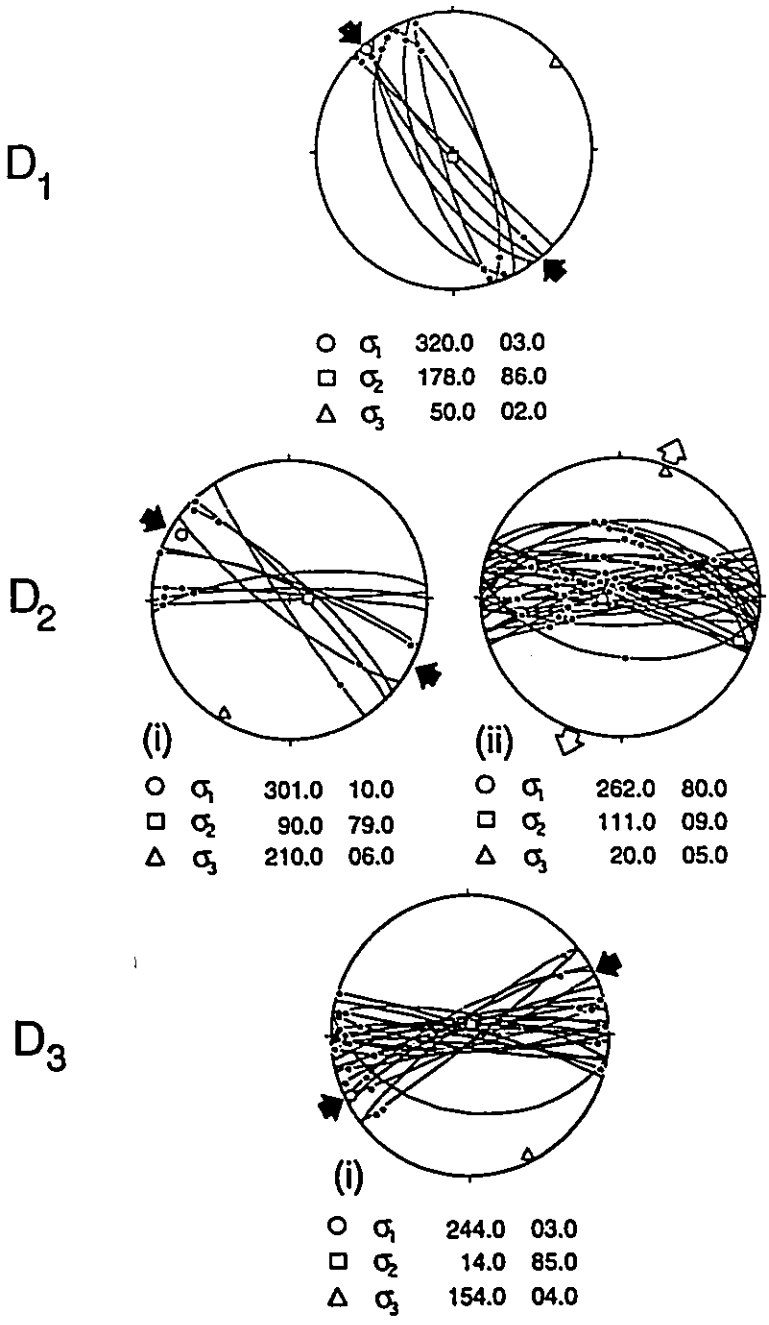

FIG. 19. Lower hemisphere Schmidt projection of principal stress directions for D_1 strike-slip faults and lineations, D_2 strike-slip faults (i), normal faults (ii) and lineations, and D_3 strike-slip faults and lineations. Associated principal horizontal stress orientations are indicated by black arrows (compression) and white arrow (extension). Calculations were carried out using a fault kinematics computer program written by Laborde *et al.* (no date).

northwest. Not enough lineation data is available for a number of D_1 northwest-oriented normal faults, but based on their orientation, a northwest intermediate principal stress (σ_2) is inferred. For the D_2 strike-slip faults, composed of both sinistral and dextral strike-slip faults, a west-northwest σ_1 is inferred. Normal faults belonging to D_2 resulted from a north-northeast-south-southwest extension and with σ_2 oriented east-southeast. Some lineations are associated with reverse faulting and consistent with west-northwest-east-southeast compression during D_2. Not enough data are available, however, to allow precise calculation of stress field orientation. Calculated σ_1 in D_3 strike-slip faults is oriented southwest.

5. SPATIAL ASSOCIATION AMONG SEISMICITY, STRUCTURES AND OTHER GEOSCIENTIFIC PARAMETERS

5.1 Spatial Association Among Seismicity, Gravity Anomalies, Magnetic Anomalies and Gravity Lineaments

5.1.1 Gravity

Spatial association was carried out between seismicity and the thirteen (13) classes of the gravity anomaly map (Fig. 20). Weights of evidence analysis results are shown in Table 6. Values in parentheses are for the 39-epicentre case (magnitude ≥2). Fig. 21a shows a plot of the cumulative proportion of points and areas for each of the gravity anomaly map classes. For the main set (62 epicentres), the peaks in contrast value correspond to classes 3 and 9 (Table 6; Fig. 21b). Class 9, however, represents the point in Fig. 21a where the difference between the cumulative proportion of points and areas is greatest and the peak in class 3 is not significant at the 95% significance level (Fig. 22a). The peak in class 9 is significant for both the main set (Table 6; Fig. 22a) and the 39-epicentre set (Table 6; Fig. 22b). In reclassifying the map into a binary map, class 9 (C=0.767; (W^+=0.443; W^-=-0.323) is then used as the cut-off point, to create a binary map for which the spatial association with epicentres is the greatest. The binary map for gravity (Fig.

FIG. 20. Gravity anomaly map. The thirteen (13) contour classes were obtained by reclassifying classes of original raster file.

GRAVITY ANOMALY MAP

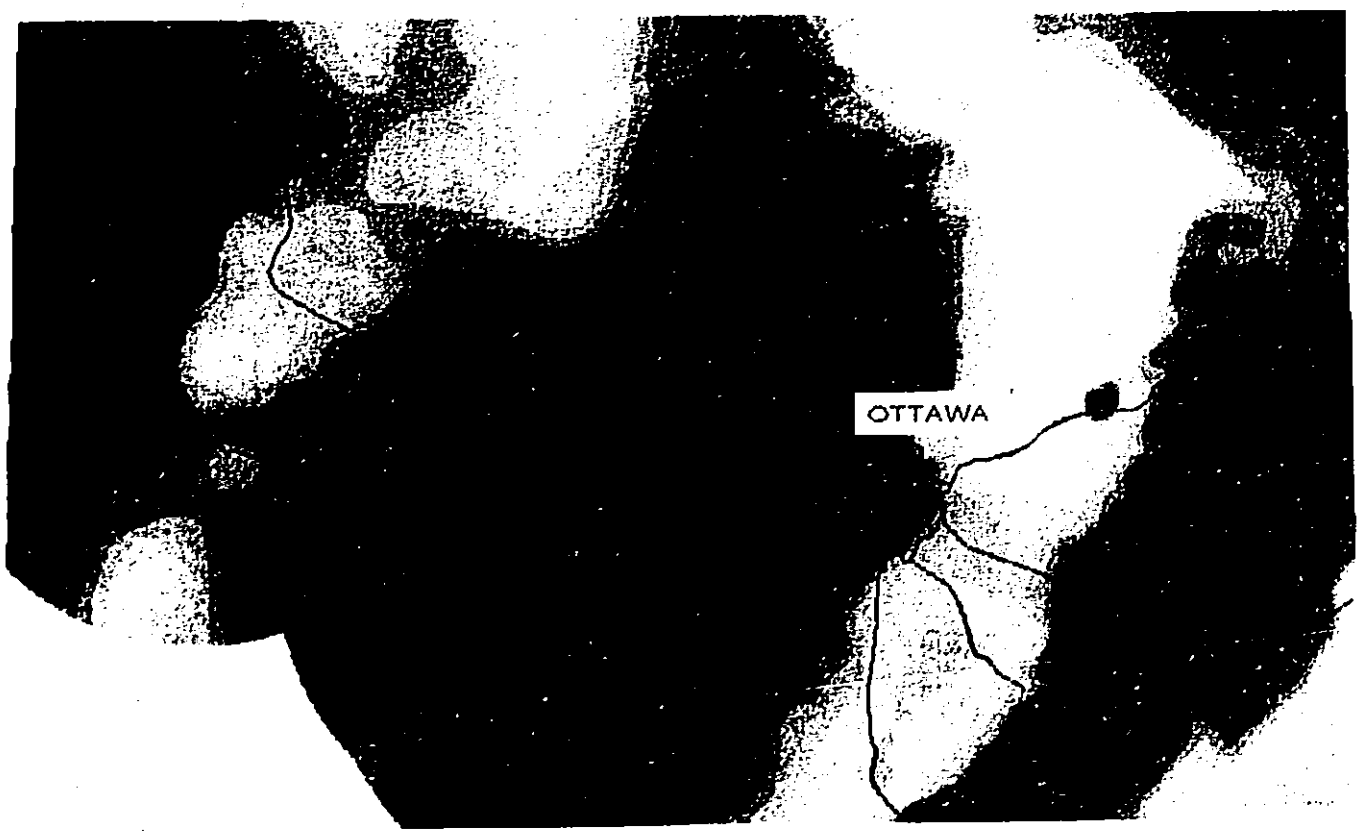

LEGEND

-51 to -38 mgal
-38 to -36 mgal
-36 to -35 mgal
-35 to -33 mgal
-33 to -32 mgal
-32 to -30 mgal
-30 to -29 mgal
-29 to -27 mgal
-27 to -26 mgal
-26 to -24 mgal
-24 to -22 mgal
-22 to -19 mgal
-19 to - 5 mgal

Highway

25 km

TABLE 6. Weighting parameters for gravity map .

Gravity Value (mgal)	Area [1]	Points [2]		W^+ [3]		s(W^+) [4]		W^- [5]		s(W^-) [6]		C [7]		s(C) [8]		Stud(C) [9]	
-51 to -38	6952	62	(39)														
-38 to -36	6508	60	(38)	0.034	(0.041)	0.130	(0.163)	-0.692	(-0.920)	0.709	(1.001)	0.726	(0.961)	0.721	(1.014)	1.007	(0.947)
-36 to -35	5918	58	(37)	0.095	(0.109)	0.132	(0.165)	-0.840	(-1.069)	0.501	(0.708)	0.936	(1.178)	0.518	(0.727)	1.806	(1.620)
-35 to -33	5308	53	(34)	0.114	(0.134)	0.138	(0.172)	-0.492	(-0.615)	0.334	(0.448)	0.606	(0.749)	0.362	(0.480)	1.675	(1.560)
-33 to -32	4658	50	(31)	0.187	(0.172)	0.142	(0.180)	-0.537	(-0.478)	0.289	(0.354)	0.725	(0.650)	0.323	(0.397)	2.247	(1.635)
-32 to -30	4032	45	(26)	0.226	(0.140)	0.150	(0.197)	-0.429	(-0.232)	0.243	(0.278)	0.656	(0.372)	0.286	(0.341)	2.296	(1.093)
-30 to -28	3445	39	(23)	0.241	(0.175)	0.161	(0.209)	-0.310	(-0.208)	0.209	(0.251)	0.550	(0.383)	0.264	(0.326)	2.085	(1.172)
-28 to -27	2912	34	(20)	0.272	(0.204)	0.173	(0.224)	-0.254	(-0.177)	0.190	(0.230)	0.526	(0.381)	0.256	(0.321)	2.053	(1.186)
-27 to -26	2315	32	(19)	0.443	(0.383)	0.178	(0.230)	-0.323	(-0.264)	0.183	(0.224)	0.767	(0.647)	0.255	(0.321)	3.002	(2.014)
-26 to -24	1927	25	(14)	0.379	(0.260)	0.201	(0.268)	-0.193	(-0.121)	0.165	(0.201)	0.572	(0.381)	0.260	(0.335)	2.198	(1.137)
-24 to -22	1495	20	(10)	0.410	(0.177)	0.225	(0.317)	-0.149	(-0.055)	0.155	(0.186)	0.559	(0.232)	0.273	(0.368)	2.045	(0.630)
-22 to -19	965	15	(7)	0.562	(0.258)	0.260	(0.379)	-0.129	(-0.049)	0.146	(0.177)	0.690	(0.306)	0.299	(0.419)	2.311	(0.732)
-19 to -0.5	379	2	(1)	-0.529	(-0.758)	0.709	(1.001)	0.024	(0.030)	0.130	(0.163)	-0.552	(-0.788)	0.721	(1.015)	-0.766	(-0.777)

Total no of points 62 (39)
Area of unit cell 2 sq kms
Total area 6952.70 unit cells or 13905.40 sq kms

1 Area enclosing region with gravity value greater than or equal to the specified gravity interval. (Area expressed in unit cells).
2 Number of epicentres occurring in region with gravity value greater than or equal to the specified gravity interval.
3 W^+ - Positive weight
4 s(W^+) - Standard deviation of W^+.
5 W^- - Negative weight
6 s(W^-) - Standard deviation of negative weight.
7 C - Contrast
8 s(C) - Standard deviation of contrast.
9 Stud(C) - Studentized contrast
Note: Values in parentheses are for the the 39-epicentre case.

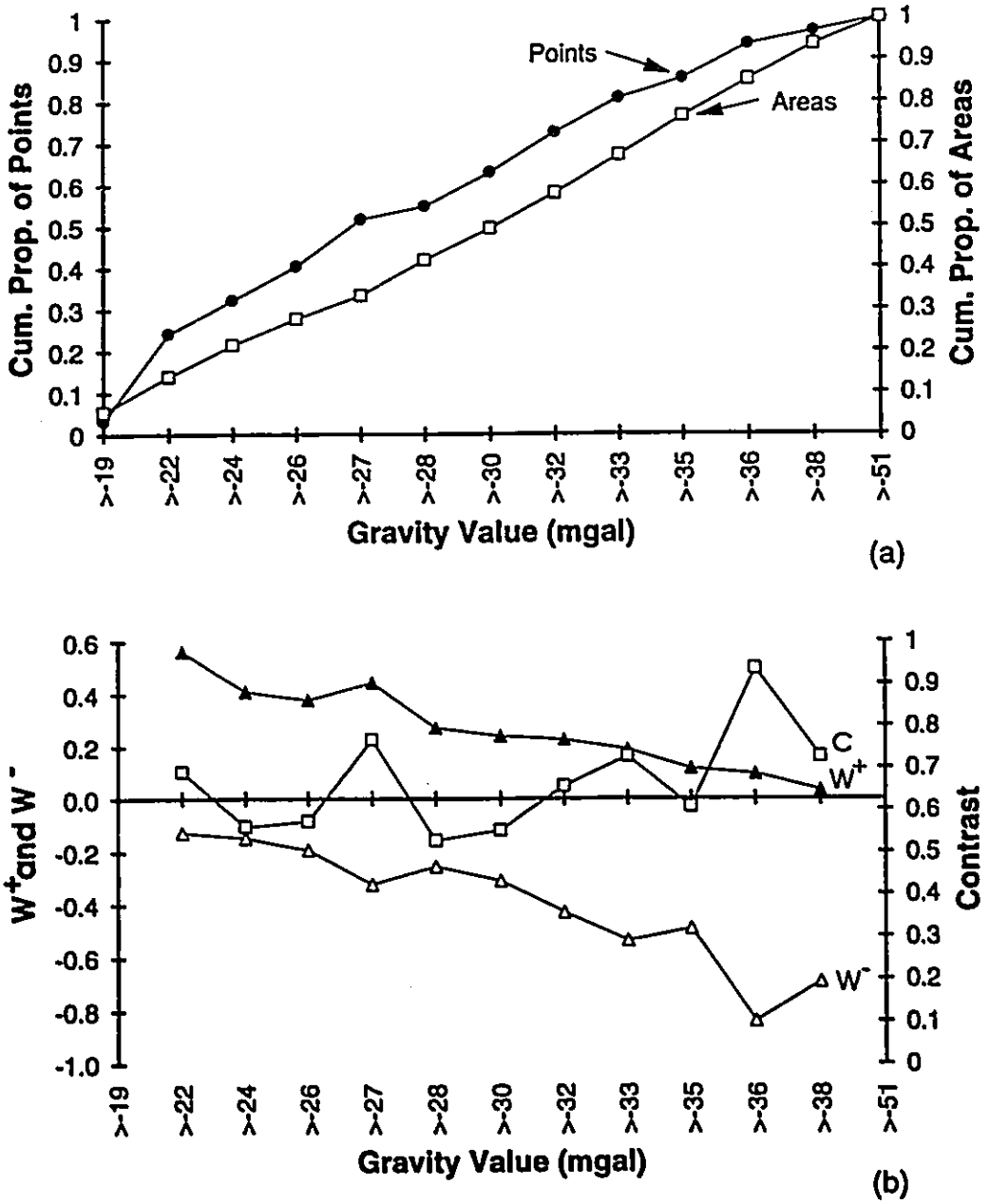

FIG. 21. (a) Plot of the cumulative proportion of points and areas for each of the gravity anomaly map classes. Note that the point distribution is consistently higher than the area distribution. For example, for the interval -28 to -27 mgals, the cumulative area proportion is 2912/6952 = 0.42 and the cumulative proportion of epicentres is 34/62 = 0.55. If the point distribution is independent of the area distribution, one would expect the two distributions to be the same. (b) Plot of contrast (C), W^+ and W^-.

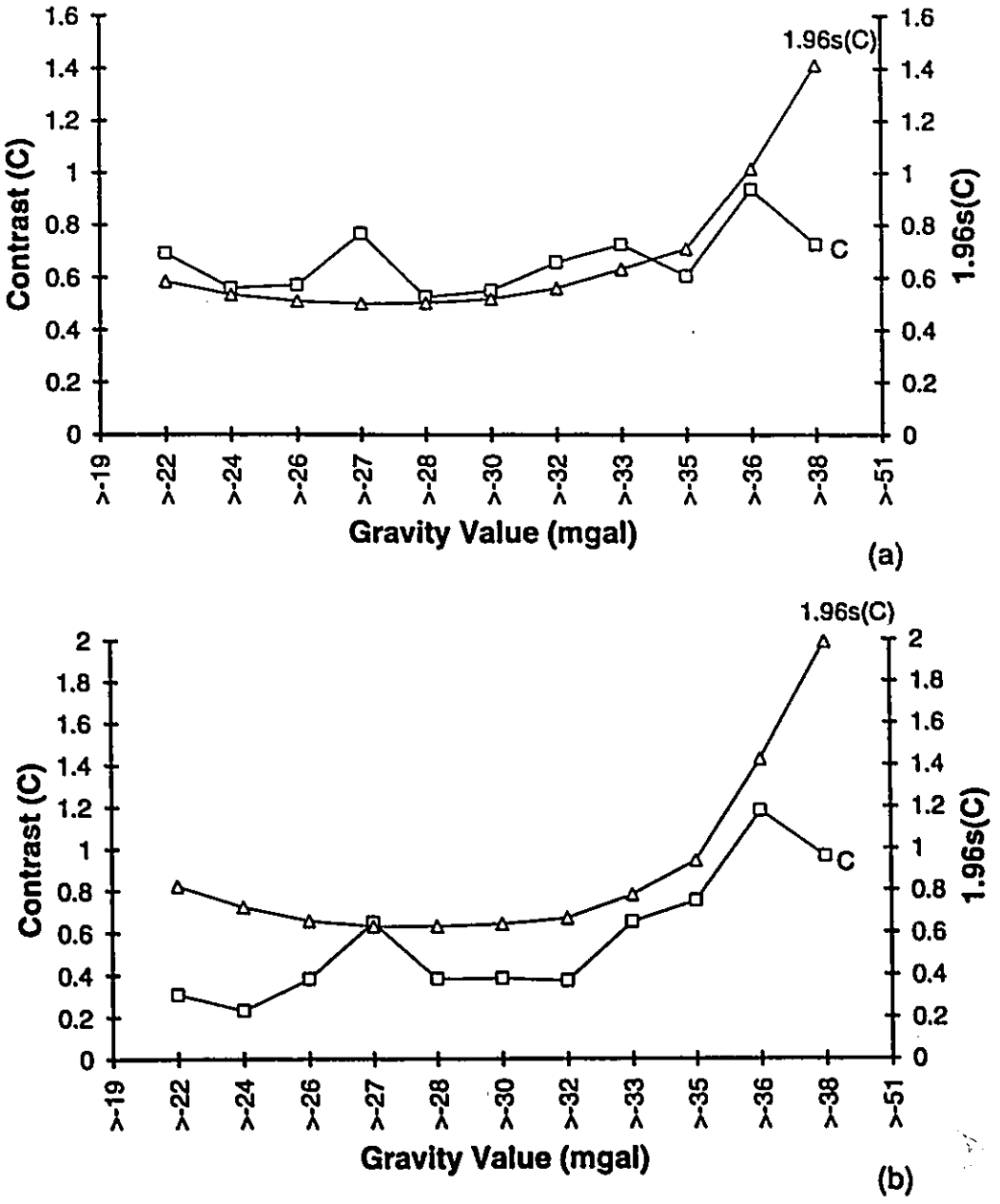

FIG. 22. Plot of contrast (C) values and 1.96 X standard deviation (s[C]) for the 62-epicentre case (a) and 39-epicentre case (b). This result suggests that gravity highs >-27 to -26 mgals are associated with more epicentres than would be expected due to chance, and that the result is independent of magnitude of the seismic event.

23) is thus composed of one class consisting of classes 9 to 13, representing gravity anomaly values of greater than -27 mgal, and another consisting of classes 1 to 8 (<-27 mgal). Class 2 (>-27 mgal) of the binary map, the zone of high magnetic anomaly, contain more epicentres than would be expected if the seismicity pattern and the binary magnetic map were independent.

5.1.2 Magnetic

Weighting parameter values obtained for the nine (9) classes of the magnetic anomaly map (Fig. 24) are shown in Table 7. Values in parentheses are for the 39-epicentre case. Cumulative proportion of points and areas for magnetics (Fig. 25a) indicate a maximum difference for class 7 (>145 NT). This corresponds to a peak in contrast (C=0.513; W^+=0.265; W^-=-0.249) shown in Fig. 25b. The peak in class 7 is significant (at 95% significance level) for both the 62-epicentre case (Figure 26a; Table 7) and the 39-epicentre case (Figure 26b; Table 7). Classes 7 to 9, representing anomaly values greater than +145 NT, therefore comprise class 2 (for pattern present) while classes 1 to 6 comprise class 1 (for pattern absent) of the binary map (Fig. 27). This result suggests that the magnetic pattern and the epicentres are not spatially independent, although the association is seen to be weak.

FIG. 23. Spatial association between seismicity and class 2 (pattern present) of the binary map for gravity. Note that the relationship with epicentres is rather weak, and does not explain the concentration of epicentres on the east side of the map.

BINARY MAP FOR GRAVITY

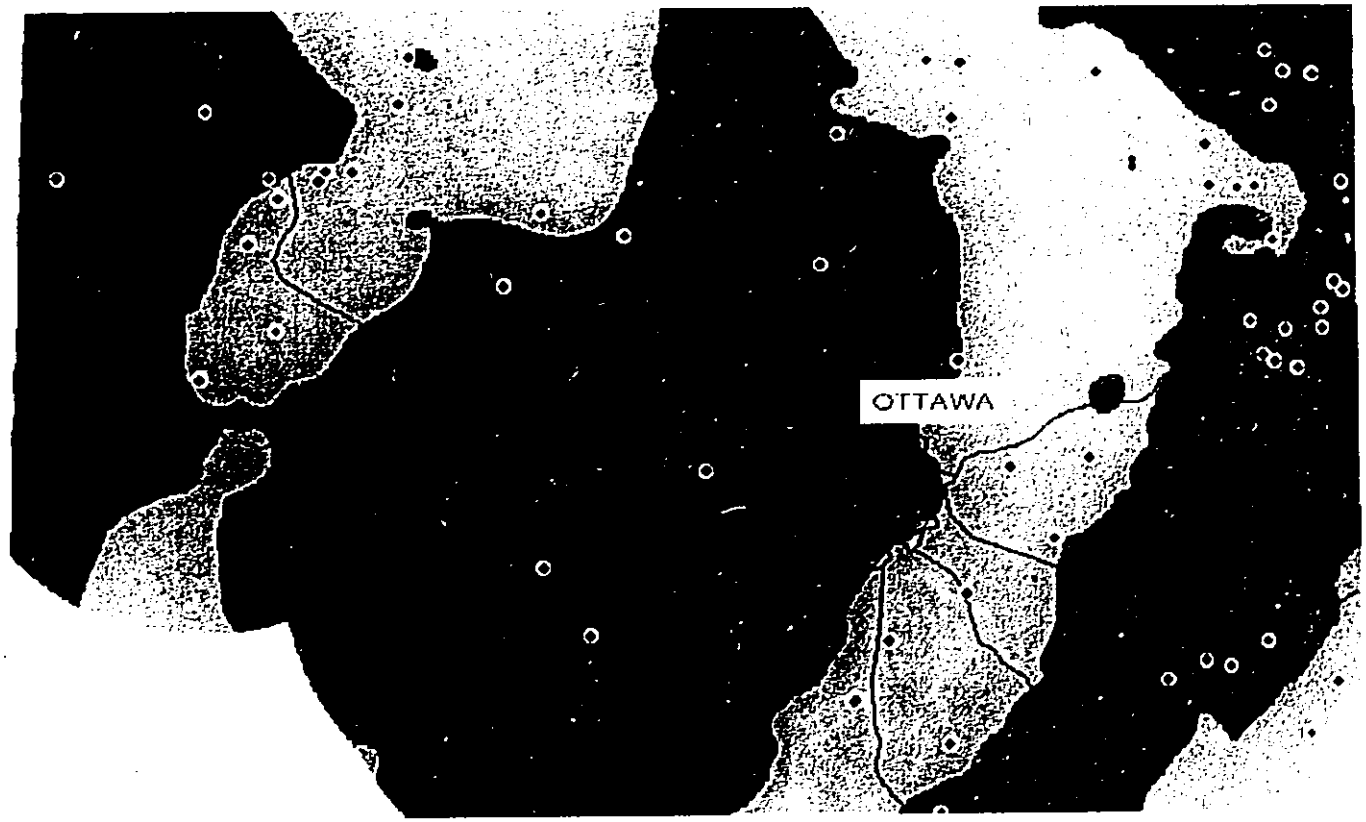

LEGEND

- < 27 mgal (Pattern absent)
- ≥ -27 mgal
- Epicentre (< 2.0 mN)
- Epicentre (≥ 2.0 mN)
- Highway

25 km

FIG. 24. Magnetic anomaly map composed of nine (9) classes derived by reclassifying the 255-class magnetic anomaly map originally in raster format.

MAGNETIC ANOMALY MAP

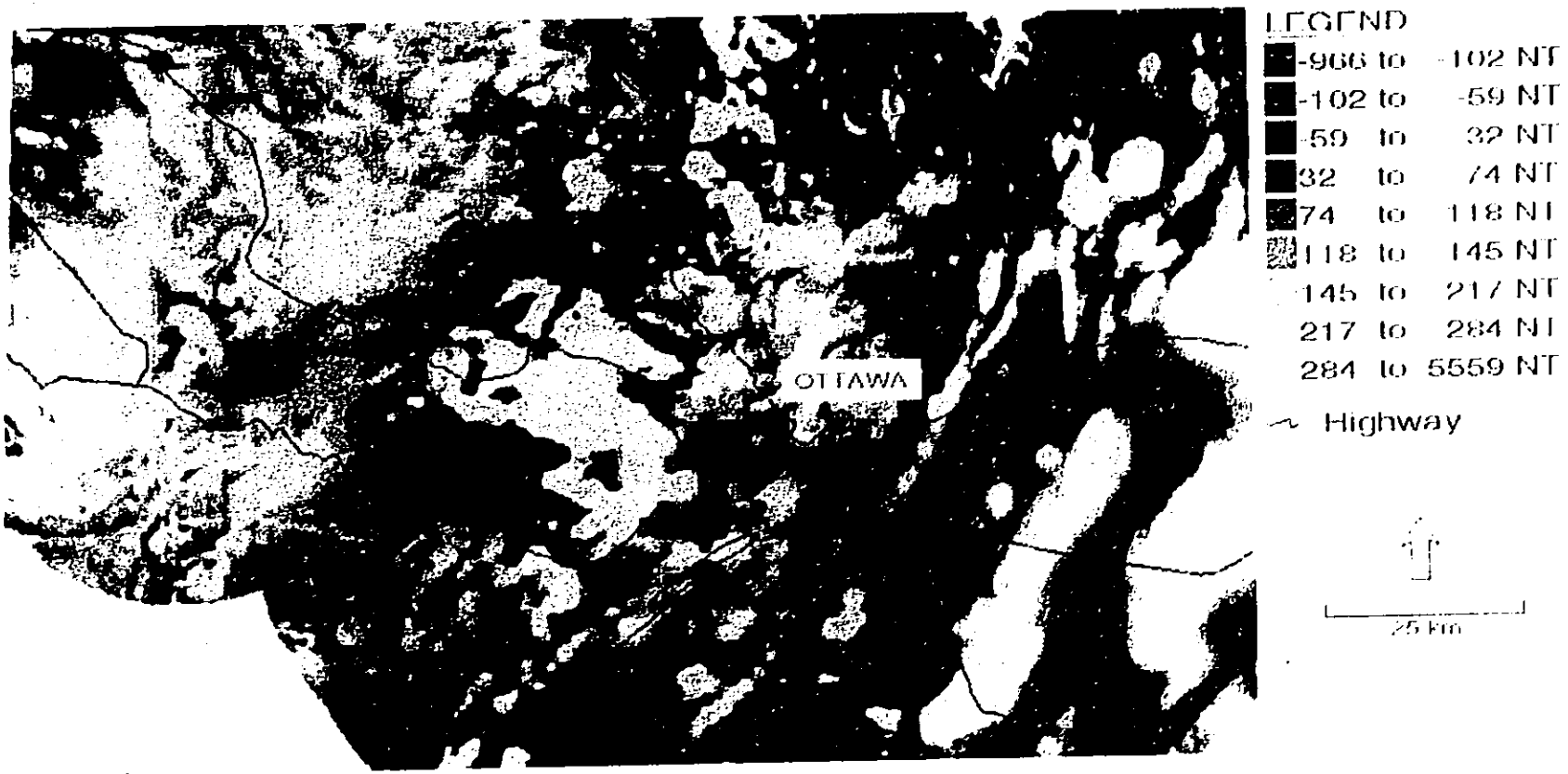

TABLE 7. Weighting parameters for magnetic map.

Magnetic Value (NT)	Area [1]	Points [2]		W^+ [3]		$s(W^+)$ [4]		W^- [5]		$s(W^-)$ [6]		C [7]		s(C) [8]		Stud(C) [9]	
-966 to -102	6952	62	(39)														
-102 to -59	5858	48	(32)	-0.086	(-0.027)	0.145	(0.177)	0.365	(0.133)	0.269	(0.379)	-0.451	(-0.159)	0.306	(0.419)	-1.475	(-0.381)
-59 to 32	5411	45	(30)	-0.071	(-0.019)	0.150	(0.183)	0.215	(0.040)	0.244	(0.334)	-0.285	(-0.052)	0.286	(0.381)	-0.996	(-0.137)
32 to 74	4318	38	(26)	-0.013	(0.071)	0.163	(0.197)	0.022	(-0.129)	0.205	(0.278)	-0.035	(0.200)	0.262	(0.341)	-0.134	(0.587)
74 to 118	3795	37	(26)	0.090	(0.201)	0.165	(0.197)	-0.120	(-0.311)	0.201	(0.278)	0.210	(0.512)	0.260	(0.341)	0.807	(1.503)
118 to 145	3266	35	(25)	0.185	(0.313)	0.170	(0.201)	-0.198	(-0.392)	0.193	(0.268)	0.384	(0.704)	0.257	(0.335)	1.491	(2.105)
145 to 217	2933	34	(25)	0.265	(0.421)	0.173	(0.201)	-0.249	(-0.479)	0.190	(0.268)	0.513	(0.900)	0.256	(0.335)	2.003	(2.687)
217 to 284	2144	23	(16)	0.186	(0.287)	0.210	(0.251)	-0.096	(-0.160)	0.161	(0.209)	0.282	(0.447)	0.264	(0.327)	1.066	(1.368)
284 to 5559	1572	18	(14)	0.252	(0.465)	0.237	(0.269)	-0.087	(-0.189)	0.153	(0.201)	0.339	(0.654)	0.281	(0.335)	1.207	(1.953)

Total no of points 62 (39)
Area of unit cell 2 sq kms
Total area 6952.55 unit cells or 13905.10 sq kms

1 Area enclosing region with magnetic value greater than or equal to the specified magnetic interval. (Area expressed in unit cells).
2 Number of epicentres occurring in region with magnetic value greater than or equal to the specified magnetic interval.
3 W^+ - Positive weight
4 $s(W^+)$ - Standard deviation of W^+.
5 W^- - Negative weight
6 $s(W^-)$ - Standard deviation of negative weight.
7 C - Contrast
8 s(C) - Standard deviation of contrast.
9 Stud(C) - Studentized contrast
Note: Values in parentheses are for the the 39-epicentre case.

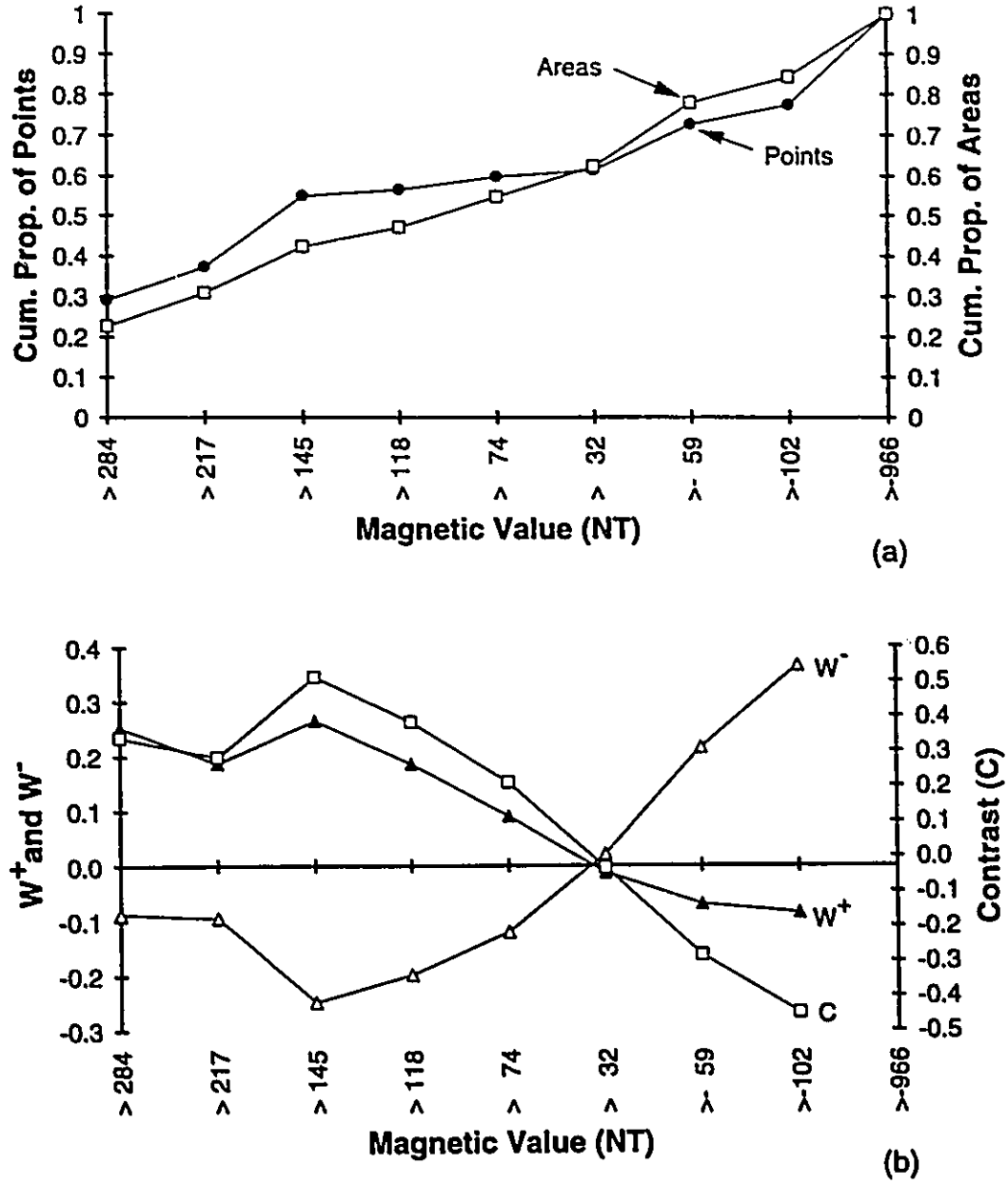

FIG. 25. (a) Cumulative proportion of points and areas for magnetics. (b) Plot of contrast (C), W^+ and W^- for each of the nine (9) classes of the magnetic anomaly map.

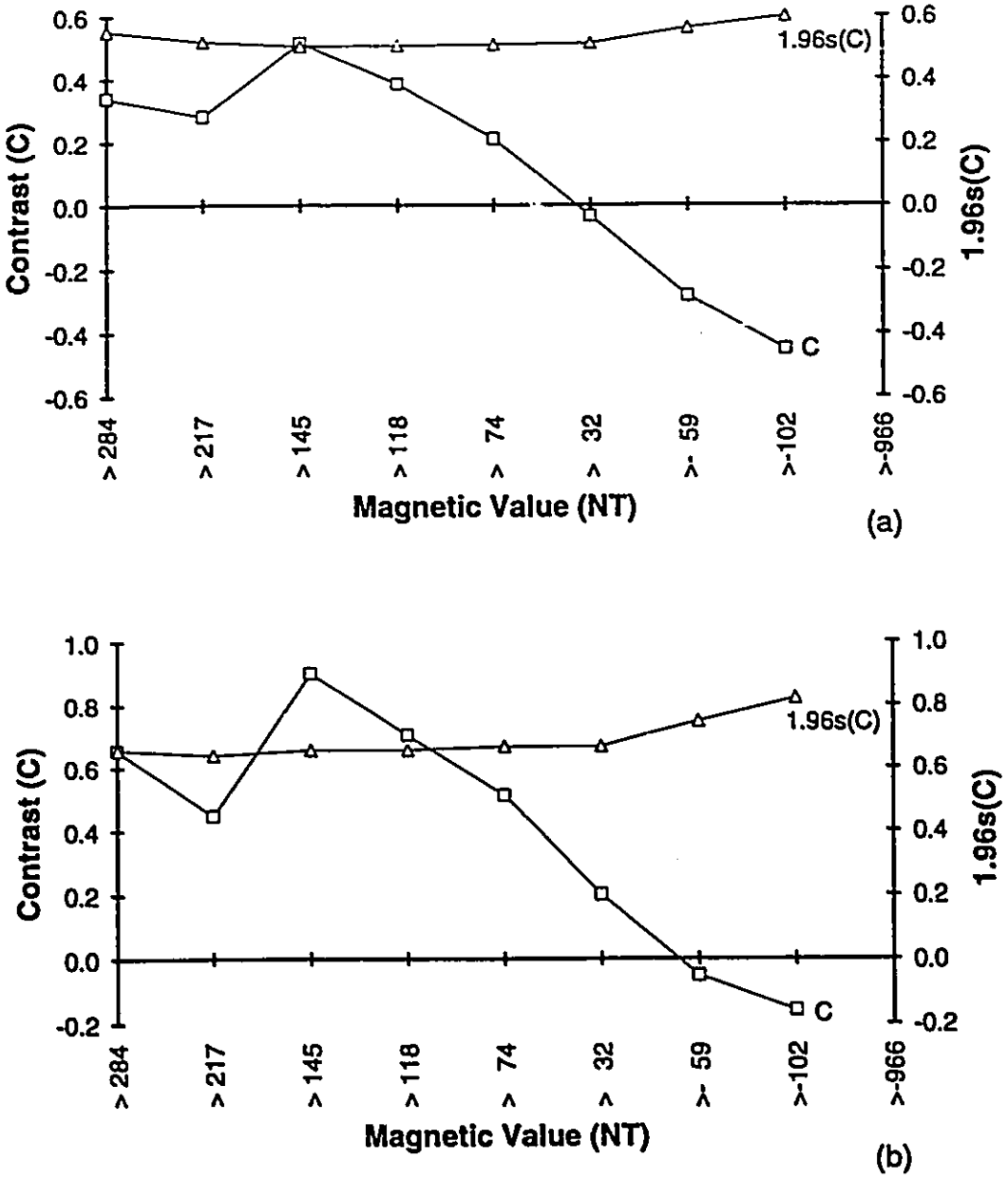

FIG. 26. Plots of contrast (C) and 1.96 X standard deviation (s[C]) for each of the nine (9) classes of the magnetic anomaly map for the 62-epicentre-case (a) and 39-epicentre case (b).

FIG. 27. Binary map derived from magnetic anomaly map, with epicentres superimposed.

BINARY MAP FOR MAGNETICS

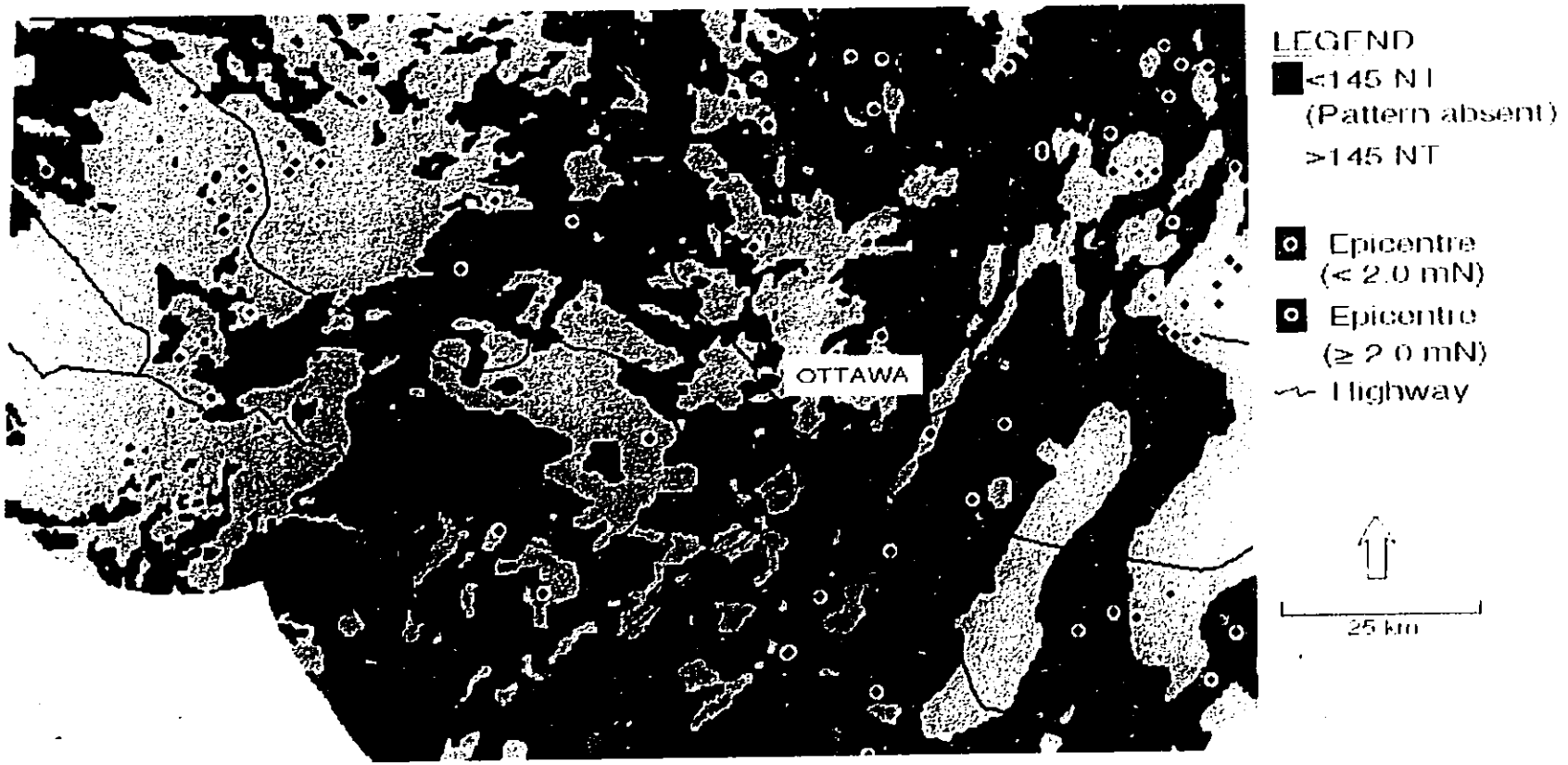

5.1.3 Geophysical Lineaments

Some of the structures within the Ottawa-Bonnechère graben that are shown in the geological map (Appendix D) are evident from the aeromagnetic anomaly map (Fig. 24). Traces of faults which have not been related to faults in geological maps and extensions of previously mapped structures can be recognized from the magnetic anomaly map. Even in sediment-covered portions of the area, faint contrast in magnetic response between downfaulted and upthrown blocks is also evident (Fig. 24). Some major buried structures are prominent in the southeastern portion of the study area where thick Ordovician sediments overlie basement rocks. Steep horizontal gradients in the gravity anomaly map of the study area (Fig. 20) delineate basement structures some of which more or less correspond to those delineated through the magnetic anomaly map. For near-surface bodies with almost vertical contacts, the lineaments corresponding to the maximum horizontal gradients of gravity occur approximately over boundaries (Dobrin and Savit 1988). This is not the case if the dip of a contact is less steep. Following Cullota *et al.*'s (1990) analytical model of structures across the terranes, the lineaments delineated in the eastern portion of the study area are expected to lie more or less directly over the structures while deviations that depend on the steepness of the contact are expected on the western side. To a certain extent, this

limits the validity of the spatial association analysis. Circular and irregular areas of high and low gravity are also common. Faint anomaly differences characterize blocks across normal faults within the graben (Fig. 20).

Estimates of contrast values for each of the gravity lineament orientation classes and buffer zones were compared. Fig. 28 indicate significant spatial association between seismicity and gravity lineament orientation class 4 (27° to 45°). Fig. 29 shows the buffer zone map for gravity lineament orientation class 4. Weighting parameters for each of the buffer zones of the gravity lineament orientation class 4 are summarized in Table 8. The difference between the cumulative proportion of points and areas for each of the buffer zones is shown in Fig. 30a. Peaks in contrast values correspond to the 13 km and 7 km buffer zones (Fig. 30b; Fig. 31a). Buffer 7 as cut-off class is preferred because of its proximity and considering that the epicentral determinations are generally not accurate to more than a few kilometres (Wetmiller *et al.* 1989). The error could be in the order of 1-5 kms and could be as much as 20 km or more in some cases. The peak in contrast value for class 7 for the 39-epicentre case (Fig. 31b) demonstrates that location errors and/or non-detection of weaker (<2.0 mN) earthquakes do not affect results for the main set. Fig. 32 shows visually the spatial association between epicentres and a binary map showing areas

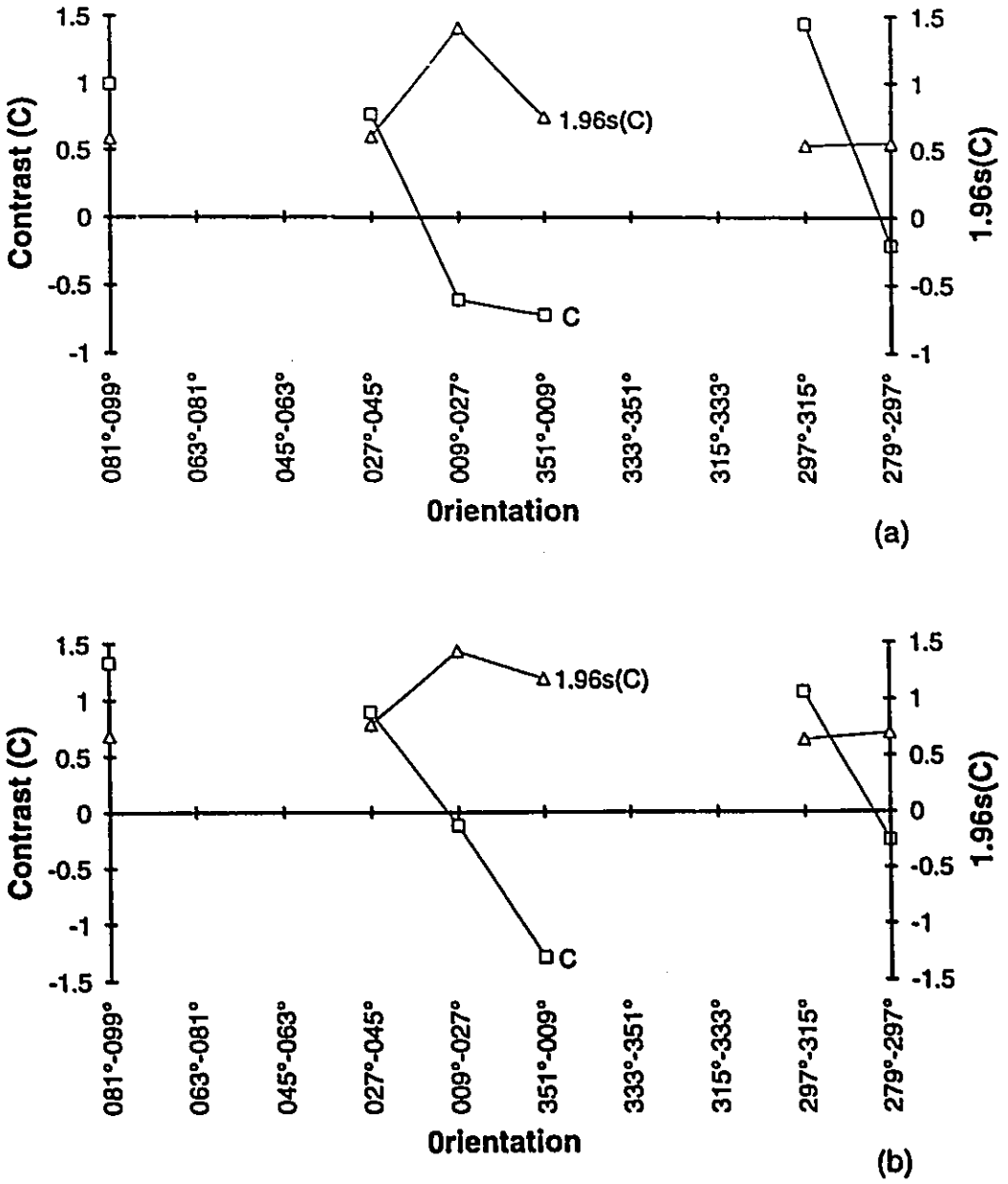

FIG. 28. Cumulative contrast (C) values and corresponding standard deviations (x1.96) for each of the gravity lineament orientation classes for the 62-epicentre case (a) and 39-epicentre case (b).

FIG. 29. Buffer zones around gravity lineaments oriented between 27° and 45°.

EPICENTRES AND NE(27°-45°) GRAVITY LINEAMENT BUFFER ZONES

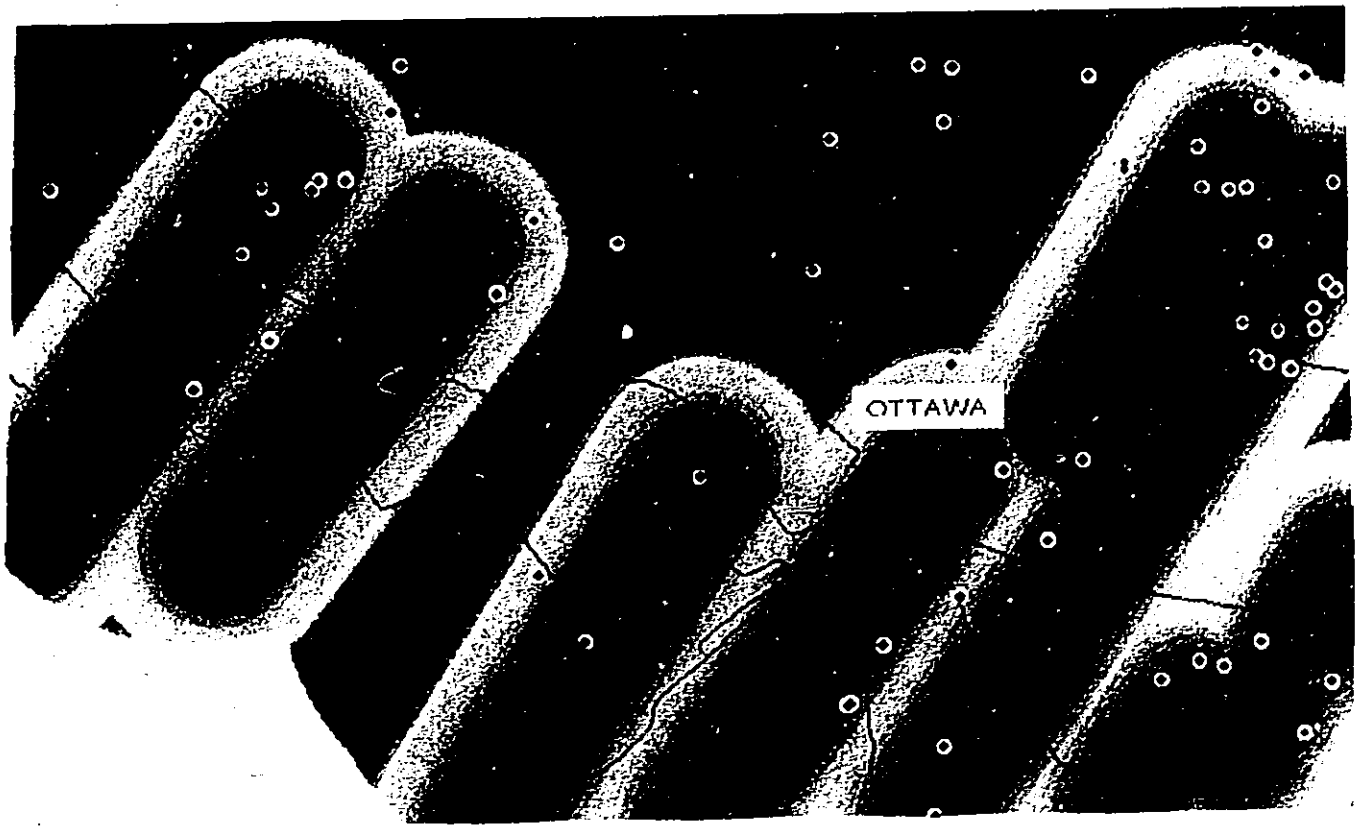

LEGEND

- 0 - 1 km
- 1 - 2 km
- 2 - 3 km
- 3 - 4 km
- 4 - 5 km
- 5 - 6 km
- 6 - 7 km
- 7 - 8 km
- 8 - 9 km
- 9 - 10 km
- 10 - 11 km
- 11 - 12 km
- 12 - 13 km
- 13 - 14 km
- 14 - 15 km
- >15 km

- Epicentre (< 2.0 mN)
- Epicentre (≥ 2.0 mN)
- Lineament
- Highway

25 km

TABLE 8. Weighting parameters for northeast (27°-45°) gravity lineament buffer zones.

Buffer Radius (km)	Area [1]	Points [2]		W^+ [3]		$s(W^+)$ [4]		W^- [5]		$s(W^-)$ [6]		C [7]		s(C) [8]		Stud(C) [9]	
1	392	4	(3)	0.135	(0.312)	0.503	(0.580)	-0.009	(-0.022)	0.132	(0.167)	0.144	(0.334)	0.520	(0.603)	0.277	(0.554)
2	783	7	(6)	0.002	(0.313)	0.380	(0.410)	-0.000	(-0.048)	0.135	(0.175)	0.002	(0.361)	0.403	(0.445)	0.004	(0.810)
3	1182	12	(10)	0.130	(0.413)	0.290	(0.318)	-0.029	(-0.110)	0.142	(0.186)	0.159	(0.524)	0.323	(0.368)	0.493	(1.422)
4	1603	15	(11)	0.048	(0.203)	0.259	(0.303)	-0.015	(-0.070)	0.147	(0.190)	0.063	(0.272)	0.298	(0.357)	0.212	(0.762)
5	2026	22	(16)	0.199	(0.344)	0.214	(0.251)	-0.095	(-0.185)	0.159	(0.209)	0.293	(0.529)	0.267	(0.327)	1.100	(1.619)
6	2431	28	(18)	0.258	(0.279)	0.190	(0.237)	-0.172	(-0.190)	0.172	(0.219)	0.430	(0.469)	0.256	(0.322)	1.677	(1.455)
7	2824	37	(22)	0.389	(0.330)	0.166	(0.214)	-0.390	(-0.311)	0.201	(0.243)	0.779	(0.641)	0.260	(0.324)	2.994	(1.979)
8	3218	40	(24)	0.336	(0.287)	0.159	(0.205)	-0.418	(-0.336)	0.214	(0.259)	0.753	(0.622)	0.267	(0.330)	2.826	(1.886)
9	3618	41	(25)	0.242	(0.210)	0.157	(0.201)	-0.351	(-0.291)	0.219	(0.268)	0.593	(0.501)	0.269	(0.335)	2.199	(1.497)
10	3989	44	(28)	0.215	(0.226)	0.152	(0.190)	-0.387	(-0.415)	0.236	(0.302)	0.602	(0.640)	0.281	(0.357)	2.142	(1.795)
11	4285	48	(31)	0.230	(0.256)	0.145	(0.180)	-0.534	(-0.629)	0.268	(0.354)	0.764	(0.885)	0.305	(0.397)	2.508	(2.227)
12	4502	50	(32)	0.222	(0.238)	0.142	(0.177)	-0.604	(-0.678)	0.289	(0.379)	0.825	(0.916)	0.322	(0.418)	2.559	(2.191)
13	4703	53	(34)	0.236	(0.255)	0.138	(0.172)	-0.806	(-0.929)	0.334	(0.448)	1.043	(1.184)	0.361	(0.480)	2.885	(2.469)
14	4878	53	(34)	0.199	(0.219)	0.138	(0.172)	-0.725	(-0.848)	0.334	(0.448)	0.925	(1.066)	0.362	(0.480)	2.558	(2.223)
15	5046	53	(34)	0.165	(0.184)	0.138	(0.172)	-0.640	(-0.763)	0.334	(0.448)	0.805	(0.948)	0.362	(0.480)	2.228	(1.975)
16	6952	62	(39)														

Total no of points 62 (39)
Area of unit cell 2 sq kms
Total area 6952.70 unit cells or 13905.40 sq kms

1 Area enclosing region the outer limit of which is defined by specified radius representing distance from lineament. (Area expressed in unit cells).
2 Number of epicentres occurring in region within a distance equal to or less than the specified radius.
3 W^+ - Positive weight
4 $s(W^+)$ - Standard deviation of W^+.
5 W^- - Negative weight
6 $s(W^-)$ - Standard deviation of negative weight.
7 C - Contrast
8 s(C) - Standard deviation of contrast.
9 Stud(C) - Studentized contrast
Note: Values in parentheses are for the the 39-epicentre case.

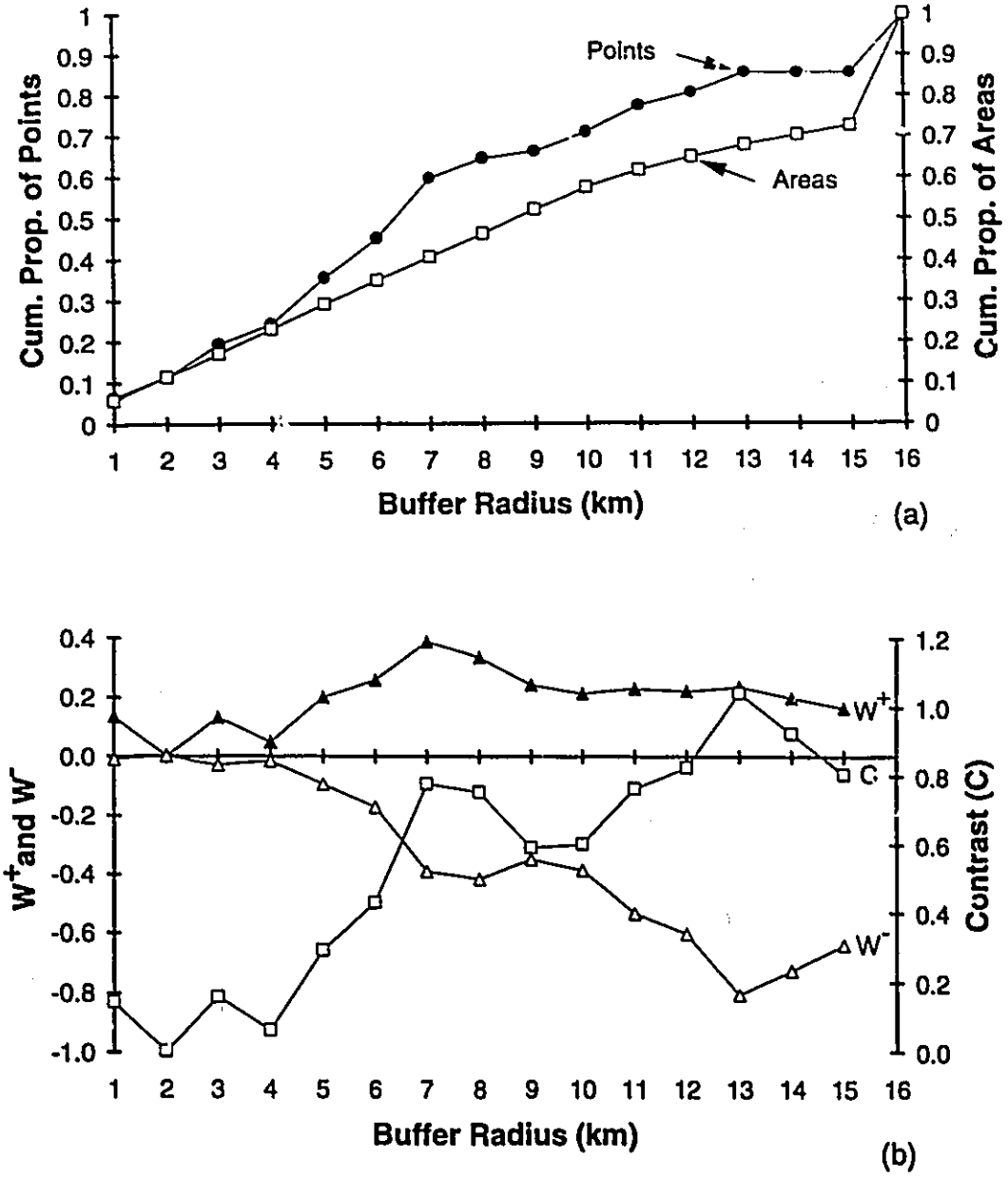

FIG. 30. (a) Cumulative proportion of points and areas for buffer zones of class 4 (27° and 45°) gravity lineaments. (b) Plot of contrast (C), W^+ and W^- for each of the buffer zones.

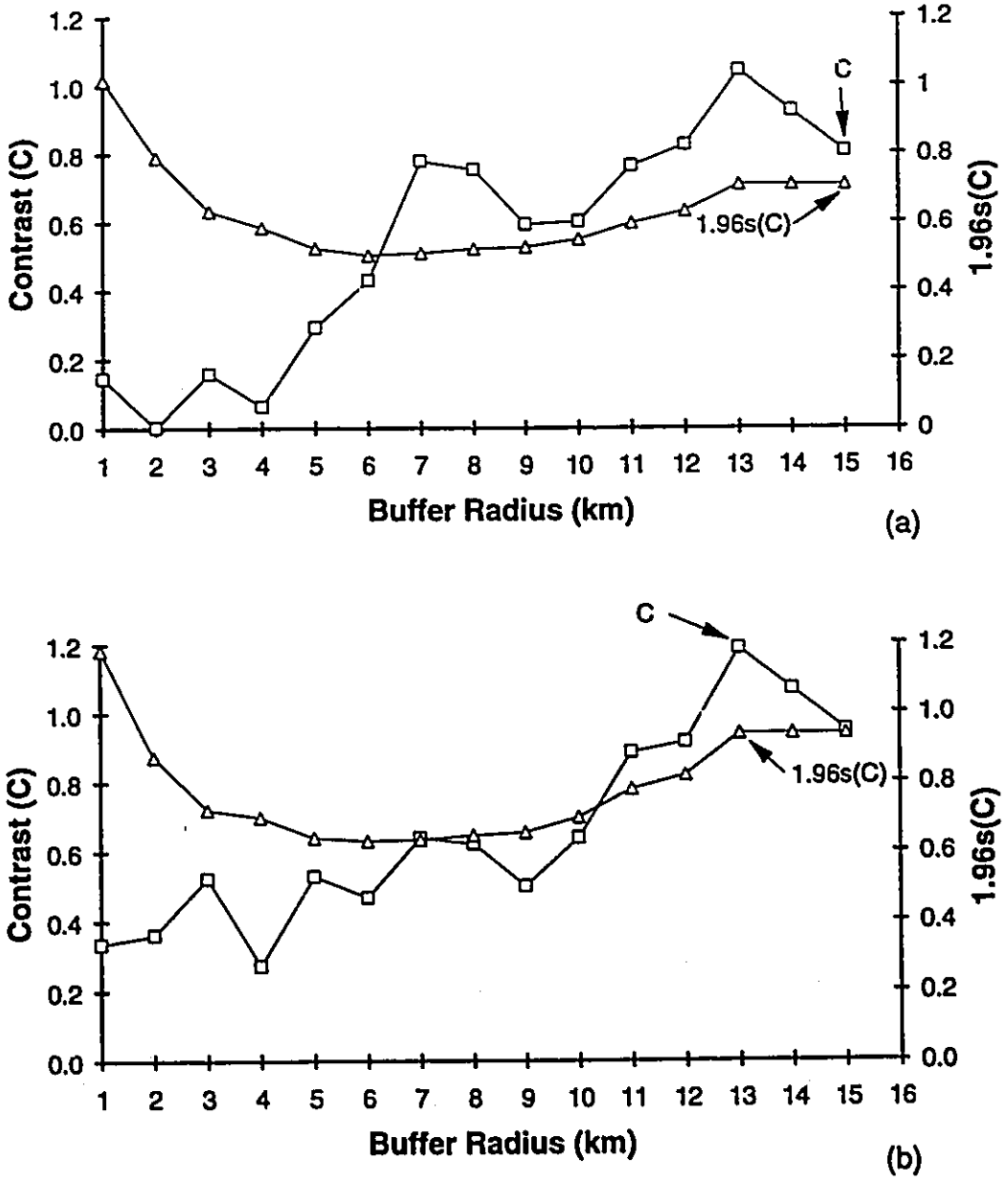

FIG. 31. Plots of contrast (C) and 1.96 X standard deviation (s[C]) for each of the class 4 (27° and 45°) gravity lineament buffer zones for the 62-epicentre case (a) and 39-epicentre case (b).

FIG. 32. Spatial association between seismicity and class 2 (pattern present) of the binary map for gravity lineament orientation class 4 (27° to 45°).

BINARY MAP FOR NE (27^0-45^0) GRAVITY LINEAMENTS

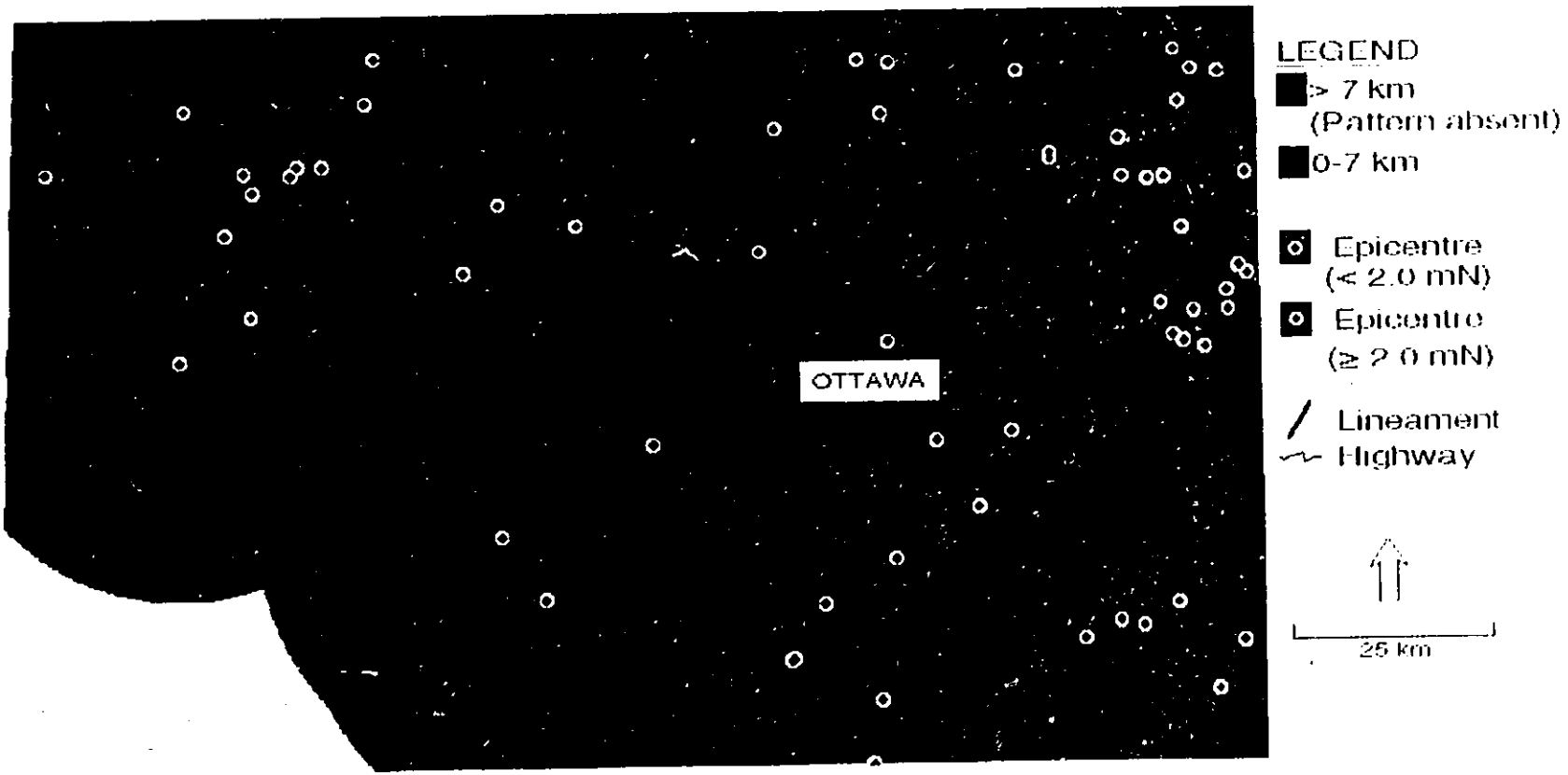

closer than 7 km to the nearest lineament. Spatial association is also estimated for orientation classes 1 (81° to 99° azimuth) and 9 (297° to 315° azimuth). No binary maps for these two classes are presented here, however, due to violation of conditional independence that results if these are included in the final combined model.

Comparison of weighting parameters computed for each of the magnetic lineament orientation classes and buffer zones indicate results similar to that for gravity lineaments (i.e. strong correlations between earthquake occurrence and orientation classes 1 (81° to 99°), 4 (27° to 45°) and 9 (297° to 315°). No binary map is presented for magnetic lineaments. Inclusion of binary maps for magnetic lineaments as evidence results in violation of conditional independence.

5.2 Spatial Association Among Seismicity and Lithotectonic Units, Lineaments Delineated From Satellite Imagery and Geological Map, and Intersections of Faults

Possible spatial association between seismicity and lithology was determined but no convincing result was obtained for any of the units except for unit Archean or Proterozoic hornblende gneiss (Appendix D). This association however is dubious as the area involved is limited in extent and the clustering of earthquakes near the unit indicate a

more probable control other than lithology (e.g. lineament intersection). Appendix F shows the major lithotectonic units of the study area and is based on published descriptions of the area's lithotectonic subdivisions (e.g. Corriveau 1990; Davidson 1986; Brock and Moore 1983; Moore 1982; Wynne-Edwards 1972). For the main set (62 epicentres), the only unit having significant correlation with seismicity is the Frontenac Terrane. For the 39-epicentre case, however, contrast value for the Frontenac terrane is not significant at 95% confidence level.

Although initial estimates suggest high spatial correlation between seismicity and orientation classes 4 (27 to 45°) and 6 (351° to 09°) and 5 (09° to 27°), no binary maps for lineaments from geological map and LANDSAT imagery (Appendix E and F) are included as evidence. The high density of lineaments (i.e. close spacing between lineaments), especially within the Frontenac terrane where most of the spatially associated lineaments are situated, and the known error associated with locating epicentres are overwhelming reasons to invalidate any association established between this set of lineaments and seismicity. Most of the 62 earthquake events recorded between 1983 and 1993 and within the study are deep-seated. Depths cluster around 15-20 kms with the deepest earthquakes occurring at 27 km (Table 3; Fig. 33). It is highly unlikely that a significant number of earthquakes

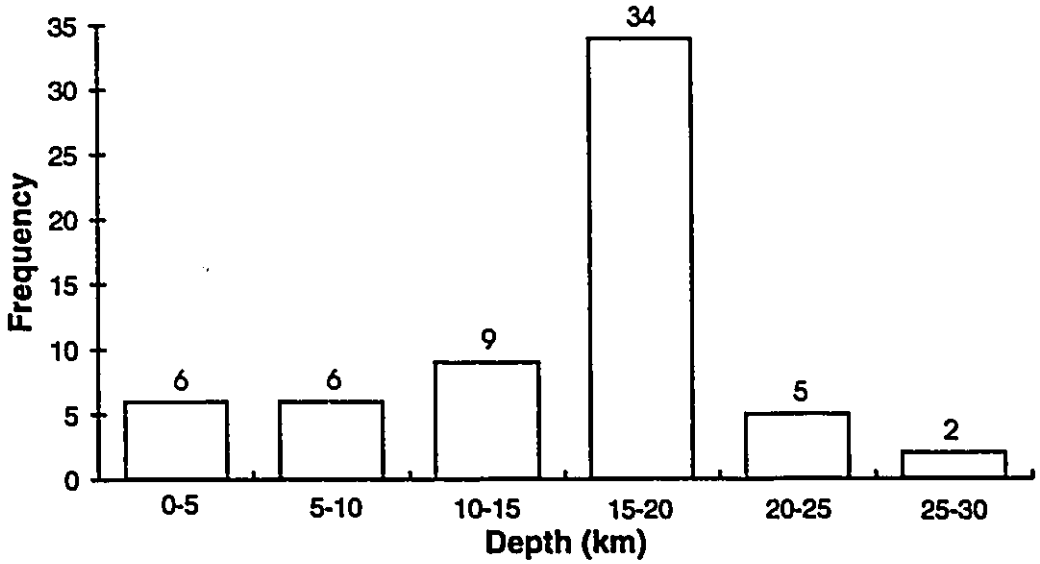

FIG. 33. Bar graph showing frequency distribution of earthquake depths.

are associated with superficial, non-throughgoing faults.

Several large and moderate earthquakes near the study area have occurred at the intersection cf major faults and examples of these, as enumerated by Wallach (1990), are the Montreal (est. M=5.6-6.0), Grand Banks (M=7.2), Timiskaming (M=6.25), Attica (M=5.8) and Cornwall-Massena earthquakes (M=5.9). The spatial association of some intraplate and interplate earthquakes with the area near the intersection of two (2) or more faults is explained by the intersection model of Andrews (1989). According to the model, previous slips along the faults render fault junctions progressively stronger barriers that later slips have to be accommodated by fresh fractures initiated in the most highly stressed region (i.e. region near junctions). Intersections of major lineaments were drawn from each of the lineament maps for gravity, magnetic, combined gravity and magnetic, geology and combined gravity, magnetic and geology. Fifteen (15) buffer zones were drawn using 1 km as radius increment. Although results are not convincing, comparison of results of contrast calculations for each of the buffer zones of the five (5) lineament intersection sets indicate gravity lineament intersections as the most spatially associated with seismicity.

5.3 Unique Conditions and Posterior Probabilities

Eight (8) binary maps, namely, gravity anomaly, magnetic anomaly, gravity lineaments (81° to 99°, 27° to 45° and 297° to 315°), magnetic lineaments (81° to 99°, 27° to 45° and 297° to 315°) were superimposed on top of each using SPAN's overlay function. Of the eight (8) binary maps, only three (3) maps (gravity, magnetic and northeast gravity lineaments) can be used as inputs without violating the assumption of conditional independence. Table 9 shows the results of the test for conditional independence. Since no G^2 value is greater than 3.84 (chi-square value the probability of which being equalled or exceeded by calculated G^2 is 5%), all pair combinations of the three (3) input binary maps passed the conditional independence test. This would not be the case if one or more of the other binary patterns were to be included. If binary maps that are highly correlated are used at the same time and, therefore, conditional independence is not satisfied, posterior probability values will be unrealistically large in some areas. A total of nine (9) map classes were derived from overlaying the gravity anomaly map, magnetic anomaly map and northeast (27°-45°) gravity lineaments. A unique conditions table (Table 10) shows the binary map class combinations for each unique conditions map class. Class 1 for each input binary map is for pattern absent while class 2 is for pattern present. The unique conditions map is presented in Fig. 34. Observed epicentres were counted after appending the unique conditions map classes on the epicentre point table (Table

TABLE 9. Partial conditional independence test 1 (points) results. (95 % fractile of theoretical chi-square is 3.84).

		A and B		A and ~B		~A and B		~A and ~B		
A	B	O	E	O	E	O	E	O	E	G^2
1	2	20(11)	18.6(10.2)	12(8)	13.4(8.8)	16(10)	17.4(10.8)	14(10)	12.6(9.2)	0.53(.24)
1	3	15(12)	18.1(12.7)	17(7)	13.9(6.3)	20(14)	16.9(13.3)	10(6)	13.1(6.7)	2.49(.21)
2	3	21(14)	20.3(14.0)	15(7)	15.7(7.0)	14(12)	14.7(12.0)	12(6)	11.3(6.0)	0.12(.00)

1 Gravity
2 Gravity Lineaments
3 Magnetics

O - Observed
E - Expected

Note: This table shows the number of epicentres observed and expected under independence, for two-by-two comparisons of binary maps. The largest value of G^2=2.49 indicates that this pair is closer to failing the conditional independence test than the other pairs, but is still less than 3.84, the critical value of chi-square at 95% probability and 1 degree of freedom.

TABLE 10. Unique conditions table for the three (3) input binary maps.

Area	Unique Conditions Map Class	Gravity	Gravity Lineaments	Magnetics	Ppost	(Ppost) X (Area)	Observed Epicentres	Residuals
1698.0330	1	1	1	1	0.0034	5.8188	6	0.1812
847.1298	2	2	1	1	0.0073	6.2238	6	-0.2238
866.4256	4	1	2	1	0.0074	6.4419	4	-2.4419
989.4467	5	1	2	2	0.0124	12.2315	12	-0.2315
1083.6580	3	1	1	2	0.0057	6.1909	8	1.8091
499.1000	6	2	1	2	0.0122	6.0971	6	-0.0971
361.6943	8	2	2	2	0.0262	9.4889	9	-0.4889
607.0789	7	2	2	1	0.0159	9.6328	11	1.3672
0.1770	9	2	1	0	0.0094	0.0017	0	-0.0017
Prior Probability		0.008917			Total	62.1274	62	
Prior Odds		0.008998						

FIG. 34. Unique conditions map generated by overlaying binary maps for gravity, magnetics and northeast (27° to 45°) gravity lineaments.

UNIQUE CONDITIONS

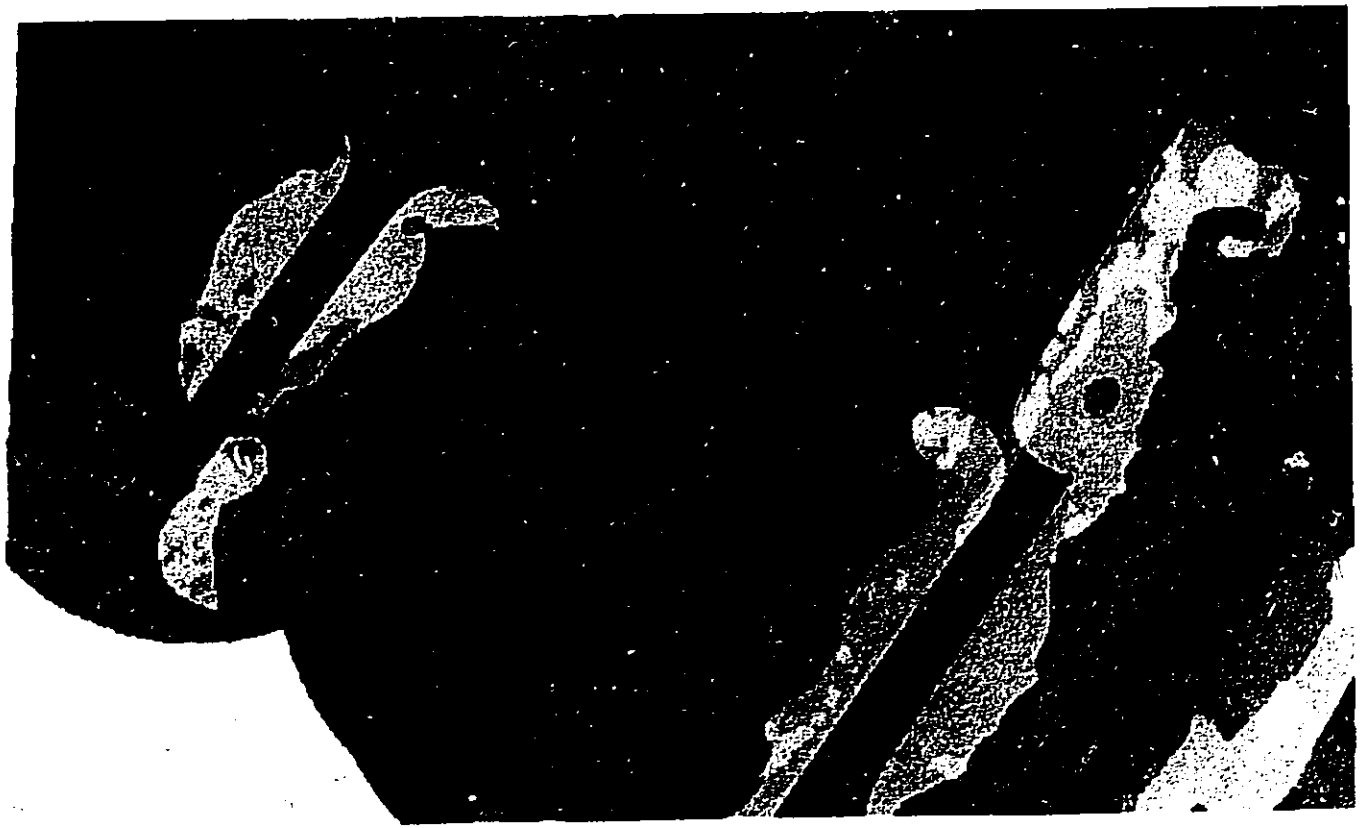

LEGEND

	G	L	M
1-	1	1	1
2-	2	1	1
3-	1	1	2
4-	1	2	1
5-	1	2	2
6-	2	1	2
7-	2	2	1
8-	2	2	2
9-	2	1	0

G - Gravity
L - NE Gravity Lineament
M - Magnetic

1 - Absence of Pattern
2 - Presence of Pattern

25 km

11).

A summary of the weighting parameters for the three (3) binary maps used as inputs in the overlaying process is presented in Table 12. Posterior probability (Ppost) values in Table 10 were based on weights contribution of each layer pattern. Posterior probability indicate the probability of occurrence of earthquakes per unit area over the eleven-year period of earthquake record. Fig. 35 is the posterior probability map generated by reclassifying the 9 unique condition classes into four classes according to the scheme presented in the legend. Posterior probability estimates for all units of the posterior probability map were found to be significant at 95% confidence level (Table 13). Differences between observed and predicted number of epicentres were noted to identify overlap areas characterized by good or bad prediction (Fig. 36). A good overall goodness-of-fit, however, is indicated by the very small difference between the sum of the observed epicentres and sum of the predicted epicentres, calculated as Ppost X Area in Table 10. A good agreement between the observed epicentres and epicentres predicted by the model is also illustrated by Fig. 37. The square of the correlation coefficient implies that the association between observed and predicted epicentres accounts for 89% of the total variability of the data. In the posterior probability map, those with highest values reflect areas of

TABLE 11 . Unique conditions map classes appended on epicentre point table. Events with magnitude <2.0 mN written in bold italics.

Latitude (Degrees)	Longitude (Degrees)	Depth	Magnitude	Map Class
45.340	-76.210	18.0	2.2	3
45.537	-76.723	18.0	3.1	8
45.589	-76.611	18.0	2.4	6
45.200	***-75.750***	***14.0***	***1.7***	***7***
45.200	-75.750	14.0	4.1	7
45.202	***-75.746***	***13.7***	***1.2***	***7***
45.083	-75.621	18.0	2.8	3
45.156	-75.607	8.5	3.3	7
45.224	-75.284	8.7	2.9	4
45.244	-75.227	13.5	2.5	4
45.238	***-75.190***	***18.0***	***1.3***	***5***
45.269	-76.139	14.2	2.1	5
45.264	***-75.697***	***18.0***	***1.7***	***7***
45.445	***-75.971***	***20.3***	***1.8***	***5***
45.316	***-75.584***	***20.7***	***1.5***	***2***
45.374	***-75.452***	***18.0***	***1.2***	***7***
45.264	-75.135	18.0	2.0	5
45.450	***-75.520***	***1.0***	***1.7***	***8***
45.460	***-75.400***	***1.0***	***1.7***	***7***
45.562	***-75.597***	***1.0***	***1.8***	***3***
45.568	***-75.141***	***18.0***	***1.8***	***4***
45.561	-75.124	20.3	3.1	5
45.604	-75.160	18.0	2.3	5
45.749	***-76.941***	***18.0***	***1.5***	***1***
45.680	-76.654	18.0	3.1	8
45.730	-76.610	18.0	2.7	8
45.752	-76.625	18.0	2.0	5
45.750	***-76.550***	***18.0***	***1.6***	***8***
45.760	***-76.540***	***18.0***	***1.8***	***8***
45.760	-76.500	18.0	2.2	6
45.639	-76.273	18.0	2.0	1
45.717	-76.219	18.0	2.3	6
45.822	-76.722	18.0	2.0	3
45.832	-76.434	18.0	2.3	6
45.883	-76.420	18.0	2.9	6
45.693	-76.094	25.4	2.0	1
45.663	-75.802	27.0	2.7	3
45.804	-75.778	0.0	2.6	3
45.689	-75.125	18.0	2.2	7
45.769	-75.336	17.1	3.5	2
45.776	-75.336	21.1	3.2	2

TABLE 11 (Cont'd)

45.749	-75.220	18.1	2.2	8
45.746	-75.179	9.6	2.4	8
45.748	-75.153	16.2	2.6	8
45.793	*-75.226*	*8.7*	*1.6*	*7*
45.822	*-75.608*	*18.0*	*1.9*	*2*
45.883	*-75.646*	*7.8*	*1.0*	*2*
45.880	*-75.595*	*18.0*	*1.9*	*2*
45.870	-75.390	22.0	2.5	6
45.834	*-75.130*	*18.0*	*1.5*	*4*
45.893	-75.137	18.0	2.6	1
45.166	-75.071	10.0	3.2	7
45.220	-75.030	5.0	2.7	7
45.554	*-75.089*	*13.7*	*1.8*	*3*
45.595	-75.107	03.8	2.5	5
45.596	-75.052	18.3	2.0	3
45.618	-75.054	12.6	3.1	5
45.637	-75.021	1.0	2.0	5
45.645	*-75.034*	*18.0*	*1.5*	*5*
45.752	*-75.023*	*18.0*	*1.7*	*5*
45.868	*-75.066*	*18.0*	*1.6*	*1*
45.871	-75.110	10.6	3.1	1

TABLE 12. Summary of weighting parameters for the three (3) input maps.

	W^+ [1]		$s(W^+)$ [2]		W^- [3]		$s(W^-)$ [4]		C [5]		s(C) [6]		Stud(C) [7]	
Magnetics	0.2647	(0.4210)	0.1725	(0.2009)	-0.2487	(-0.4785)	0.1896	(0.2677)	0.5134	(0.8995)	0.2564	(0.3347)	2.0027	(2.6874)
Gravity	0.4432	(0.3831)	0.1780	(0.2304)	-0.3234	(-0.2642)	0.1832	(0.2241)	0.7666	(0.6473)	0.2554	(0.3214)	3.0015	(2.0142)
Gravity Lineaments	0.3888	(0.3304)	0.1655	(0.2140)	-0.3898	(-0.3105)	0.2006	(0.2430)	0.7786	(0.6410)	0.2601	(0.3238)	2.9940	(1.9792)

1 W^+ - Positive weight
2 $s(W^+)$ - Standard deviation of W^+.
3 W^- - Negative weight
4 $s(W^-)$ - Standard deviation of negative weight.
5 C - Contrast
6 s(C) - Standard deviation of contrast.
7 Stud(C) - Studentized contrast
Note: Values in parentheses are for the the 39-epicentre case.

FIG. 35. Posterior probability map generated by reclassifying the unique conditions map classes.

POSTERIOR PROBABILITY

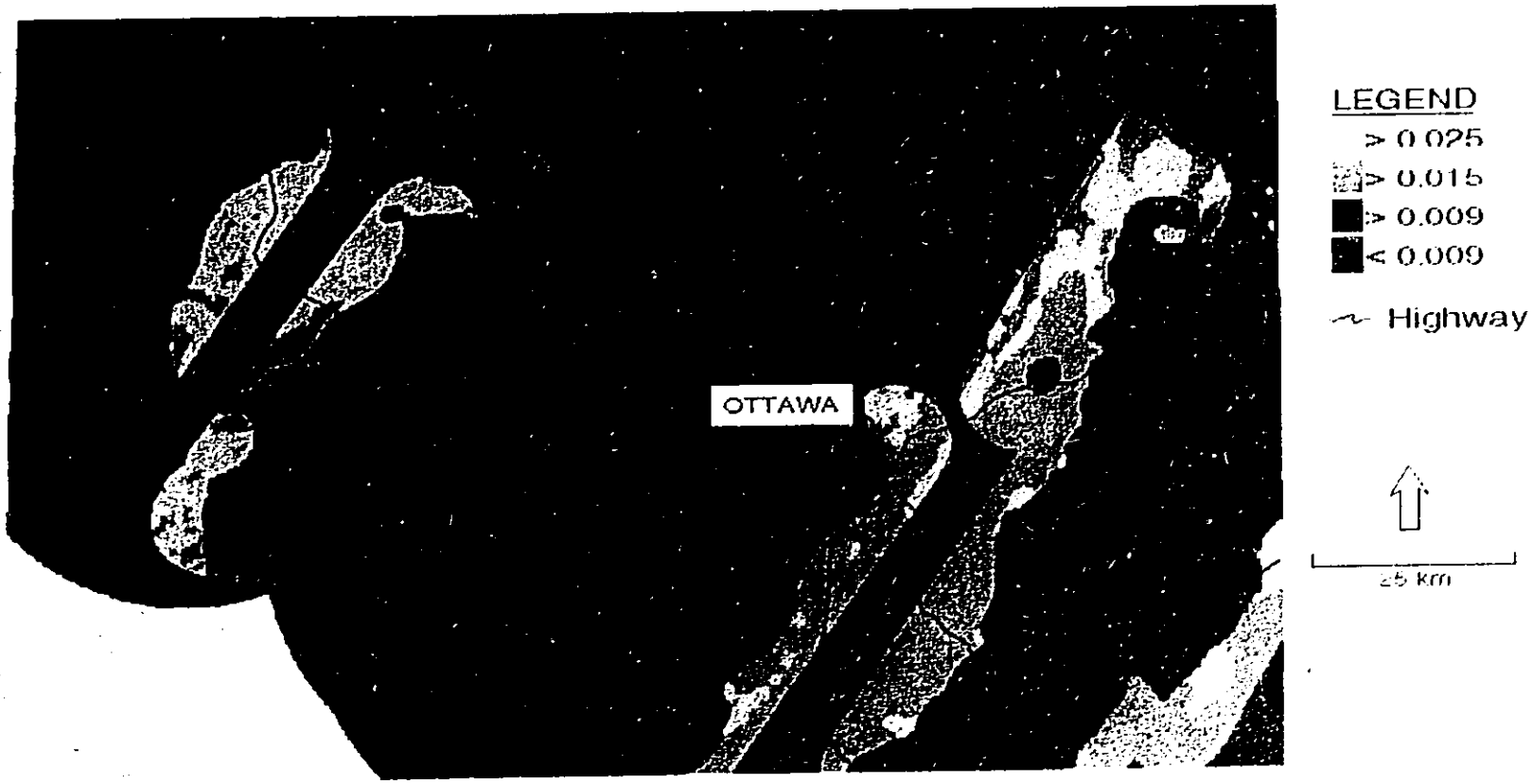

TABLE 13. Uncertainty estimates for posterior probability.

Area	Unique Conditions Map Class	Number of Epicenters	Ppost	s(Ppost) (weights)	s(Ppost) (missing)	s(total)	Stud(Ppost)
1698.0330	1	6	0.0034	0.0012	-	0.0012	2.8185
847.1298	2	6	0.0073	0.0026	-	0.0026	2.8398
866.4256	4	4	0.0074	0.0025	-	0.0025	2.9744
989.4467	5	12	0.0124	0.0040	-	0.0040	3.0594
1083.6580	3	8	0.0057	0.0020	-	0.0020	2.8905
499.1000	6	6	0.0122	0.0042	-	0.0042	2.9135
361.6943	8	9	0.0262	0.0085	-	0.0085	3.0867
607.0789	7	11	0.0159	0.0053	-	0.0053	2.9995
0.1770	9	0	0.0094	0.0028	0.0026	0.0038	2.4631
	Total	62					

FIG. 36. Residuals for overlap conditions indicating areas where good (or bad) predictions were made.

RESIDUALS

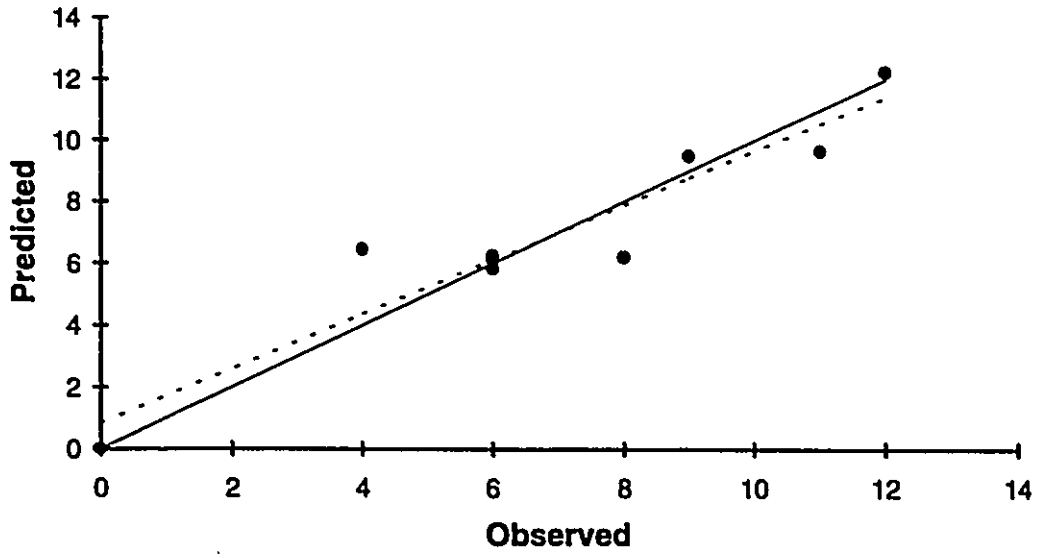

FIG. 37. Observed epicentres plotted against predicted epicentres. Dashed line represents the best-fitting line derived through regression. r^2 value is 0.89. Solid line represents one-to-one correspondence between observed and predicted epicentres (i.e line with 45° slope).

high magnetic and gravity values along and near northeast gravity lineaments.

6. SYNTHESIS AND INTERPRETATIONS

6.1 Episodes Of Faulting And Corresponding Tectonic Events

This field investigation of structural geology has for the first time documented the relative ages and history of faulting in the Ottawa-Hull area. Treatment of data gathered also made possible the determination of the evolution of the paleostress field. The paleostress field orientation in the Ottawa-Bonnechère graben has apparently rotated counterclockwise from northwest to southwest. This has caused the formation in the Ottawa-Hull area of several generations of faulting. During successive faulting periods, some pre-existing faults were reactivated.

Strike-slip faults and some normal faults that belong to the oldest generation of structures (D_1) in the area are related to northwest-southeast compression and northeast-southwest extension. The second generation of structures (D_2) consist of strike-slip faults, thrust and normal faults related to west-northwest-east-southeast compression and north-northeast-south-southwest extension. The far larger number of normal faults involved is an indication of the extension-dominated nature of D_2. D_3 structures include strike-slip, thrust, and normal faults. Compression associated with D_3 was oriented southwest-northeast to north-northeast-

south-southwest.

Absolute ages ascribed to the dykes encountered in the Ottawa-Hull area, particularly those at Francon Quarry, provide an indication as to the range of time during which the D_2 faults were formed. The emplacement of Cretaceous carbonatite dykes was associated with D_2 structures, formed under the stress regime associated with opening of the Atlantic ocean during the Mesozoic. There are no absolute age data available for the D_1 and D_3 faults. D_2 structures may be associated with the opening of the Atlantic Ocean during the Mesozoic and subsequent plate collision favourable to the development of extensional faulting at high angles to the collisional plate margins and compression causing the formation of strike-slip and thrust faults. D_3 structures are consistent with the post-Cretaceous stress field in eastern North America. D_1 structures are kinematically congruent with the compressional direction associated with the closing of the proto-Atlantic ocean during the Paleozoic, a possibility which is supported by the maximum principal stress axis calculated for D_1 strike-slip faults.

No categorical reference regarding relative ages of relatively large and well known faults within or near the Ottawa-Hull (including the Gloucester, Eardley and Hazeldean faults) recognized by Wilson (1946a) was made. Their relative

ages, however, could be inferred based on their orientations, knowledge of relative ages of studied faults and associated structures, and orientation of paleostress fields in the Ottawa-Hull area. The essentially northwest-oriented Gloucester fault could have originated as a D_1 normal or strike-slip fault and subsequently reactivated during D_2 and D_3. The east-west- to northwest-oriented Hazeldean and Eardley faults are more likely to have started mainly as normal faults during D_2 and subsequently reactivated as strike-slip faults during D_3. Further fieldwork could provide evidence of the history of movement on these regionally important faults.

6.2 Recent Crustal Deformation

The most recent tectonic movements in the Ottawa-Hull area are associated with surface deformation features such as pop-ups observed in quarry floors and offset boreholes (Fig. 38) commonly seen in roadcuts. Pop-ups reported from different locations in the Ottawa-Hull area commonly trend west-northwest to northwest (Adams 1982; Wallach 1990). Offset boreholes are observed to be displaced, by bedding-parallel slip, towards the east-northeast or west-southwest, an orientation supported by J. Wallach's (Personal communication 1992) documentation. This orientation is consistent with the orientation of the current stress field

FIG. 38. Boreholes along a roadcut at the St. Laurent Boulevard in Hull, Québec displaced by bedding-parallel slip towards the east-northeast.

in North America as determined through various methods (Yang and Aggarwal 1981; Hasegawa *et al.* 1985; McKay 1986; Adams and Basham 1989; Zoback 1992), and with the northeast trend of the greatest principal horizontal stress associated with D_3.

6.3 Possible Origin of Faults

The regional stress field that generate faults is primarily caused by plate movement (Richardson *et al.* 1979; Solomon *et al.* 1980; Hasegawa and Adams 1981; Talwani and Rajendran 1991). D_1 faults may have resulted mainly from reactivation of pre-existing basement structures that propagated into overlying sedimentary units, during compression attendant with the final closure of the Iapetus in the Paleozoic. D_2 normal faults most likely formed mainly from reactivation of D_1 fractures or basement faults, that eventually propagated into overlying sediments, perpendicular or at high angles to Paleozoic fold belts during the opening of the Atlantic Ocean in the Mesozoic. D_2 strike-slip faults may have developed obliquely with respect to the collisional front. Alternatively, some basement structures at high angles to the collisional front may have developed as strike-slip faults as a result of minute rotation of stress orientation. Similarly, D_3 strike-slip and normal faults most likely formed as a result of reactivation of pre-existing structures that are favourably oriented, during compression attendant with

compression following Mesozoic extension.

Given that the regional stress field is due primarily to plate movement (Richardson *et al.* 1979; Solomon *et al.* 1980; Hasegawa and Adams 1981; Talwani and Rajendran 1991), the local stress field may be perturbed by mechanisms and conditions such as deglaciation, continental collision, large sedimentary loads and pore pressure causing switches in the style of faulting (Talwani and Rajendran 1991). Such mechanisms may explain the co-occurrence of different types of faults during the same period of deformation. The co-occurrence of strike-slip faults and normal faults during D_1 might indicate that values of σ_1 and σ_2 were probably close. Assuming that the magnitudes of σ_1 and σ_2 were not very different during this period, the relative positions of σ_1 and σ_2 would have been very sensitive to changes due to small changes in magnitude of either horizontal or vertical stresses. For an initial state wherein σ_1 was horizontal and σ_2 was vertical, an interchange in the positions of σ_1 and σ_2 may be caused, for instance, by erosion resulting in uplift, turning the σ_2 to σ_1 and strike- slip faults to normal faults.

D_2 normal faults and strike-slip faults are more abundant than D_1 normal faults and strike-slip faults. The trends of σ_1 calculated for D_2 strike-slip faults and σ_2 calculated for

D_2 normal faults are almost parallel, with apparent change in position of σ_1 from horizontal to a vertical position. Apart from erosion, uplift due to igneous activity might also account for the switch from strike-slip faulting to normal faulting. Although this period appears to be accompanied by igneous activity, it is doubtful that igneous intrusion during the Mesozoic was a major factor in modifying the stress field, as igneous bodies intruded during this period are not abundant. The reverse may be the case, that is, faulting may have controlled emplacement of igneous bodies.

The co-occurrence of strike-slip faults and normal faults during D_3 also indicate that values of σ_1 and σ_2 were probably close. The interchange in the positions of σ_1 and σ_2 during D_3 may be the result of long-term uplift due to erosion, aided by extension due to regional compression associated with northeast-trending σ_1, as suggested for the recent normal faults in eastern Metro Toronto (Mohajer *et al.* 1992), and in southeastern Lake Ontario (Thomas *et al.* In press). Several northeast-trending normal faults having orientations similar to the northeast trend of nearby major gravity lineaments suggest possible reactivation of basement faults during D_3. Although northeast-oriented normal faults could form under the current stress field, none were found in the study area. Such faulting, however, has been documented in metropolitan Toronto area where a normal fault in interglacial sediments, and

oriented 065°-55°, cuts and displaces a second normal fault (Wallach 1994). In addition, northeast-oriented normal faulting was postulated to explain the displaced seismic reflectors, recorded by Thomas *et al.* (1993) in unconsolidated sediments in the southeastern portion of Lake Ontario. subsequent work by Thomas (unpublished) revealed that the displacement occurred along features which originate in the underlying Paleozoic bedrock, thereby confirming that those features are faults.

6.4 Spatial Association Among Seismicity, Structures and Geophysical Anomalies

Recent deformation is also demonstrated by the occurrence of weak to moderate earthquakes within the study area. Using the weights of evidence model, weak spatial associations of seismicity with high gravity and magnetic anomalies were obtained. Weak association was also established between seismicity and three orientation classes of gravity and magnetic lineaments (81° to 99°, 27° to 45° and 297° to 315°). The orientations of geophysical lineaments associated with earthquakes are consistent with the expected orientations of lineaments that might be activated given the orientation of the current stress field in eastern North America. The direction of the current stress field as inferred from focal mechanism solutions is northeast (Sbar and Sykes 1973, 1977;

Yang and Aggarwal 1981; Hasegawa et al. 1985; Adams and Basham 1989; Zoback 1992). This direction is similar to the orientation derived based on fault lineation data from the youngest generation of faults (D_3) in the Ottawa-Hull area and to the direction of the principal compressional stress of the region attributed to spreading along the mid-oceanic ridge in the North Atlantic (Richardson *et al.* 1979; Solomon *et al.* 1980; Hasegawa and Adams 1981; Talwani and Rajendran 1991). Focal mechanism solutions from earthquakes in eastern north America indicating types of movement and orientations of faults and orientations of the greatest principal horizontal compressive stress (Sbar and Sykes 1973, 1977; Aggarwal and Sykes 1978; Horner *et al.* 1978, 1979; Herrmann 1979; North *et al.* 1989; Pulli and Toksöz 1981; Yang and Aggarwal 1981; Mauk *et al.* 1982; Seborowski *et al.* 1982; Schlesinger-Miller et al 1983; Houlday *et al.* 1984; Seeber and Coles 1984; Wetmiller *et al.* 1984; Wahlström 1987; Burke *et al.* 1989; Lamontagne 1987; Adams and Basham 1989, 1991; Zoback 1992) show mostly reverse displacements on northwest-striking surfaces, and dextral slip on north-northeast to northeast-trending planes.

The northeast geophysical lineaments probably originated as ductile faults during the Grenvillian orogeny. Brittle faulting indicated by their association with present-day seismicity may have also affected the northeast ductile faults during earlier deformation episodes following Grenvillian

orogeny. Although no sufficient evidence is currently available to establish the origin of the northwest and east-northeast to east-southeast lineaments in the basement rocks, these could be related to deformation episodes earlier than D_1. Although most of the large-scale structures delineated from geophysical anomaly maps are basement faults that are associated with earlier deformation periods, some of these may be linked directly to known, younger surface faults (e.g. Gloucester, Eardley and Hazeldean) that cut the Paleozoic sedimentary cover. It is possible that some Pre-cambrian structures propagated into the Paleozoic cover during D_1, D_2 and D_3. Field evidence should be gathered, if any, to verify this hypothesis.

7. CONCLUSIONS AND SUGGESTIONS FOR FURTHER STUDY

This work has documented families of Phanerozoic faults in the Ottawa-Hull area based on fault-plane orientations and kinematics, and has established their relative ages and movement histories based on cross-cutting and offset relationships. The families of faults belong to three (3) generations. These are, from oldest to youngest: 1) D_1 structures including sinistral and dextral strike-slip faults and some normal faults, 2) D_2 structures consisting of sinistral and dextral strike-slip faults, thrust faults and normal faults, and 3) D_3 structures including sinistral and dextral strike-slip faults, thrust faults and normal faults.

Absolute ages ascribed to the dykes encountered in the Ottawa-Hull area provide an indication as to the range of time during which the D_2 faults were formed. D_2 faults are associated with the emplacement of carbonatite dykes during the early Cretaceous period. There is no absolute age data available for the D_1 and D_3.

Kinematic analysis of faults and fault surface features demonstrate an evolution in the orientation of the paleostress field where the greatest principal horizontal stress (σ_1) has rotated counterclockwise by about 90°. Maximum principal stress axis calculated for D_1 strike-slip faults suggests that

D_1 structures were generated by northwest-southeast compression attendant with the closing of the proto-Atlantic ocean during the Paleozoic. Maximum principal horizontal stress axis obtained for D_2 structures are consistent with the compressional direction associated with the opening of the Atlantic ocean. Plate collision attendant to this event was favourable to the development of strike-slip and thrust faults, and extensional faulting at high angles to the collisional plate margins. D_3 structures are consistent with the post-Cretaceous, northeast-southwest compression in eastern North America. The occurrence of different types of faults during each period of deformation indicate perturbations in the stress field, due to plate movement, resulting in switches in the style of faulting.

Using the weights of evidence model, weak spatial association of seismicity with gravity and magnetic anomalies were obtained. Weak associations were also established between seismicity and three (3) orientation classes of gravity and magnetic lineaments (81° to 99°, 27° to 45° and 297° to 315°). The northeast lineaments represent ductile faults that originated during the Grenvillian orogeny and have been reactivated by brittle faulting since the Grenvillian orogeny. The northwest and east-northeast to east-southeast lineaments are also probably Pre-Cambrian features that have been reactivated in the basement and overlying Paleozoic rocks.

Their orientations are similar to the orientations of some families of D_1 to D_3 faults. Some of these lineaments may be directly linked to known faults.

Maps of elevated probabilities of occurrence per unit area for an 11-year period was generated. Areas characterized by the overlap of high magnetic anomaly, high gravity anomaly and zones within 7 kms from northeast gravity lineaments are associated with highest posterior probabilities.

Pre-existing structures can be reactivated in later, different strain episodes, as demonstrated in this paper, and by the occurrence of large earthquakes during historic times along ancient geological structures in eastern North America (Sykes 1978; Slemmons and dePolo 1986). Large historical events such as the 1811 and 1812 New Madrid earthquakes and 1886 Charleston earthquake demonstrate that favourably-oriented, pre-existing faults, including sediment-covered, major basement faults in intraplate regions, are prone to reactivation under later stress regimes. Once major crustal fractures are formed, they may serve as loci for tectonic movements over a long period of time, i.e. major faults tend to be reactivated if tectonic stresses are favourably oriented. It is believed that the current principal stress in the earth's crust in eastern North America trends east-northeast to northeast, an orientation favourable for possible

reactivation of faults in the Ottawa-Bonnechère graben. In the Ottawa-Hull area, a major urban agglomeration, possible reactivation of faults belonging to the families defined here under the current stress field cannot be discounted. For instance D_1 and D_2 strike-slip, normal and thrust faults, and D_2 and D_3 strike-slip and normal faults, due to their orientations with respect to the direction of the current maximum horizontal principal stress, are prone to reverse and strike-slip faulting, respectively. Similarly-oriented structures older than D_1 are also prone to reactivation.

Evidence of recent displacement of faults and lineaments spatially associated with seismicity should be gathered. This could be done using displacement studies in outcrops with Quaternary sediment cover. The lack of young sediments in the Ottawa-Hull area and eastern Canada, however, means evidence will be gathered almost always from deformed bedrock exposures where it is very difficult to distinguish neotectonic from older deformation. Nevertheless, structural studies in bedrock outcrops covering a larger area will help to better understand the sequence and kinematic characteristics of deformation periods. It would then be easier to identify those structures that are the result of more recent activity.

Basement faults, concealed or with only very subtle surface expressions, need further investigation employing

seismological, geophysical, geological, conventional and satellite geodesy, and remote-sensing techniques. The information derived would be very useful in identifying earthquake source zones. Stratigraphic and structural studies including the analysis of boreholes would help in the determination of the orientation, continuity and history of movement of subsurface structures.

Future studies should also address possible spatial association between seismicity and intersections of faults to provide additional constraint in assessing earthquake source zones, hazards and risks. The largest historical earthquakes in the region (e.g. Montreal, est. M=5.6-6.0; Grand Banks, M=7.2; Timiskaming, M=6.25; Attica, M=5.8, and; Cornwall-Massena earthquakes, M=5.9) have occurred at intersections of faults. As more earthquakes are recorded, more significant results may be obtained from the analysis of epicentre distribution with respect to intersections of faults.

REFERENCES

Adams, J. 1982. Stress-relief buckles in the McFarland quarry, Ottawa. Canadian Journal of Earth Sciences, 19: 1883-1887.

Adams, J. 1989. Crustal stresses in eastern Canada. *In* Earthquakes at North-Atlantic Passive Margins: Neotectonics and Postglacial Rebound. *Edited by S.* Gregersen and P. W. Basham. Kluwer Academic Publishers, The Hague.

Adams, J. and Basham, P. 1989. The seismicity and seismotectonics of Canada east of the Cordillera. Geoscience Canada, 16: 3-16.

Adams, J. and Basham, P. W. 1991. The seismicity and seismotectonics of eastern Canada. *In* Neotectonics of North America. *Edited by* D. B. Slemmons, E. R. Engdahl, M. D. Zoback, and D. D. Blackwell. Geological Society of America, Geology of North America, Decade Map Volume, Boulder, Colorado.

Adams, J., Sharp, J. and Connors, K., 1989a. Revised epicenters for earthquakes in the lower St. Lawrence

seismic zone, 1928-1968. Geological Survey of Canada, Open File 2072, 82 pp.

Adams, J., Sharp, J. and Stagg, M., 1988. New focal mechanisms for southeastern Canadian earthquakes. Geological Survey of Canada, Open File 1892, 109 pp.

Adams, J., Sharp, J. and Stagg, M., 1988. New focal mechanisms for southeastern Canadian earthquakes - Volume II. Geological Survey of Canada, Open File 1995, 97 pp.

Aggarwal, Y. P. and Sykes, L. R. 1978. Earthquakes, faults and nuclear power plants in southern New York and Northern New Jersey. Science, 200: 425-429.

Agterberg, F. P., 1989b. Systematic approach to dealing with uncertainty of geoscience information in mineral exploration. Proc. 22nd APCOM Symposium, Chapter 18, pp. 165-178.

Agterberg, F. P. and Bonham-Carter, G. F. 1990. Deriving weights of evidence from geoscience contour maps for the prediction of discrete events. XXII International Symposium APCOM, pp. 381-395.

Agterberg, F. P., Bonham-Carter, G. F. and Wright D. F., 1988.

Integration of Geological Datasets for Gold Exploration in Nova Scotia. Photogram. Eng. Remote Sensing, **54**: 1585-1592.

Agterberg, F. P., Bonham-Carter, G. F. and Wright, D. F. 1990. Statistical pattern integration for mineral exploration. *In* Computer applications in Resource Exploration. *Edited by* G. Gaal. Pergamon Press, New York.

Andrews, D. J. 1989. Mechanics of fault junctions. Journal of Geophysical Research, **94**: 9389-9397.

Basham, P. W., Weichert, D. H. and Berry, M. J. 1979. Regional Assessment of seismic hazard in eastern Canada. Bulletin of the Seismological Society of America, **69**: 1567-1602.

Beardsley, R. W. and Cable, M. S. 1983. Overview of the evolution of the Appalachian Basin: Northeastern Geology, **5**: 137-145.

Bolton, T. E. and Liberty, B. A. 1972. Geology of the national capital area: Lower Paleozoic stratigraphy. Field Excursions B23 to B27 Guidebook. 24th International Geological Congress, Montreal, pp. 15-23.

Bonham-Carter, G. F. 1991. Spatial data integration of geoscientific maps using GIS. *In* Geographic Information Systems:Principles and Applications. *Edited by* D.J. McGuire, M.F. Goodchild and D.W. Rhind. Longman, London.

Bonham-Carter, G. F. In Press. Geographic Information Systems for Geoscientists: Modelling with GIS. Pergamon Press, Oxford.

Bonham-Carter, G. F. and Agterberg, F. P., 1990. Application of a Microcomputer-based Geographic Information System to Mineral Potential Mapping. *In* Microcomputers in Geology. *Edited by* T. Hanley and D. F. Merriam. Pergamon Press, Oxford.

Bonham-Carter, G. F., Agterberg, F. P. and Wright, D. F. 1988. Integration of geological data sets for gold exploration in Nova Scotia. Photogrammetric Engineering and Remote Sensing, **54**: 1585-92.

Bonham-Carter, G. F., Agterberg, F. P. and Wright, D. F. 1990. Weights of evidence modelling: a new approach to mapping mineral potential. Geological Survey of Canada, Paper 89-9, pp. 171-83.

Brock, B. S. and Moore, J. M. 1983. Chronology, chemistry, and tectonics of igneous rocks in terranes of the Grenville Province, Canada. Geological society of America Abstracts with Programs, 15: 533.

Burke, K. and Dewey, J. F. 1973. Plume-generated triple junctions: Key indicators in applying plate tectonic model to old rocks. Journal of Geology, 81: 406-433.

Burke, K. B. S., Wetmiller, R. J., Lamontagne, M., Carr, M. J. and Hickey, C. 1989. Microearthquake survey of the Miramichi, New Brunswick, epicentral region, 1985. Canadian Journal of Earth Sciences, 26: 2567-2577.

Campbell, D. L. 1978. Investigation of the stress concentration mechanism for intraplate earthquakes. Geophysical Research Letters, 5: 477-479.

Corriveau, L. 1990. Proterozoic subduction and terrane amalgamation in the southwestern Grenville province, Canada: Evidence from ultrapotassic to shoshonitic plutonism. Geology, 15: 614-617.

Cullota, R. C.. Pratt, T. and Oliver, J. 1990. A tale of two sutures: COCORP'S deep seismic surveys of the Grenville province in the eastern U.S. midcontinent. Geology, 18:

646- 649.

Davidson, A. 1986. New interpretations in the southwestern Grenville Province. *In* The Grenville Province. *Edited by* J. M. Moore, A. Davidson and A. J. Baer. Geological Association of Canada, Special Paper 31, pp.61-74.

Derry, Booth, Michener and Wahl and Ontario Geological Survey. 1989. Limestone Industries of Ontario, Volume II - Limestone Industries and Resources of Eastern and Northern Ontario; Ontario Ministry of Natural Resources, Land Management Branch, 196 p.

Dewey, J. F. 1969. The evolution of the Caledonian/Appalachian orogen. Nature, **222**: 124-128.

Dewey, J. F. and Bird, J. M. 1984. Mountain belts and the new global tectonics. *In* Orogeny (Benchmark Papers in Geology, V. 62); *Edited by* J. G. Dennis. Hutchinson Ross Publishing Company, Stroudsburg.

Dobrin, M. B. and Savit C. H. 1988. Introduction to Geophysical Prospecting (4th ed.). McGraw-Hill Book Company,New York.

Du Berger, R., Roy D. W., Lamontagne M., Woussen G., North, R.

G. and Wetmiller, R. J. 1991. The Saguenay (Québec) earthquake of November 25, 1988: seismologic data and geologic setting. *In* Intraplate. Deformation, Neotectonics, Seismicity, and the State of Stress in Eastern North America. *Edited by* J.-C. Mareschal. Tectonophysics, **186**: 59-74.

Durney, D. W. and Ramsay, J. G. 1973. Incremental strains measured by syntectonic crystal growth. *In* Gravity and Tectonics. *Edited by* K. A. DeJong and R. Scholten. John Wiley and Sons, New York.

Eby, G. N. 1984. Geochronology of the Monteregian Hills alkaline igneous province, Québec. Geology, **12**: 468-470.

Etchecopar, A., Vasseur, G. and Daignieres, M. 1981. An inverse problem in microtectonics for the determination of stress tensors from fault striation analysis. Journal of Structural Geology, **3**: 51-65.

Fleiss, J. L. 1981. Statistical Methods for Rates and Proportions (2nd ed.), John Wiley and Sons, New York.

Fleuty, M. J. 1975. Slickensides and slickenlines. Geological Magazine, **112**:319-321.

Forsyth, D. A. 1977. Relationships between seismicity, free-air gravity and structure in arctic and eastern Canada (abstract). Earthquake Notes, **48**: 15.

Forsyth, D. A. 1981. Characteristics of the Western Québec seismic zone. Canadian Journal of Earth Sciences, **18**: 103- 119.

Gittins, J., MacIntyre, R. M., and York, D. 1967. The ages of carbonatite complexes in eastern Canada. Canadian Journal of Earth Sciences, **4**, 651-655.

Goodacre, A. K., Bonham-Carter, G. F., Agterberg, F. P. and Wright D. F. 1993. A statistical analysis of the spatial association of seismicity with drainage patterns and magnetic anomalies in western Québec. Tectonophysics, **217**: 285-305.

Groshong, R. H. Jr. 1988. Low-temperature deformation mechanisms and their interpretation. Geological Society of America Bulletin, **100**: 1329-1360.

Halls, H. C. 1978. The late Precambrian Central N. American rift system - a survey of recent geological and geophysical investigations. *In* Tectonics and Geophysics of Continental Rifts. *Edited by* I. B. Ramberg

and E.R. Neumann. D. Reidel Publ. Co., Dordrecht.

Hancock, P. L. 1985. Brittle Microtectonics: principles and practice. Journal of Structural Geology, 7: 437-457.

Hanmer, S. 1988. Ductile thrusting at mid-crustal level, southwest Grenville Province: Canadian Journal of Earth Sciences, 25: 1049-1059.

Hasegawa, H. S. and Adams, J. 1981. Crustal stresses and seismotectonics in eastern Canada, Earth Physics Branch Open-File Report 81-12, 62 pp.

Hasegawa, H. S., Adams, J. and Yamazaki, K. 1985 . Upper crustal stresses and vertical stress migration in eastern Canada. Journal of Geophysical Research, 90: 3637-3648.

Herrmann, R. B. 1979. Surface wave focal mechanisms for eastern North America earthquakes with tectonic implications. Journal of Geophysical Research, 84: 3543-3552.

Hewitt, D. F. 1964. Precambrian - Paleozoic contact relationships in eastern Ontario. Guidebook to Geology of central Ontario. American Association of Petroleum

Geologists and Society of Economic Paleontologists and Mineralogists, pp.9-13.

Hofmann, H. J. 1972. Stratigraphy of the Montreal area: 24th International Geological Congress, Montreal, Guidebook for excursions, B-03.

Hogarth, D. D., Rushforth, P. and McCorkell, R. H. 1988. The Blackburn carbonatites, near Ottawa, Ontario: dykes with fluidized emplacement. Canadian Mineralogist, 26: 377-390.

Hon, V. 1970. A study of some post Cambrian dike rocks in southeastern Ontario. B.Sc. thesis, Carleton University, Ottawa, Ont.

Horner, R. B., Stevens, A. E., Hasegawa, H. S. and Leblanc, G. 1978. Focal parameters of the July 12, 1975, Maniwaki, Québec earthquake - An eaxample of intraplate seismicity in eastern Canada. Bulletin of the Seismological Society of America, 68: 619-640.

Houlday, M., Quittmeyer, R., Mrotek, K. and Statton, C. T. 1984. Recent seismicity in north- and east-central New York State. Earthquake Notes, 55: 16-20.

Illies, J. H. 1981. Mechanism of graben formation, Tectonophysics, 73: 249-266, 1981.

Kay, G. M. 1942. Ottawa-Bonnechère graben and Lake Ontario homocline. Geological Society of America Bulletin, 53: 585- 646.

Keppie, J. D. 1977a. Tectonics of Southern Nova Scotia. Nova Scotia Department of Mines, Paper 77-1, 34 p.

Keppie, J. D. 1977b. Plate tectonic interpretation of Paleozoic world maps (with emphasis on circum-Atlantic orogens and southern Nova Scotia). Nova Scotia Department of Mines, Paper 77-3, 45p.

Kumarapeli, P. S. 1976. The St. Lawrence rift system, related metallogeny and plate tectonic models of Appalachian evolution. *In* Metallogeny and Plate Tectonics. *Edited by* D. F. Strong. Geological Association of Canada, Special Paper 14, pp. 301-320.

Kumarapeli, P. S. 1978. The St. Lawrence paleo-rift system: a comparative study, *In* Tectonics and Geophysics of Continental Rifts. *Edited by* I. B. Ramberg and E.R. Neumann. D. Reidel Publ. Co., Dordrecht.

Kumarapeli, P. S. 1985. Vestiges of Iapetan rifting in the craton west of the northern Appalachians. Geoscience Canada, **12**: 55-59.

Kumarapeli, P. S., and Saull, V. A. 1966. The St. Lawrence valley system: A North American equivalent of the East African rift valley system. Canadian Journal of Earth Sciences, 3: 639-658.

Lamontagne, M. 1987. Seismic activity and structural features in the Charlevoix region, Québec. Canadian Journal of Earth Sciences, **24**: 2118-2129.

Liberty, B. A. 1964. Middle Ordovician stratigraphy of the Lake Simcoe area, Ontario. Guidebook to Geology of central Ontario. American Association of Petroleum Geologists and Society of Economic Paleontologists and Mineralogists, pp. 14-35.

Liberty, B. A. 1967. Ordovician stratigraphy of Southern Ontario: The Ottawa Valley problem. Abstracts, Geological Association of Canada and Mineralogical Association of Canada, International Meeting, pp.49-50.

Long, L. T. 1976. Speculations concerning southeastern

earthquakes, mafic intrusions, gravity anomalies and stress amplification. Earthquake Notes, **47**: 29-35.

Lumbers, S. B. 1976. Geological setting of alkalic rock-carbonatite complex in eastern Canada. *In* Proceedings - International Symposium on Carbonatites, Pacos de Calelos, Brazil.

MacDonald, G. and Harrison, J. E. 1979. Ottawa-Hull sheet. Geological Survey of Canada, Map 1508A, scale 1: 125 000.

Mareschal, J.-C. and Zhu P.-D. 1989. Focal Mechanism of small earthquakes and the stress field in the western Québec Adirondack region. Tectonophysics, **166**: 163-174.

Mauk, F. J., Christensen, D. and Henry, S. 1982. The Sharpsburg, Kentucky earthquake, 27 July 1980: Main shock parameters and isoseismal maps. Bulletin of the Seismological Society of America, **72**: 221-236.

McGinnis, L. D. and Ervin, C. P. 1974. Earthquakes and block tectonics in the Illinois Basin. Geology, **2**: 517-519.

McKay, D. A. 1986. Roblindale Quarry stress measurements: Preliminary evaluation-phase 1. Ontario Hydro Research Division, Report No. 86-43-p., 144 pp.

McKeown, A. F. 1975. Hypothesis: mafic intrusives and their contact zones are source zones of many earthquakes in central and southeastern United States (abstract). Earthquake Notes, **46**:53.

McKerrow, W. S. and Cocks, L. R. M. 1977. The location of the Iapetus Ocean suture in Newfoundland. Canadian Journal of Earth Sciences, **14**: 488-499.

Means, W. D. 1987. A newly recognized type of slickenside lineation. Journal of Structural Geology, **9**: 585-590.

Miyashiro, A. 1982. Precambrian orogenies, *In* Orogeny. *Edited by* A. Miyashiro, K. Aki and A. M. Celal Sengor. John Wiley and Sons, Chichester.

Miyashiro, A. 1982. Theory of orogeny based on plate tectonics: Various aspects of the theory of orogeny based on plate tectonics. *In* Orogeny. *Edited by* A. Miyashiro, K. Aki and A. M. Celal Sengor. John Wiley and Sons, Chichester.

Mohajer, A. A., Eyles, N. and Rogojina, C. 1992. Neotectonic faulting in metropolitan Toronto: Implications for earthquake hazard assessment in the Lake Ontario region. Geology, **20**: 1003-1006.

Moore, J. M. and Thompson, P. H. 1980. The Flinton Group: A late PreCambrian metasedimentary succession in the Grenville Province of eastern Ontario. Canadian Journal of Earth Sciences, **17**: 1685-1707.

Moore, J. M., Jr. 1982. Stratigraphy and tectonics of the Grenvillian Orogen in eastern Ontario. Ottawa-Carleton Center for Geoscience Studies, Grenville Workshop, Program and Abstracts, p. 7.

Mueller, St. 1970. Geophysical aspects of graben formation in continental rift systems, *In* Graben Problems. *Edited by* J. H. Illies and St. Mueller. E. Schweizerbart'sche Verlagsbuchhandlung, Sttutgart.

Murthy, G. S. 1971. The paleomagnetism of diabase dikes from the Grenville Province. Canadian Journal of Earth Sciences, **8**: 802-812.

Norris, D. K. 1967. Structural analysis of the Queensway folds, Ottawa, Canada. Canadian Journal of Earth Sciences, **4**: 209-321.

Norris, D. K., and Barron, K. 1969. Structural analysis of features on natural and artificial faults. Geological Survey of Canada, Paper 68-52, pp. 136-167.

North, R. G., Wetmiller, R. J., Adams, J., Anglin, F. M., Hasegawa, H. S., Lamontagne, M., DuBerger, R., Seeber, L. and Armbruster, J., 1989. Preliminary results from the November 25, 1988 Saguenay (Québec) earthquake. Seismological Research Letters, 60: 89-93.

Petit, J. P. 1987. Criteria for the sense of movement on fault surfaces in brittle rocks. Journal of Structural Geology, 9: 597-608.

Philpotts, A. R. 1978. Rift-associated igneous activity in Eastern North America. *In* Petrology and Geochemistry of Continental Rifts. *Edited by* E. R. Neumann and I. B. Ramberg. D. Reidel Publishing Company, Dordrecht.

Pintson, H., P. S. Kumarapeli and Morency, M. 1985. Tectonic significance of the Tibbit Hill Volcanics: Geochemical evidence from Richmond Area, Québec. In Current Research, Part A. Geological Survey of Canada, Paper 85-1A, pp. 123- 130.

Pulli, J. J. and Toksöz, M. N. 1981. Fault plane solutions for northeastern United States earthquakes. Bulletin of the Seismological Society of America, 71: 1875-1882.

Rankin, D. W. 1976. Appalachian salients and recesses:late

Precambrian continental break up and the opening of the Iapetus Ocean. Journal of Geophysical Research, **81**: 5605-5619.

Richardson, R. M., Solomon, S. C. and Sleep, N. H. 1979. Tectonic stress in the plates. Rev. Geophysical Space Physics, **17**: 981-1019.

Roche, A. and Wohlenberg, J. 1970. Magnetic measurements in Alsace, Baden and Pfalz. *In* Graben Problems. *Edited by* J. H. Illies and St. Mueller. E. Schweizerbart'sche Verlagsbuchhandlung, Sttutgart.

Sanford, B. V. and Baer, A. J. 1971. Geology of southern Ontario, Ontario-Québec-U.S.A. Geological Survey of Canada, Map 1335A, scale 1:1 000 000.

Sbar, M. L. and Sykes, L. R. 1973. Contemporary stress and seismicity in eastern North America: an example of intra-plate tectonics. Geological Society of America Bulletin, **84**: 1861-1882.

Sbar, M. L. and Sykes, L. R. 1977. Seismicity and lithospheric stress in New York and adjacent areas. Journal of Geophysical Research, **82**: 5771-5786.

Schenck, P. E. 1971. Southeastern Atlantic Canada, northwestern Africa and continental drift. Canadian Journal of Earth Sciences, 8: 1218-1251.

Schlesinger-Miller, E. A., Barstow, N. L. and Kafka, A. L. 1983. The July 1981 earthquake sequence near Cornwall, Ontario, and Massena, New York. Earthquake Notes, 54: 11-26.

Seborowski, K. D., Williams, G., Kelleher, J. A. and Statton, C. T. 1982. Tectonic implications of recent earthquakes near Annsville, New York. Bulletin of the Seismological Society of America, 72: 1601-1609.

Seeber, L. and Coles, K. S. 1984. Seismicity in the Central Adirondacks with emphasis on the Goodnow, October 7, 1983 epicentral zone and its geology. In New York Geological Association Fieldtrip Guidebook. Edited by D. B. Potter. 56th Annual Meeting, Clinton, New York, 334-352.

Sengor, A. M. C., Burke, K. and Dewey, J. F. 1978. Rifts at high angles to orogenic belts: tests for their origin and the upper Rhine graben as an example. American Journal of Science, 278: 24-40.

Shafiqullah, M. 1971. K-Ar ages of some igneous rocks in

eastern Canada. Unpublished Manuscript, Carleton University, Ottawa, Ont.

Slemmons, D. B. and dePolo, C. M. 1986. Evaluation of active faulting and associated hazards. *In* Active Tectonics, Studies in Geophysics. *Edited by* R. E. Wallace. National Academy Press, Washington D. C.

Smith, W. E. T. 1962. Earthquakes of eastern Canada and adjacent areas 1534-1927. Publications of the Dominion Observatory, **26**: 271-301.

Smith, W. E. T. 1966. Earthquakes of eastern Canada and adjacent areas 1928-1959. Publications of the Dominion Observatory, **32**: 87-121.

Solomon, S. C., Richardson, R. M. and Bergman, E. A. 1980. Tectonic stress: models and magnitudes. Journal of Geophysical Research, **85**: 6086-6092.

Steele-Petrovich, H. M. 1986. Lithostratigraphy and a summary of the paleoenvironments of the lower Middle Ordovician sedimentary rocks, upper Ottawa valley, Ontario. *In* Current Research, part B. Geological Survey of Canada, Paper 86-1B, pp. 493-506.

Sykes, L. R. 1978. Intraplate seismicity, reactivation of pre-existing zones of weakness, alkaline magmatism, and other tectonism postdating continental fragmentation. Rev. Geophys. Space Phys., **16**: 621-688.

Talwani, P. and Rajendran, K. 1991. Some seismological and geometric features of intraplate earthquakes. *In* Intraplate Deformation, Neotectonics, Seismicity, and the State of Stress in Eastern North America. Edited by Mareschal, J.-C. Tectonophysics, **186**: 19-41.

Teskey, D. J. 1989. Statistical interpretation of aeromagnetic data. *In* Statistical Applications in the Earth Sciences. *Edited by* F. P. Agterberg and G. F. Bonham-Carter. Geological Survey of Canada, Paper 89-9, pp. 49-55.

Thomas, R. L., Wallach, J. L., McMillan, R. K., Bowlby, J. R., Frape, S., Keyes, D., and Mohajer, A. A. 1993. Recent Deformation in the bottom sediments of western and southeastern Lake Ontario and its association with major structures and seismicity. Geographie Physique et Quaternaire, **47**: 325-331.

Twiss, R. J. and Moores, E. M. 1992. Structural Geology. W. H. Freeman and Company, New York.

US Geodynamics Committee. 1989. Transects D_1 to D_4: Eastern Canada and North Atlantic Ocean. *In* North American Continent-Ocean Transects Program. National Academy Press, Washington, D. C.

US Geodynamics Committee. 1989. Transect E_2: New York Appalachian Basin to Baltimore Canyon Trough. *In* North American Continent-Ocean Transects Program. National Academy Press, Washington, D. C.

Uyeno, T. T. 1974. Conodonts of the Hull Formation, Ottawa Group (Middle Ordovician), of the Ottawa-Hull Area, Ontario and Québec. Geological Survey of Canada Bulletin, **248**: 31.

van Breemen, O. and Davidson, A. 1989. U-Pb zircon ages of granites and syenites in the Central Metasedimentary Belt, Grenville Province, Ontario. *In* Radiogenic Age and Isotopic Studies: Report 2. Geological Survey of Canada, Paper 88-2, p. 45-50.

van Breemen, O. and Hanmer, S. 1986. Zircon morphology and U-Pb geochronology in active shear zones: Studies on syntectonic intrusions along the northwest boundary of the Central Metasedimentary Belt, Grenville Province, Ontario. Geological Survey of Canada, Special Paper 86-

1B, pp. 775-784.

Wahlström, R., 1987. Focal Mechanisms of earthquakes in southern Québec, southeastern Ontario, and northeastern New York with implications for regional seismotectonics and stress field characteristics. Bulletin of the Seismological Society of America, 77: 891-924.

Wallach, J. L. 1990. The onset of the current stress field in eastern North America. *In* Magnec '89 Annual Report. Edited by J. A. Heginbottom and J. L. Wallach. Geological Survey of Canada, Open File Report 2275.

Wallach, J. L. 1994. AECB assessment of Geological Survey of Canada Open File Report #2652 entitled "Late Quaternary faulting in the Rouge River Valley, Southern Ontario: seismotectonic or glaciotectonic?", Unpublished, Atomic Energy Control Board, Ottawa, Ont.

Watson, G. P. and Rencz, A. N. 1989. Data integration studies in northern New Brunswick. *In* Statistical Analysis in the Earth Sciences. *Edited by* F. P. Agterberg and G. F. Bonham-Carter. Geological Survey of Canada, Paper 89-9, pp. 185-191.

Watson, G. P., Rencz, A. N. and Bonham-Carter, G. F. 1989.

Computers assist prospecting. GEOS, 18: 8-15.

Wetmiller, R. J., Adams, J., Anglin, F. M., Hasegawa, H. S. and Stevens, A. E. 1984. Aftershock sequences of the 1982 Miramichi, New Brunswick earthquakes. Bulletin of the Seismological Society of America, 74: 621-653.

Wetmiller, R. J., Drysdale, J. A., Horner, R. B. and Lamontagne, M. 1989. Canadian Earthquakes - 1985-86. Geological Survey of Canada, Paper 88-14, p. 1.

Wiener, R. W., McLelland, J. M. Isachsen, Y. W. and Hall L. M. 1984. Stratigraphy and structural geology of the Adirondack Mountains, New York: Review and synthesis. *In* The Grenville Event in the appalachians and Related Topics. *Edited by* M. J. Bartholomew. Geological Society of America, Special Paper 194, pp. 1-52.

Williams, D. A. and Rae, A. M. 1983. Paleozoic geology of the Ottawa-St. Lawrence Lowland, southern Ontario. Ontario Geological Survey, Miscellaneous Paper 116, pp. 107-110.

Williams, D. A., Rae, A. M. and Wolf, R. R. 1984. Paleozoic geology of the Ottawa area, southern Ontario. Ontario Geological Survey, Map P. 2716, Geological Series -

Preliminary Map, scale 1: 50 000.

Williams, D. A. and Telford, P. G. 1986 . Paleozoic geology of the Ottawa area. Field Trip 8 Guidebook, Geological Association of Canada - Mineralogical Association of Canada - Canadian Geophysical Union Joint Annual Meeting, Ottawa '86, 25 p.

Williams, D. A. and Telford, P. G. 1987. Structure and Ordovician Stratigraphy of the Ottawa area, southern Ontario. Geological Society of America Centennial Field Guide - Northeastern Section, 5:349-352.

Williams, D. A., Telford, P. G., McCracken and Brunton, F. R. 1992. Cambrian-Ordovician Geology of the Ottawa Region. Fieldtrip Guidebook No. 2. Canadian Paleontology Conference - II Ottawa '92, 51 p.

Wilson, A. E. 1938a. Ottawa sheet (east half). Geological Survey of Canada, Map 413A, scale 1: 63 360.

Wilson, A. E. 1938b. Ottawa sheet (west half). Geological Survey of Canada. Map 413A, scale 1: 63 360.

Wilson, A. E. 1946. Geology of the Ottawa-St. Lawrence Lowland, Ontario and Québec. Geological Survey of

Canada, Memoir 241.

Wilson, A. E. 1946. Ottawa-Cornwall sheet. Department of Mines and Resources, Map 852A, scale 1:253 440.

Wilson, A. E. 1946. Structural map of the Ottawa-St.Lawrence Lowland. Geological Survey of Canada, scale 1:340 833.

Wolf, R. R., and Dalrymple, R. W. 1984. Sedimentology of the Cambro-Ordovician sandstones of eastern Ontario. *In* Geoscience Research Grant Program, Summary of Research, 1983-84. *Edited by* V.G. Milne. Ontario Geological Survey, Miscellaneous Paper 121, pp. 240-252.

Wright, D. F. 1988. Data integration and geochemical evaluation of Meguma terrane, Nova Scotia, for gold mineralization. M. Sc. Thesis, University of Ottawa, Ottawa, Ont.

Wynne-Edwards, H. R. 1972. The Grenville Province. *In* Variations in Tectonic Styles in Canada. *Edited by* R. A. Price and R. J. W. Douglas. Geological Association of Canada, Special Paper 11, pp. 163-182.

Yang, J. P., and Aggarwal, Y. P. 1981. Seismotectonics of Northeastern United States and adjacent Canada. Journal

of Geophysical Research. **86**: 4981-4998.

Zoback, M. L. 1992. Stress field constraints on intraplate seismicity in eastern North America. Journal of Geophysical Research. **97**: 11,761-11,782.

APPENDIX A

Weights of evidence method

The first step in calculating weights of evidence involves the determination of prior probability. The positive (W^+) and negative weights (W^-) are then calculated for each class of each map layer being considered as input in the overlaying process, using conditional probability ratios. The calculation of statistical weights is based on the areal correspondence of earthquake epicentres with map patterns. W^+ and W^- are estimated using the following formulas:

$$W^+ = \log_e\{P(B|D)/P(B|\bar{D})\}$$

$$W^- = \log_e\{P(\bar{B}|D)/P(\bar{B}|\bar{D})\}$$

Positive weight (W^+) is for pattern present and is a measure of the ratio between the proportion of points present within the pattern with respect to the total points present and the proportion of the pattern area with respect to the total area. Negative weight (W^-) is for pattern absent and indicates the ratio between the proportion of points lying outside the pattern with respect to the total points present and the proportion of area outside the pattern with respect to the total area. Contrast (C) is the difference of the positive and negative weights ($[W^+]-[W^-]$), and is also the

natural logarithm of the odds ratio (see page 30.

Expressions used to indicate whether the magnitudes of W^+, W^- and C are large enough to be statistically significant, are given by the following variance estimates:

$$s^2(W^+) = [1/\text{area}(B \cap D)] + [1/\text{area}(B \cap \bar{D})]$$

$$s^2(W^-) = [1/\text{area}(\bar{B} \cap D)] + [(1/\text{area}(\bar{B} \cap \bar{D})]$$

$$s^2(C) = [1/\text{area}(B \cap D) + 1/\text{area}(B \cap \bar{D})] + [1/\text{area}(\bar{B} \cap D) + 1/\text{area}(\bar{B} \cap \bar{D})]$$

The **'studentized'** value of C tests the hypothesis that there is lack of spatial association (i.e., C = 0). The hypothesis can be rejected with values greater than 1.96. The expression for the studentized value of C is given by:

$$\text{stud}(C) = C/s(C)$$

Each layer is simplified to produce a binary pattern reflecting the presence or absence of a given condition. The idea of measuring spatial association between points and multi-class maps (ordered), the treatment of cumulative class intervals as binary cases and the method to simplify multi-class maps to binary maps is discussed in section 3.2. The class number corresponding to the peak in contrast (C) value is usually taken as the cut-off class when reclassifying the

layer into only two classes. The input map layers are overlaid using SPANS to generate a unique conditions map consisting of map classes representing all areas of possible overlap between classes of the binary maps.

For each unique conditions map class, the posterior probability, representing the likelihood of earthquake occurrence and based on the weights of binary patterns that formed the unique conditions map class, is determined. Posterior probability is useful in predicting, in a spatial sense, the occurrence of earthquakes per unit area over a given period of time. Posterior probability is given as:

$$P = O_{post}/(1+O_{post})$$

where O_{post} = Posterior odds

$$= \exp\{\log_e O_{prior} + \sum_{j=1}^{n} W_j^k\}$$

k = + (for pattern present) or - (for pattern absent)

O_{prior} = Prior odds

Using the posterior probability values obtained, the unique conditions map is reclassified into desired number of classes depending on the range of probability values for locating earthquakes for display purposes.

Two tests for conditional independence were applied, namely: 1) pairwise test, that is, the application of a test

for conditional independence of each possible combination of two input binary maps with respect to the mineral occurrence points, and; 2) a test for the overall conditional independence assumption by applying an overall goodness-of-fit test.

The pairwise test involves the use of the following equation:

$$G^2 = -2\sum_{i=1}^{4} x_i \log_e(\hat{m}_i / x_i)$$

where x_i = observed number of epicentres (unit cells) occurring for one of the 4 overlap conditions between the two patterns, B_1 and B_2.

$\hat{m}_i$ = expected number of epicentres, calculated assuming conditional independence.

The calculation of observed values are made as for a contingency table test, where the table is restricted to locations where epicentres occur only. The following is a contingency table for cells where epicentres are present only:

A: Observed values

Pattern 2 \ Pattern 1	B_1	$\bar{B}_1$	
B_2	$N\{B_1 \cap B_2\} = X_1$	$N\{\bar{B}_1 \cap B_2\} = X_2$	$N\{B_2\}$
$\bar{B}_2$	$N\{B_1 \cap \bar{B}_2\} = X_3$	$N\{\bar{B}_1 \cap \bar{B}_2\} = X_4$	$N\{\bar{B}_2\}$
	$N\{B_1\}$	$N\{\bar{B}_1\}$	

B. Expected values under conditional independence for the four cells of the table are calculated from the product of the marginal totals divided by the grand total. Thus for cell 1 (both patterns present), the expected value ($\hat{m}_1$) is given by:

$$\hat{m}_1 = \frac{N\{B_1\}N\{B_2\}}{N\{B_1\} + N\{\bar{B}_1\} + N\{B_2\} + N\{\bar{B}_2\}}$$

and

$$\hat{m}_2 = \frac{N\{\bar{B}_1\}N\{B_2\}}{N\{B_1\} + N\{\bar{B}_1\} + N\{B_2\} + N\{\bar{B}_2\}}$$

$$\hat{m}_3 = \frac{N\{B_1\}N\{\bar{B}_2\}}{N\{B_1\} + N\{\bar{B}_1\} + N\{B_2\} + N\{\bar{B}_2\}}$$

$$\hat{m}_4 = \frac{N\{\bar{B}_1\}N\{\bar{B}_2\}}{N\{B_1\} + N\{\bar{B}_1\} + N\{B_2\} + N\{\bar{B}_2\}}$$

The hypothesis of conditional independence of B_1 and B_2

with respect to the points will be rejected if G^2 is large and one of the patterns can be deleted from the final combined model.

The test for the overall conditional independence assumption is applied after the final posterior probability map has been calculated. The total number of predicted epicentres is calculated from the sum of the product of posterior probability and area of each unique condition. Using weights of evidence, the predicted total almost always is larger than the observed total, and the discrepancy is a measure of the failure of the conditional independence assumption.

APPENDIX B

Software and operations used to extract information

The main software used for this work was SPANS (Spatial Analysis System) version 5.2 and 5.3 on OS/2 operating system from INTERA TYDAC Technologies Inc. SPANS is a quadtree-based GIS which uses a raster data structure with a variable pixel size. The maximum raster image resolution is 2" by 2" (32,768 X 32,7680) pixels. SPANS facilitates the integration of data from various sources and of different formats including raster and vector files. It allows data to be easily transferred between many external PC-based applications using ASCII and other file formats. SPANS also provides a comprehensive array of analytical and modelling tools that facilitates customized statistical operations.

Vector files such as geological boundaries, drainage lines and lineaments were generated by digitizing from source maps or by directly creating these within SPANS. The geological map and lineaments from LANDSAT imagery were digitized using the TYDIG software and exported into SPANS. Lineaments digitized from various maps were edited and, if necessary, combined using the FORTRAN programs VECED and VMERGE, respectively. The geophysical data (magnetic and gravity), originally in raster format, were transformed into

maps and were likewise further reclassified into fewer units. Point seismic files were created within SPANS from imported seismic data. A SPANS-compatible table file (Tba) was created from raw seismic data in table format (pik) using a FORTRAN program (pntba) before exporting it into SPANS.

A number of FORTRAN programs written by the Geological Survey of Canada for analysis and intermediate processing of data was used outside SPANS. These programs include CLASSLIN, CONTRAST/WTS, PREDICT AND G2OUT. The CLASSLIN program classifies lineaments into orientation classes allowing the lineament file(s) to be exported into SPANS and broken down into orientation classes for subsequent analysis. Both WTS and CONTRAST programs calculate weights of evidence parameters. The CONTRAST program, however, is applicable only for binary maps, whereas WTS produces W^+, W^- and related statistics for multi-class maps. The PREDICT program was used to estimate weights of evidence parameters including posterior probability for binary map patterns that were used as overlays. The program carries out other modelling methods as well, such as logistic regression, but these were not applied in the thesis. G2OUT was used to test pairwise conditional independence between the binary maps.

APPENDIX C

Hardware

Computer work was carried out at the Department of Geology's GIS laboratory using at any time one of the workstations that are connected to a network to facilitate laser printer-sharing and higher data storage capacity. Each workstation consists of a 80486 IBM PC/AT compatible computer operating at a clock speed of 33 MHz with ISA 16 bit bus internal architecture and 8 Mb of total system memory. Each system is equipped with a SCSI disk controller, 120 Mb hard drive, two high-density floppy drives (5¼ and 3½ inch), non-interlaced super VGA 14 inch color monitor, and an ATI Technologies Inc. Graphics ULTRA graphics accelerator video card which provides 256 colors at a monitor resolution of 1024 by 768 pixels. A more capable workstation operates with 12 Mb RAM, 220 Mb hard drive, a Sony CDU-7101W external CD-ROM drive unit and a 17 inch color monitor. Both types of workstations run under the OS/2 operating system (version 1.21) in Presentation Manager mode with a serial mouse.

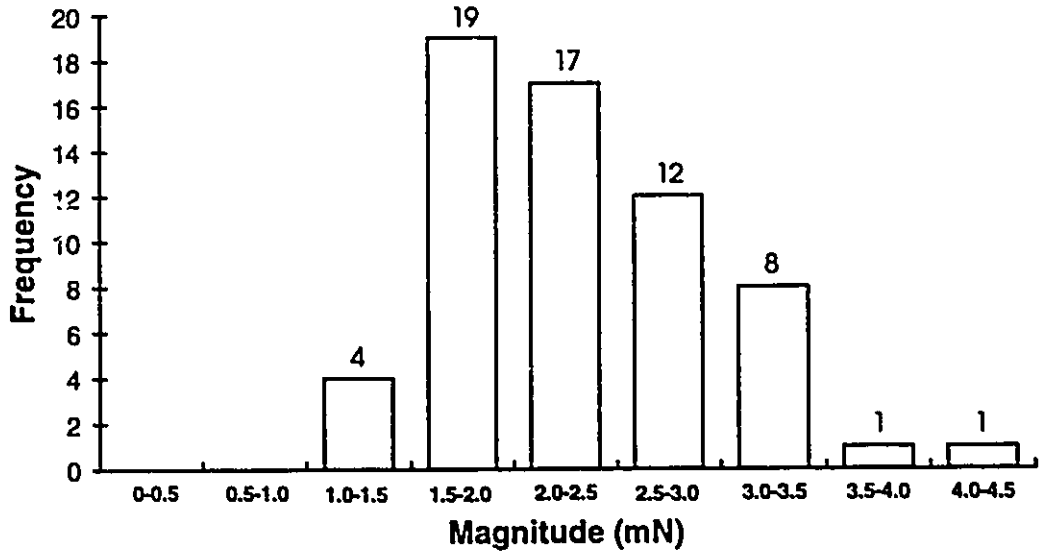

APPENDIX D. Frequency distribution of earthquake magnitude.

APPENDIX E. Regional geology and structures within the study area. After Sanford and Baer's (1971) 1: 1 000 000 scale geological compilation.

GEOLOGY AND STRUCTURES

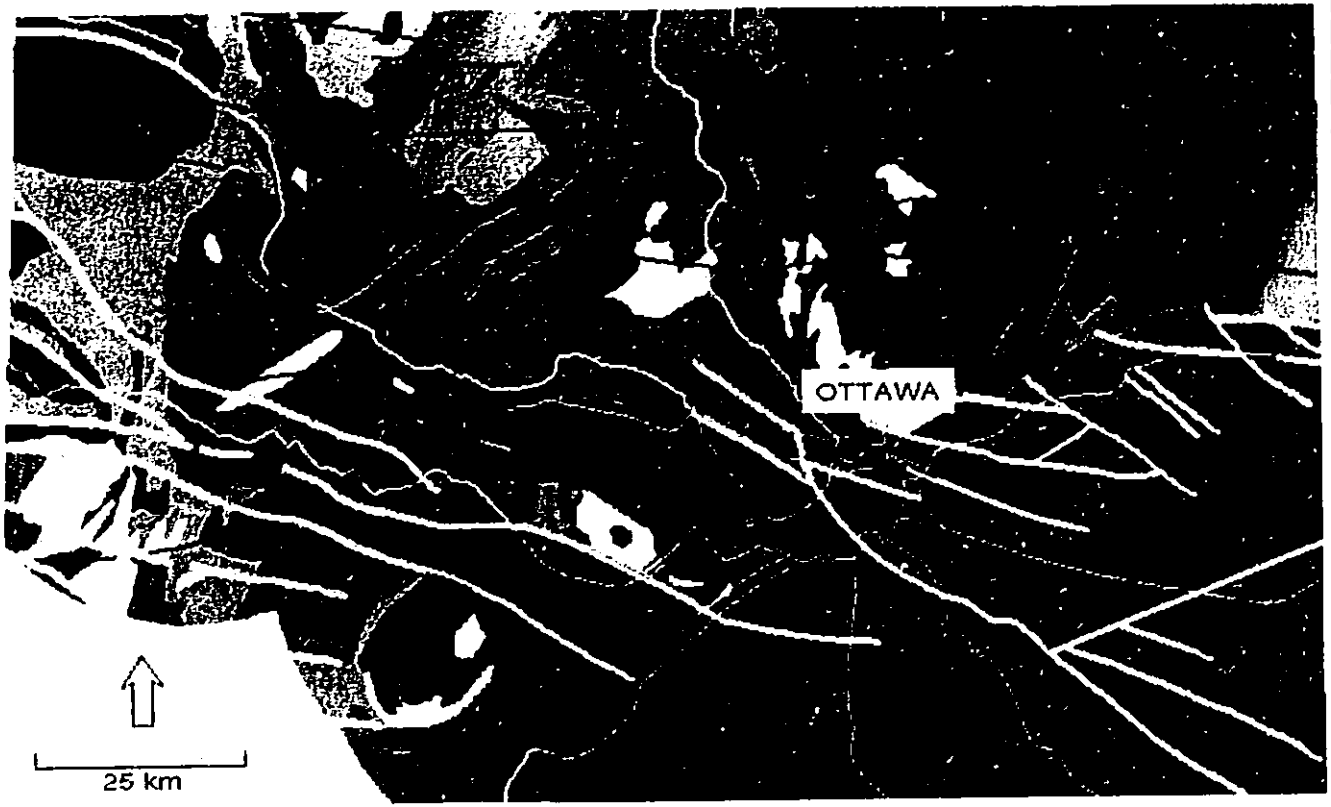

LEGEND

- Ordovician sediments
- Hy Syenite
- Hy-h' Hornblende syenite
- Hy-h Hypersthene syenite
- Hg Granite
- Hg-b Biotite potassic granite
- Hgk Potassic granite
- Hdi Diorite
- Hb Gabbro
- Hmc Marble
- Hq Quartzite
- Hcg Conglomerate
- Hvd Andesite
- Hm Amphibolite
- Hn Paragneiss
- An-b Biotite gneiss
- An bh' Hblende biotite gneiss
- An-h' Hornblende gneiss
- Anqf Biotite qtz feld gneiss
- Pg Granite
- Pn-s Granite-garnet-biot gneiss
- Pmg Migmatite
- Pnqf Biot. qtz-feld'thic gneiss
- gk Potassic granite
- gd Granodiorite
- ub Ultrabasics
- nm Hornblende gneiss
- n-h' Amphibole-hy'thene gneiss

Fault
Dykes
Highway

APPENDIX F. Lineaments from satellite imagery superimposed on map of main lithotectonic units.

LINEAMENTS AND MAIN LITHOTECTONIC UNITS